Goldstone Bosons in a Crystalline Chiral Phase

Goldstone Bosonen in einer Kristallinen Chiralen Phase
Zur Erlangung des Grades eines Doktors der Naturwissenschaften (Dr. rer. nat.)
genehmigte Dissertation von M.Sc. Marco Schramm, geb. in Frankfurt am Main
Tag der Einreichung: 29.06.2017, Tag der Prüfung: 24.07.2017
Darmstadt 2017 — D 17

1. Gutachten: PD Dr. Michael Buballa
2. Gutachten: Prof. Dr. Jens Braun

TECHNISCHE UNIVERSITÄT DARMSTADT

Fachbereich Physik
Institut für Kernphysik
NHQ

Goldstone Bosons in a Crystalline Chiral Phase
Goldstone Bosonen in einer Kristallinen Chiralen Phase

Genehmigte Dissertation von M.Sc. Marco Schramm, geb. in Frankfurt am Main

1. Gutachten: PD Dr. Michael Buballa
2. Gutachten: Prof. Dr. Jens Braun

Tag der Einreichung: 29.06.2017
Tag der Prüfung: 24.07.2017

Darmstadt 2017 — D 17

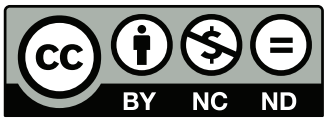

Abstract

The phase diagram of strong interaction matter is expected to exhibit a rich structure. Different models have shown, that crystalline phases with a spatially varying chiral condensate can occur in the regime of low temperatures and moderate densities, where they replace the first-order phase transition found for spatially constant order parameters.

We investigate this inhomogeneous phase, where in addition to the chiral symmetry, translational and rotational symmetry are broken as well, in a two flavor Nambu–Jona-Lasinio model. The main goal of this work is to describe the Goldstone bosons in this phase, massless excitations that occur for spontaneously broken symmetries.

We take one of the simplest possible modulations, the chiral density wave, and show how to derive the quark propagator of the theory analytically, by means of transformations in chiral and momentum space. We apply this to a test case for the gap equation.

We show the derivation of Nambu-Goldstone modes in the inhomogeneous phase and find, that for our case only three different modes have to be taken into account. We proceed to calculate the Goldstone boson related to the breaking of spatial symmetry, which can be related to the neutral pion. By evaluating a Bethe-Salpeter equation, we can show, that we have indeed found a Goldstone boson and give its dispersion relation in terms of momenta perpendicular, as well as parallel to the mass modulation.

Zusammenfassung

Im Phasendiagramm stark wechselwirkender Materie wird eine reiche Struktur erwartet. Verschiedene Modelle haben gezeigt, dass kristalline Phasen mit einem räumlich veränderlichen chiralen Kondensat bei niedriger Temperatur und mittleren Dichten auftreten können und dort den Phasenübergang erster Ordnung überlagern, der für räumlich konstante Ordnungsparameter erwartet wird.

Wir untersuchen diese inhomogene Phase, in der zusätzlich zur chiralen Symmetrie auch Translations- und Rotationssymmetrie gebrochen sind, in einem Zwei-Flavor-Nambu–Jona-Lasinio Modell. Das Hauptziel dieser Arbeit ist die Beschreibung der Goldstone Bosonen, masselose Anregungen, die bei spontan gebrochenen Symmetrien auftreten.

Wir arbeiten mit einer der einfachsten möglichen Modulationen, der chiralen Dichtewelle, und zeigen wie man den Quarkpropagator der Theorie analytisch herleitet. Wir wenden dies auf den Testfall der Gapgleichung an.

Wir diskutieren die Herleitung der Nambu-Goldstone Moden der inhomogenen Phase und erhalten, dass für unseren Fall nur drei verschiedene Moden zu betrachten sind. Weiterhin berechnen wir das Goldstone Boson, das mit dem Brechen der räumlichen Symmetrie zusammenhängt, welches mit dem neutralen Pion in Verbindung gebracht werden kann. Mit Hilfe einer Bethe-Salpeter Gleichung zeigen wir, dass wir tatsächlich ein Goldstone Boson gefunden haben und berechnen dessen Dispersionsrelation in Abhängigkeit von Impulsen, senkrecht sowie longitudinal zur Massenmodulation.

Contents

1 Introduction

Since the advent of Quantum Chromodynamics (QCD) [1, 2], the standard model of particle physics has been tried and tested and found to be the most reliable framework available to describe subatomic particles. The discovery of the Higgs boson [3, 4, 5, 6] provides the last cornerstone for an already successful theory. The standard model is capable of describing all known microscopic degrees of freedom and encapsulates three of the four fundamental forces, namely the electromagnetic force, the weak nuclear force and the strong force. Only gravity resists to be integrated into this framework, but since its effects are only relevant at very large scales, it has a negligible effect on the quantum nature of the universe.

The strong interaction is the force with the largest magnitude in the standard model. It is described in an elegant way in Quantum Chromodynamics, which is an $SU(3)$ gauge theory with quarks and gluons as fundamental degrees of freedom. The theory has three color charges, red, green and blue, and anti-colors respectively. The coupling of QCD has a strong dependence on the energy scale, as can be seen in Figure 1.1. This exhibits some of the hallmark features of QCD. At large energies or short distances the coupling is small and quarks can be treated as free particles. This phenomenon is the asymptotic freedom [7, 8], a discovery which was awarded the Nobel prize in 2004. At low energies or large distances the coupling is very strong, which makes the theory inaccessible to perturbative methods, that worked reliably in quantum electrodynamics. One of the most important and probably least understood features of QCD is confinement. In the vacuum only colorless objects can be observed, despite large experimental efforts [9].

This means quarks and gluons can only appear in bound states, the most common are three quarks of different colors forming baryons and a quark and an antiquark forming a meson. More exotic combinations are theoretically possible and there are a number of candidates for bound states of four quarks (tetraquarks, two quarks and two antiquarks) [10, 11] and even five quarks (pentaquarks, four quarks and one antiquark) are believed to have been observed [12]. Another possible state would be the so called glueballs [13, 14], which is a theorized colorless object containing entirely gluons.

Another important feature of QCD is the dynamical chiral symmetry breaking. The Lagrangian of the theory for the light quarks, up and down, approximately fulfills chiral symmetry, but in the vacuum this approximate symmetry is dynamically broken, giving rise to a large chiral condensate. If the symmetry was exact, we would find massless Goldstone bosons, in accordance with the Goldstone theorem [15], which would be massless pions. The fact that pions are very light compared to all other bound states of QCD is a testament for the validity of the approximate symmetry and its spontaneous breakdown. This mechanism generates an effective quark mass, the so called constituent quark mass.

The low energy regime is of particular interest when investigating the phase structure of strong interaction matter. An exemplary plot of the phase diagram is given in Figure 1.2. In its simplest form the phase diagram describes a transition between the phase where quarks and gluons are confined and chiral symmetry is dynamically broken and a phase where the quarks and gluons can appear freely and the chiral symmetry is (approximately) restored, the so called

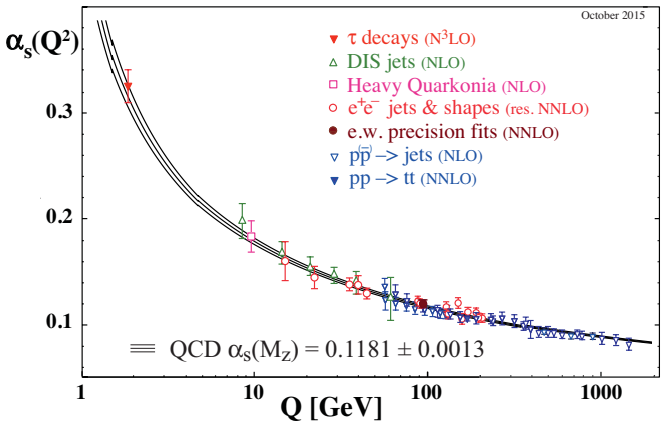

Figure 1.1.: The running coupling of QCD, taken from the particle data group [16].

quark-gluon plasma (QGP). At high temperatures and low densities first principle calculations predict a crossover transition, while for low temperatures and high densities some models show a first-order transition. This claim however can not yet be backed up by first principle calculations or experiments, but should the first-order transition exist it would necessitate a critical end point, after which the crossover occurs. At low temperatures and high densities more exotic phases are expected, like color-superconducting phases.

With the current technology, experimentally as well as theoretically, only the regime of low densities is accessible.

On the theory side lattice gauge theory is a powerful method to solve QCD from first principles, by applying Monte-Carlo methods to the QCD partition function and solving the full theory [17]. The computational effort is enormous and the calculations get more involved with smaller quark masses, which is why only in recent years the computing capacities are available to calculate at realistic quark masses [18]. The introduction of chemical potentials, which would be needed to access the low temperature, high density regime, turns out to be rather difficult. This well known Fermion sign problem [19] states, that the introduction of a finite chemical potential gives rise to a complex part in the Fermion determinant. Since the Fermion determinant is used as probability weight, the method breaks down. There are several efforts to circumvent this problem. Purely imaginary chemical potentials [20, 21] can be used and the hope is, to get a better understanding from these to the real phase structure. Some progress has been made by applying a Taylor expansion in μ/T to the theory [22, 23, 24], but this is of course limited to small ratios. In recent years other methods are being developed, like the complex Langevin [25, 26] method, but while they look promising, no reliable results have been obtained, yet.

On the experimental side large particle colliders are the tool of choice. Especially the Large Hadron Collider (LHC) at CERN in Geneva and the Relativistic Heavy Ion Collider (RHIC) at the Brookhaven National Laboratory in Long Island have delivered outstanding results and have driven our understanding of strong interaction matter considerably. Due to the high energies they are designed to work with, they can only access the high temperature, low density regime, according to the thermal model [27, 28]. Only future facilities, like the Facility for Antiproton and Ion Research (FAIR) in Darmstadt and the Nuclotron-based Ion Collider fAcility (NICA) in Dubna hold the promise to operate at lower energies and might come into the region of the expected first-order phase transition.

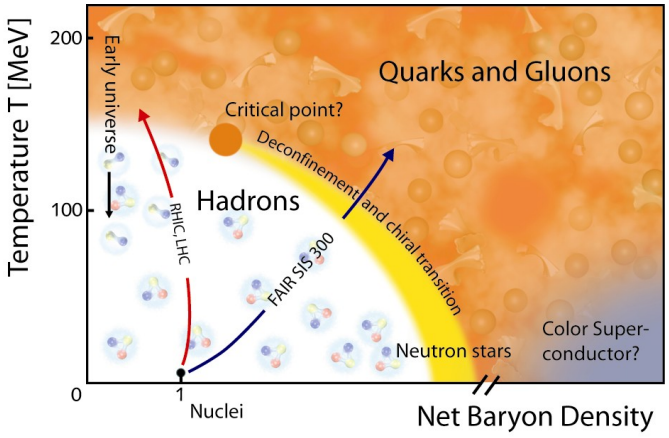

Figure 1.2.: Sketch of the phase diagram of strong interaction matter [38]

So in order to explore the regime of high densities, only model calculations and effective theories are available. These either share only certain symmetries and degrees of freedom with QCD or start from the full theory, but introduce approximations, which are believed to be reasonable, but cannot be controlled from a first principle standpoint.

One promising ansatz are Dyson-Schwinger equations [29, 30, 31], which start from the full theory and expand it in terms of functional derivatives of the source fields. This method is exact, but in practice any Dyson-Schwinger equation depends on higher functional derivatives, which yields an infinite stack of equations. To perform calculations one has to truncate the equation system at some point, which makes for an uncontrolled approximation, because the effect of higher-order equations can in principle be quite large. Another method to tackle QCD is via Functional Renormalization Group methods [32], where one starts from a classical action and integrates out momentum shells, to arrive at the full quantum action of the theory. Some progress on vacuum calculations has been made utilizing this method [33, 34], but again, truncations are needed to obtain results.

Model calculations circumvent some of these problems, but instead mirror only select aspects of QCD. Especially a proper introduction of confinement is difficult in models without gluons and color degrees of freedom. A model that yields good results in the low energy sector is for example the Quark Meson model (QM model), where the forces between quarks are transmitted via the exchange of mesons. In recent years the description of real-time quantities, like spectral functions and transport coefficients, were obtained in a functional renormalization framework with promising results [35, 36, 37].

The model we want to focus on in this thesis is the Nambu–Jona-Lasinio (NJL) model [39, 40], which shares the (approximate) chiral symmetry with QCD. It was conceived before the development of QCD as a hadronic model exhibiting an energy gap, similar to super conductors, but has since been repurposed. Since it is one of the simplest model mirroring the chiral symmetry of QCD it has been used for investigating strong interaction for decades, see for example [41, 42]. In its original form it uses only scalar and pseudo-scalar interactions, but it can be extended with other interaction terms to describe for example vector mesons [43, 44] or color superconductivity [45, 46].

Here we want to use the model to investigate the occurrence of an inhomogeneous phase, a phase where the order parameter, the chiral condensate, varies periodically in space, resembling

a crystal. This behavior is well known in the context of (color-) superconductors and pion condensates. The concept of an inhomogeneous ground state was first brought up by Overhauser in the context of density waves in nuclear matter [47] and later for super conductors by Fulde and Ferell [48] and Larkin and Ovchinnikov for sinusoidal modulations [49]. In lower dimensional models, such as the 1+1 dimensional Gross-Neveu model [50] and the NJL_2 model analytical solutions have been found, showing it to be the true ground state [51]. Those solutions were brought to the 3+1 dimensional NJL model some years ago [52] and have been heavily investigated since, see [53] for a review.

These studies show, that the first-order phase transition from the homogeneous model is completely covered by the inhomogeneous phase and the critical point is replaced by a Lifschitz point [54], when considering a standard NJL model. The occurrence of an inhomogeneous phase is quite stable against different model extensions. The inclusion of vector interactions [55, 56] and the extension to isospin asymmetric matter [57] show a robust inhomogeneous phase for a reasonable range of parameters. There have also been advances to include spatially modulated condensates in more sophisticated models, like the Quark-Meson model [58] and Dyson-Schwinger equations [59], where the inhomogeneous phase appears as well.

Most modern studies of inhomogeneous strong interaction matter use only one-dimensional modulations, for a work on two-dimensional order parameters see [60], since higher dimensional modulations increase the computational cost tremendously. From condensed matter physics it is known however, that one-dimensional crystals are unstable against thermal fluctuations, a property known as Landau-Peierls instability [61]. The thermal fluctuations are not taken into account in most works, which explains the apparent stability of one-dimensional modulations. The few exceptions [62, 63] work in a Ginzburg-Landau approach, which is only valid close to the homogeneous critical point, where a loss of the long-range order was found. This loss is due to the occurrence of phonons, quasiparticles related to the spontaneous breaking of rotational and translational symmetries and act as a massless Goldstone mode. In condensed matter physics, phonons are associated with vibrations of crystal layers.

In order to better understand the properties of the inhomogeneous phase and the influence of thermal fluctuations at lower temperatures, studies in the full model are needed. In this work we want to investigate the Goldstone modes appearing through the breaking of rotational and translational symmetry in the inhomogeneous phase and the occurrence of mesons, such as the sigma meson and the pion.

Structure of this thesis

After this introductional chapter we proceed to give a more in depth overview of Quantum Chromodynamics in Chapter 2, before we introduce our model and give an overview over relevant derivations and results that are of importance to our work in Chapter 3. In Chapter 4 we will develop a formalism to derive propagators analytically in the inhomogeneous phase for a certain modulation of the mass function. Afterwards we give a description of the relevant Goldstone modes directly from the symmetries of the model in Chapter 5. We will show how to derive a Bethe-Salpeter equation to describe mesonic degrees of freedom in Chapter 6, where we will go thoroughly through the calculations needed to describe sigma meson and uncharged pion, which doubles as a Goldstone mode. We will conclude this thesis by summarizing our findings and give an outlook for further interesting research in Chapter 7.

2 Quantum Chromodynamics

In this chapter we review some of the important properties of QCD and its symmetries.

2.1 QCD Basics

Quantum Chromodynamics is the fundamental quantum field theory of strong interactions. It describes quarks, which each have six different flavors, spin, electric and color charge. The force is transmitted by eight gluons, which carry spin and color. QCD is a non-abelian $SU(3)$ gauge theory, obeying locality, local gauge symmetry, renormalizability and Poincaré invariance. This leads to the QCD Lagrangian

$$\mathcal{L}_{QCD} = \overline{\psi}\left(i\gamma^{\mu}D_{\mu} - \hat{m}\right)\psi - \frac{1}{4}F^{a}_{\mu\nu}F^{\mu\nu}_{a}. \tag{2.1}$$

In the first part, the Dirac part, ψ and $\overline{\psi} = \psi^{\dagger}\gamma_0$ describe the quark fields, which are spinors with four Dirac, $N_f = 6$ flavor and $N_c = 3$ color components. $\hat{m}$ is a diagonal $N_f \times N_f$-dimensional matrix of the bare masses generated by the Higgs mechanism and the covariant derivative is given by

$$D_{\mu} = \partial_{\mu} + igA^{a}_{\mu}\frac{\lambda_a}{2}, \tag{2.2}$$

with the strong coupling constant g, the gluon field A^{a}_{μ} and the Gell-Mann matrices λ_a, describing the a-th generator of $SU(3)$. The second part of Equation 2.1 contains the field strength tensor

$$F^{a}_{\mu\nu} = \partial_{\mu}A^{a}_{\nu} - \partial_{\nu}A^{a}_{\mu} - gf^{abc}A^{b}_{\mu}A^{c}_{\nu}, \tag{2.3}$$

with the totally anti-symmetric structure constant f^{abc} defined by

$$if^{abc}\lambda^{c} = [\lambda^{a}, \lambda^{b}]. \tag{2.4}$$

It describes the kinetics of the gluons and the gluon self interaction. These self interactions are an important feature of QCD that is in contrast to QED, where photons can not interact with each other, and is responsible for the non-abelian nature of the theory.

The masses of the differently flavored quarks are distinct, from the two lightest flavors, up and down quarks with only a few MeV, ranging up to 173 GeV for the top quark [16].

As already indicated in the last chapter, the QCD coupling constant is energy dependent, see Figure 1.1, where α_S relates to g via the relation $g^2 = 4\pi\alpha_S$. This leads to asymptotic freedom, the effect that quarks behave as free particles at very high energies or very short distances. At low energies however, this leads to the need of a non-perturbative treatment of the theory.

2.2 Symmetries in QCD

The Lagrangian exhibits certain symmetries. It is invariant under local $SU_C(3)$ gauge transformations

$$\psi(x) \to U(x)\psi(x), \tag{2.5}$$

$$F_{\mu\nu} \to U(x)F_{\mu\nu}U^\dagger(x), \tag{2.6}$$

$$A_\mu \to U(x)\left(A_\mu(x) - \frac{i}{g}\partial_\mu\right)U^\dagger(x), \tag{2.7}$$

with the transformation matrix

$$U(x) = \exp\left\{\frac{i}{2}\alpha^a(x)\lambda_a\right\}, \tag{2.8}$$

where $\alpha^a(x)$ is a real valued rotation angle.

Of particular interest for us is the *chiral symmetry*, which is only an approximate symmetry. We regard the two flavor case, where only up and down quarks contribute to the Lagrangian. Since their masses are much lower than the masses of the other quark flavors, we can reasonably focus on only these two. If we take the two masses to be equal, the QCD Lagrangian is invariant under the transformations

$$\psi \to \exp\{-i\alpha_a\tau_a\}\psi, \qquad \overline{\psi} \to \exp\{i\alpha_a\tau_a\}\overline{\psi}, \tag{2.9}$$

with a real angle α_a and the Pauli matrices τ_a in isospin space. This is an $SU_V(2)$ symmetry, which is called isospin symmetry. If we furthermore demand the quark masses to be zero, the so called *chiral limit*, we find the additional symmetry

$$\psi \to \exp\{-i\alpha_a\gamma_5\tau_a\}\psi, \qquad \overline{\psi} \to \exp\{-i\alpha_a\gamma_5\tau_a\}\overline{\psi}. \tag{2.10}$$

This is an axial symmetry, $SU_A(2)$ [1]. Combined those two symmetries can be written as

$$SU_V(2) \otimes SU_A(2) \simeq SU_R(2) \otimes SU_L(2), \tag{2.11}$$

the chiral symmetry. In the QCD vacuum, the chiral symmetry is spontaneously broken, to the $SU_V(2)$, by a finite chiral condensate $\langle\overline{\psi}\psi\rangle$ which acts as an order parameter. According to the Goldstone theorem [64, 15], a spontaneously broken continuous symmetry leads to the appearance of a massless mode, which in case of QCD in the chiral limit, are the pions.

Chiral symmetry is only an approximate symmetry, hence the finite pion mass. But since the up and down quark masses are much smaller than the characteristic scale of QCD, $m_{u,d} \ll \Lambda_{QCD}$, it is a reasonable approximation, which is further supported by the fact, that the pions are very light compared to all other hadrons.

At high temperatures or high densities the chiral symmetry is (approximately) restored and the chiral condensate is small.

In addition the QCD Lagrangian is invariant under a global $U_V(1)$ transformation

$$\psi \to \exp\{-i\alpha\}\psi, \qquad \alpha \in \mathbb{R}, \tag{2.12}$$

which corresponds to conservation of baryon number.

We will see the same chiral symmetry in our model in the next chapter, which allows us to make qualitative predictions of what might occur in the full QCD.

[1] Strictly speaking this is not a group, since it is not closed. The combination with the $SU_V(2)$ however constitutes a group.

3 The Nambu–Jona-Lasinio Model

The calculations in this work are done in the Nambu–Jona-Lasinio model [39, 40]. In this chapter we go over some of the known properties of the model.

We will start by giving a general overview of the features of the model, independent of any assumptions we make in later sections.

We will continue by deriving the homogeneous solutions for the constituent quark mass and introduce mesons into the model. Since the expressions for the inhomogeneous mesons get quite complicated, but behave similar in lots of ways, this will give a more understandable outline for the procedure in the next chapters.

Afterwards, we will introduce inhomogeneous condensates and review some of the features of the inhomogeneous phase. We will discuss this via the formalism introduced in previous works, were the diagonalization of the Hamiltonian is a key aspect, for a more comprehensive review see [65].

We will conclude by a discussion of different regularization techniques and the choice of parameters in this work.

3.1 The Lagrangian of the Model and its Features

We start from the Lagrangian of the NJL model for two flavors

$$\mathcal{L}_{NJL} = \overline{\psi}\left(i\partial\!\!\!/ - \underline{m}\right)\psi + G_S\left[\left(\overline{\psi}\psi\right)^2 + \left(\overline{\psi}i\gamma_5\tau^a\psi\right)^2\right], \tag{3.1}$$

where ψ and $\overline{\psi}$ describe the quark fields, $\underline{m} = \mathrm{diag}(m_u, m_d)$ is the diagonal matrix of the bare quark masses for up and down quarks and G_S is the coupling constant for both interaction parts. The interaction is a four-point interaction with a scalar $\Gamma_\sigma = \mathbb{1}$ and three pseudo-scalar channels $\Gamma_\pi^a = i\gamma_5\tau^a$. In the course of this thesis we will mostly consider diagonal contributions in flavor space, so it is useful to define $\Gamma_\pi := \Gamma_\pi^3 = i\gamma_5\tau^3$.

This Lagrangian shares symmetries with the QCD Lagrangian, namely the approximate chiral symmetry. In the same limits, equal bare quark masses for $SU_V(2)$ and vanishing bare quark masses for $SU_A(2)$, we obtain the chiral symmetry $SU_L(2) \otimes SU_R(2)$ as we did in the previous chapter. Furthermore it exhibits the $U_V(1)$ symmetry of QCD.

Due to the four-point interaction and the resulting dimensionful coupling constant, the model is not renormalizable. We have to apply a regularization scheme to treat the occurring divergences in the integrals. The parameters of this regularization will be fitted to vacuum observables, but they will still influence the results of the model. We will discuss different regularization schemes in a later section.

Nonetheless the NJL model is a valuable tool, since it is a relatively simple model sharing chiral symmetry with QCD and can give qualitative insights into the theory of strong interactions.

3.2 Homogeneous NJL Model

In the homogeneous phase we assume that all observables are space-time independent. We will discuss this in the context of the gap equation, which will give us a self-consistent result for the constituent quark mass. Afterwards we will introduce the formalism to include two-body excitations in the model and give results for the sigma-meson and pion masses.

3.2.1 Gap Equation

In this formalism we deal with the theory in terms of propagators. The propagator from the free theory is given in the standard way

$$iS_0(p) = i\frac{\not{p} + m}{p^2 - m^2 + i\epsilon} \tag{3.2}$$

and can be found in any text book on quantum field theory.

To include the interactions of the NJL Lagrangian, we derive dressed values from the Dyson equation in Hartree approximation

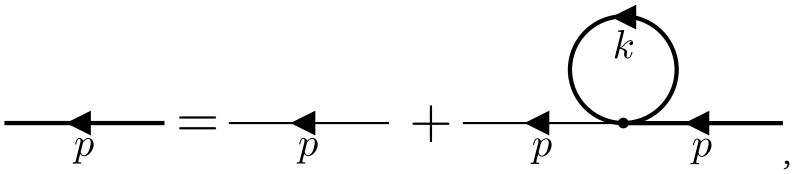

, (3.3)

where thin lines represent the bare propagators, Equation (3.2), and thick lines represent dressed propagators

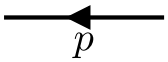

$$= iS(p) = i\frac{\not{p} + M}{p^2 - M^2 + i\epsilon}, \tag{3.4}$$

where M represents the *constituent quark mass*, the effective mass of a quark. As we will see later, this mass corresponds to the *chiral condensate* $\langle\overline{\psi}\psi\rangle$ and will serve as an order parameter for chiral symmetry breaking. In accordance with the Feynman rules for fermions we have to integrate and trace over the loop in Equation (3.3).

This way of deriving the constituent quark mass is referred to as the Hartree (-Fock) equation [1] or the gap equation and is equivalent to the mean-field approximation, which we will emphasize in the next section.

The diagrammatic equation (3.3) can be written as

$$iS(p) = iS_0(p) + iS_0(p)(-i\Sigma)iS(p), \tag{3.5}$$

[1] Although in the literature this is often described as the Hartree-Fock approximation, in the form presented here the Fock term, an additional exchange term, is omitted. This can be done, because this term only gives an offset to the coupling constant, which we can get rid off by a redefinition of the coupling constant.

with the self-energy

$$-i\Sigma = \quad . \tag{3.6}$$

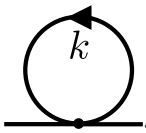

Multiplying Equation (3.5) with $S^{-1}(p) = \not{p} - M$ from the right and $S_0^{-1}(p) = \not{p} - m$ from the left yields after some rearranging

$$iS^{-1}(p) = iS_0^{-1}(p) - i\Sigma, \tag{3.7}$$

which inserting the explicit expression gives the conditional equation for M

$$M = m + \Sigma, \tag{3.8}$$

where we should note, that Σ is in itself dependent on M.

The self-energy can be determined by evaluating the loop

$$-i\Sigma = -i\sum_N \Sigma_N = \sum_N 2iG_N\Gamma_N \int \frac{d^4k}{(2\pi)^4}\,(-\mathrm{Tr}\,[\Gamma_N iS(k)]) \tag{3.9}$$

$$\Rightarrow \qquad \Sigma = \sum_N 2G_N\Gamma_N \int \frac{d^4k}{(2\pi)^4}\,\mathrm{Tr}\,[\Gamma_N iS(k)]\,. \tag{3.10}$$

We have to sum over all possible interactions, which in our case, after neglecting non-diagonal flavor contributions, are just the two Γ_σ and Γ_π. In explicit form this reads

$$\Sigma = 2G_S\left(i\mathbb{1}\int \frac{d^4k}{(2\pi)^4}\,\mathrm{Tr}\,[\mathbb{1}S(k)] - i\gamma_5\tau^3\int \frac{d^4k}{(2\pi)^4}\,\mathrm{Tr}\left[\gamma_5\tau^3 S(k)\right]\right), \tag{3.11}$$

where we note that the second trace vanishes, due to the trace over a single Pauli matrix.

We can calculate the first trace

$$2iG_S\int \frac{d^4k}{(2\pi)^4}\,\mathrm{Tr}\,[\mathbb{1}S(k)] = 2iG_S\int \frac{d^4k}{(2\pi)^4}\,\mathrm{Tr}\left[\frac{\not{k}+M}{k^2-M^2+i\epsilon}\right] \tag{3.12}$$

$$= 8N_fN_cG_S\,i\int \frac{d^4k}{(2\pi)^4}\,\frac{M}{k^2-M^2+i\epsilon}. \tag{3.13}$$

To solve this integral for finite temperatures T and finite chemical potentials μ, we introduce the Matsubara formalism, also known as the imaginary time formalism. This method uses the similarities between the expectation value of an operator in a quantum statistical thermal ensemble

$$\langle\mathcal{O}\rangle = \frac{\mathrm{Tr}\,(\mathcal{O}\exp(-\beta H))}{\mathrm{Tr}(\exp(-\beta H))}, \qquad \beta = \frac{1}{T} \tag{3.14}$$

and the quantum field theory expectation value at imaginary time $\tau = it$, see for example [66] for more details. For our practical calculations, this leads to a transformation of the four-momentum integral of the form

$$i\int \frac{d^4k}{(2\pi)^4} f(k_0,\vec{k}) \to -T\sum_{m=-\infty}^{\infty}\int \frac{d^3k}{(2\pi)^3} f(i\omega_m+\mu,\vec{k}), \tag{3.15}$$

with fermionic *Matsubara frequencies*

$$i\omega_m = (2m+1)\pi i T, \qquad m\in\mathbb{Z}. \tag{3.16}$$

In the self-energy this reads

$$\Sigma = -8N_fN_cG_ST\sum_m\int \frac{d^3k}{(2\pi)^3}\frac{M}{(i\omega_m+\mu)^2-\vec{k}^2-M^2} \tag{3.17}$$

$$= -8N_fN_cG_ST\sum_m\int \frac{d^3k}{(2\pi)^3}\frac{M}{(i\omega_m+\mu)^2-E_k^2}, \tag{3.18}$$

where in the second step we defined the homogeneous energy eigenvalues

$$E_k = \sqrt{\vec{k}^2+M^2}. \tag{3.19}$$

We can perform the Matsubara sum analytically, see Appendix B.1, and find

$$\Sigma = 8N_fN_cG_SM\int \frac{d^3k}{(2\pi)^3}\left(\frac{1}{2E_k}-\frac{1}{2E_k}[n_F(E_k-\mu)+n_F(E_k+\mu)]\right), \tag{3.20}$$

with Fermi distributions for quarks and antiquarks

$$n_F(z) = \left[1+\exp\left(\frac{z}{T}\right)\right]^{-1}. \tag{3.21}$$

The first summand in this integral is divergent and we have to apply a regularization scheme, which we will discuss later in this chapter.

Overall we arrive at the gap equation for M

$$M = m-8N_fN_cG_SM\int \frac{d^3k}{(2\pi)^3}\left(\frac{1}{2E_k}-\frac{1}{2E_k}[n_F(E_k-\mu)+n_F(E_k+\mu)]\right). \tag{3.22}$$

The integrals have to be solved numerically. This equation can have more than one solution. To determine the energetically preferred one we have to solve for the grand potential, the derivation of which we will not do here, but discuss for the inhomogeneous ansatz in the next section in greater detail and also give the homogeneous limit there.

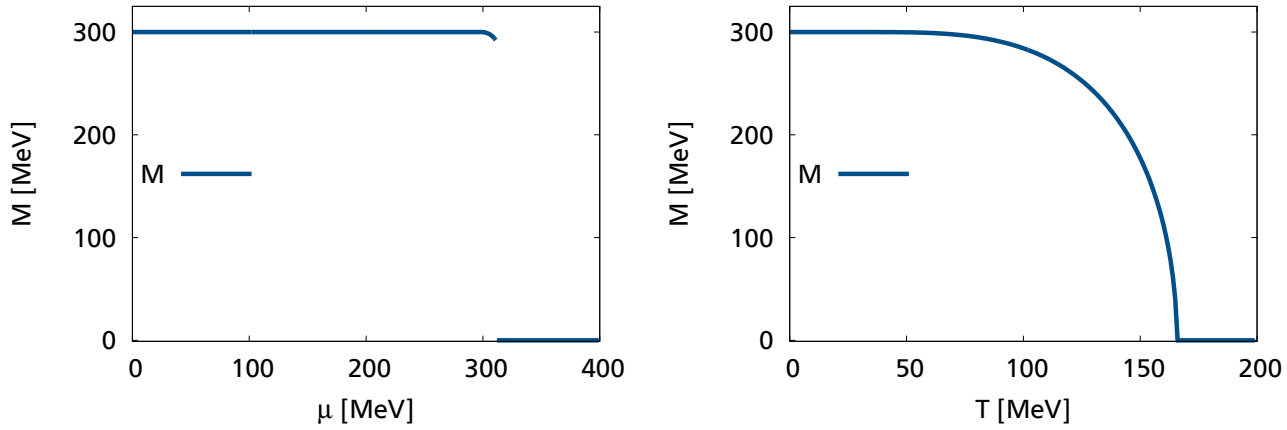

Figure 3.1.: Homogeneous results for the constituent quark mass, as a function of μ for vanishing temperature (left) and as a function of T for vanishing chemical potential (right).

Results

With the formalism largely in place, we will discuss the homogeneous results for the constituent quark mass here.

We apply the regularization scheme described in Section 3.4 and should note here that all calculations are done in the chiral limit ($m = 0$).

In Figure 3.1 we have plotted the resulting constituent quark masses obtained from Equation (3.22). Again in the region where there is more than one solution, the energetically preferred one has been chosen. On the left, where the temperature is vanishing, we show M as a function of chemical potential, we see the constituent quark mass stays constant below a chemical potential equal to the constituent mass in the vacuum ($\mu < M_{vac}$). This property is known as the Silverblaze property [67], which states that the mass cannot change until the energy density is non-zero. Beyond this point in chemical potential, the mass decreases before it drops to zero at $\mu_{crit.} = 312$ MeV. This is the *chiral restoration phase transition*, since, as already discussed, M acts as an order parameter. Here it is a clear first-order transition, indicated by the discontinuity in the order parameter. Since we operate in the chiral limit, after the phase transition M is exactly zero.

If we consider vanishing chemical potential instead and look at the constituent mass along the temperature axis as shown on the right side of Figure 3.1, we see, that this sharp transition is not visible here. Instead we find a much smoother decrease in M until it reaches 0 at a critical temperature $T_{crit.} = 166$ MeV. The transition is continuous, but not continuous differentiable, with respect to the first derivative in T, which indicates a second-order phase transition. This is again a feature of the chiral limit, were we to include a finite bare quark mass, we would find a crossover instead of a phase transition. The first-order transition at low temperatures would persist.

We can combine the results into an overview of the phase structure, as shown in the phase diagram in Figure 3.2. Here the dashed line indicates a phase transition of second order, while the solid line indicates a first-order phase transition. The tricritical point is marked by the red dot and it is located at $T_{CEP} = 75$ MeV and $\mu_{CEP} = 267$ MeV.

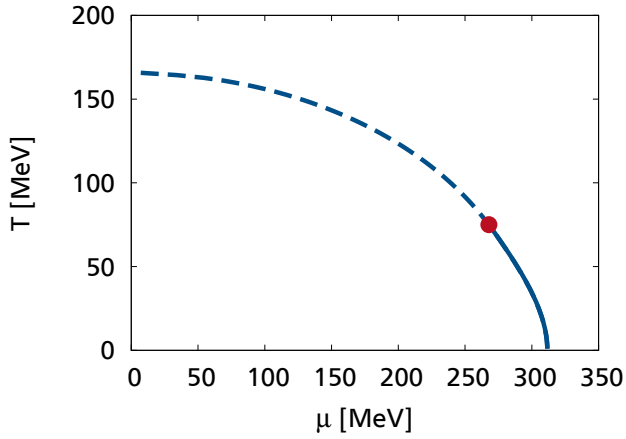

Figure 3.2.: Phase diagram of the homogeneous NJL model, depicted as function of μ and T. The solid line indicates a first order phase transition and the dashed line indicates a second order phase transition. The dot marks the tricritical point.

3.2.2 Bethe-Salpeter Equation and Mesons

In the NJL model one can explain mesons as collective excitations, despite the lack of confinement. To do this we use the *Bethe-Salpeter equation* (BSE) [68], which allows the description of two-body bound states. In random phase approximation the BSE reads

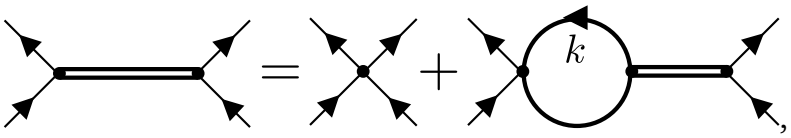

(3.23)

which is a resummation of the form

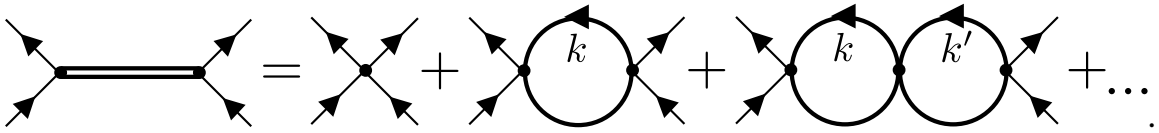

(3.24)

The left hand side is the scattering matrix $\hat{T}$, which we will interpret as the meson later on. We can write the diagrammatic equation (3.23) in explicit form as

$$i\hat{T} = i\hat{K} + i\hat{K}\left(-i\hat{J}\right)i\hat{T}, \tag{3.25}$$

with the bare scattering kernel

$$\hat{K} = \Gamma_{M'} K_{M'M} \Gamma_M = \Gamma_{M'} 2G_S \delta_{M'M} \Gamma_M \tag{3.26}$$

and the polarization loop $\hat{J}$. We separate the external vertices from the polarization loop and write

$$J_{M'M} = \Gamma_{M'} \hat{J} \Gamma_M. \tag{3.27}$$

We write the scattering matrix as

$$\hat{T} = -\Gamma_{M'} D_{M'M} \Gamma_M, \tag{3.28}$$

where $D_{M'M}$ acts as a meson propagator.

We can calculate the polarization loop for $M, M' \in \{\sigma, \pi\}$

$$-iJ_{M'M}(p) = \tag{3.29}$$

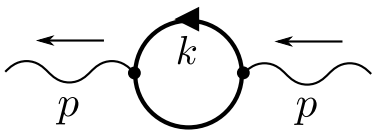

$$= \int \frac{d^4k}{(2\pi)^4} \operatorname{Tr}\left[\Gamma_{M'} S(k+p) \Gamma_M S(k)\right]. \tag{3.30}$$

From evaluating the traces, we see that for our vertices, no mixing of different flavors occurs. This means we can write all equations with a single flavor index M. We can rewrite the BSE as

$$-D_M = 2G_S - 2G_S J_M D_M. \tag{3.31}$$

We can solve this equation for D_M

$$D_M(p) = -2G_S \left[1 - 2G_S J_M(p)\right]^{-1}. \tag{3.32}$$

The calculations for the polarization loop can be found in Appendix B.2.1 and we end up with

$$J_\sigma(i\omega_m, \vec{p}) = 4N_f N_c i I_1 - 2N_f N_c ((i\omega_m)^2 - \vec{p}^2 - 4M^2) i I_2(i\omega_m, \vec{p}), \tag{3.33}$$

$$J_\pi(i\omega_m, \vec{p}) = 4N_f N_c i I_1 - 2N_f N_c ((i\omega_m)^2 - \vec{p}^2) i I_2(i\omega_m, \vec{p}), \tag{3.34}$$

where $i\omega_m = 2\pi i m T$ are bosonic Matsubara frequencies and the integrals are given by

$$iI_1 = T \sum_n \int \frac{d^3k}{(2\pi)^3} \frac{1}{(i\omega_n + \mu)^2 - \vec{k}^2 - M^2}, \tag{3.35}$$

$$iI_2(i\omega_m, \vec{p}) = -T \sum_n \int \frac{d^3k}{(2\pi)^3} \frac{1}{\left[(i\omega_n + \mu)^2 - \vec{k}^2 - M^2\right]\left[(i\omega_n + i\omega_m + \mu)^2 - (\vec{k} + \vec{p})^2 - M^2\right]}, \tag{3.36}$$

with $i\omega_n$ the fermionic Matsubara frequencies and the integral iI_1, that we have already solved in Section 3.2.1. For the integral iI_2 we refer to Appendix B.2.2.

To give the masses of the sigma-meson and pion, we use the pole approximation, where we assume

$$D_M^+(p_0, \vec{p}) \approx \frac{g_{Mqq}^2}{p_0^2 - \vec{p}^2 - m_M^2}, \tag{3.37}$$

with the coupling of the meson to two quarks g_{Mqq} and the mass of the meson m_M. We have to treat p_0 and $\vec{p}$ separately, since the medium breaks Lorentz invariance. In practice we will search for the poles in Equation (3.32) and determine the mass as the solution of the equation

$$1 - 2G_S \operatorname{Re}\left(J_M^+\left(p_0 = \pm\sqrt{m_M^2 - \vec{p}^2}, \vec{p}\right)\right) \stackrel{!}{=} 0. \tag{3.38}$$

We will give the results in the next section.

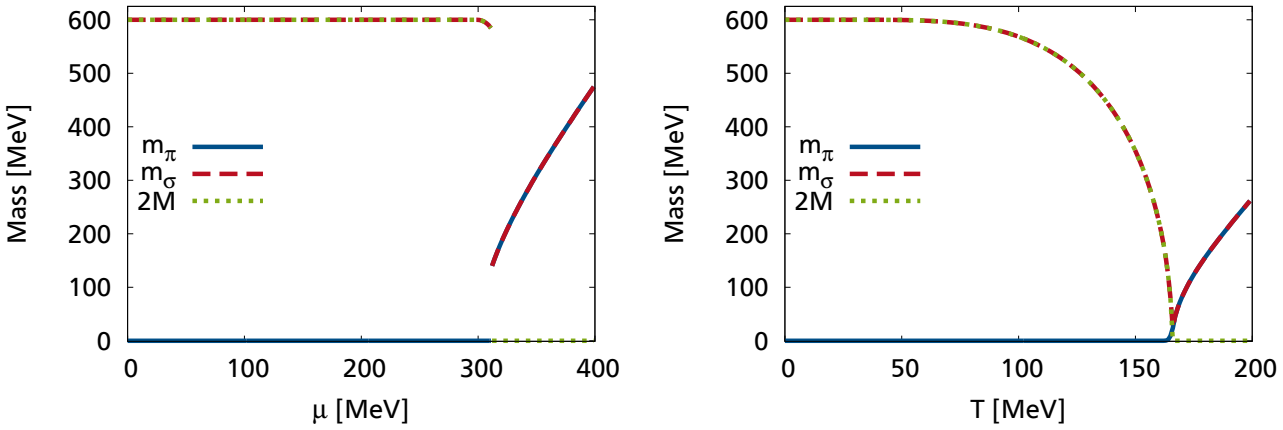

Figure 3.3.: Masses of the mesons and twice the constituent quark mass as a function of chemical potential (left) and temperature (right), both at vanishing external three-momentum.

Results

With the formalism laid out we can calculate the masses of the sigma-meson and the pion in pole approximation. In Figure 3.3 we see that both as a function of chemical potential and as a function of temperature the pion mass vanishes in the region where the chiral symmetry is broken. This is to be expected, since the pions act as Goldstone bosons of the spontaneously broken chiral symmetry. In addition we can show this analytically, with the result from Equation (3.22) and by entering Equation (3.34) into Equation (3.38) and calculate that for any non-trivial solution of the gap equation $p_0^2 = \vec{p}^2$ fulfills the condition, as the prefactor of iI_2 lets the second part vanish. The mass of the sigma-meson is always twice the constituent quark mass in the broken phase, which is visible from a similar argument as for the pion.

At the phase transition to the chirally restored phase, the sigma mass drops to zero as does the constituent quark mass. In the restored phase itself, the two meson masses are degenerate and finite. The former is also obvious, since the polarization loops for both mesons, Equations (3.33) and (3.34) are the same if the constituent quark mass is zero. The different order of the phase transition for finite temperature and finite chemical potentials respectively is also visible from Figure 3.3, the same discontinuities we saw in the constituent quark mass are reflected in the meson masses as well.

In Figure 3.4, we show the dispersion relation for both sigma-meson and pion. In the broken phase (left), the masses remain unchanged with increasing three momentum, while in the restored phase (right) we see both masses remaining degenerate and falling with increasing external three momentum.

3.3 Inhomogeneous NJL model

To present the inhomogeneous phase in this section we take a similar approach to other works, see for example [52, 65]. We will derive the grand potential as the central quantity that enables us to calculate all thermodynamic observables and determine solutions to the gap equation from stationary conditions in the potential. This formalism is used widely, but has his limitations.

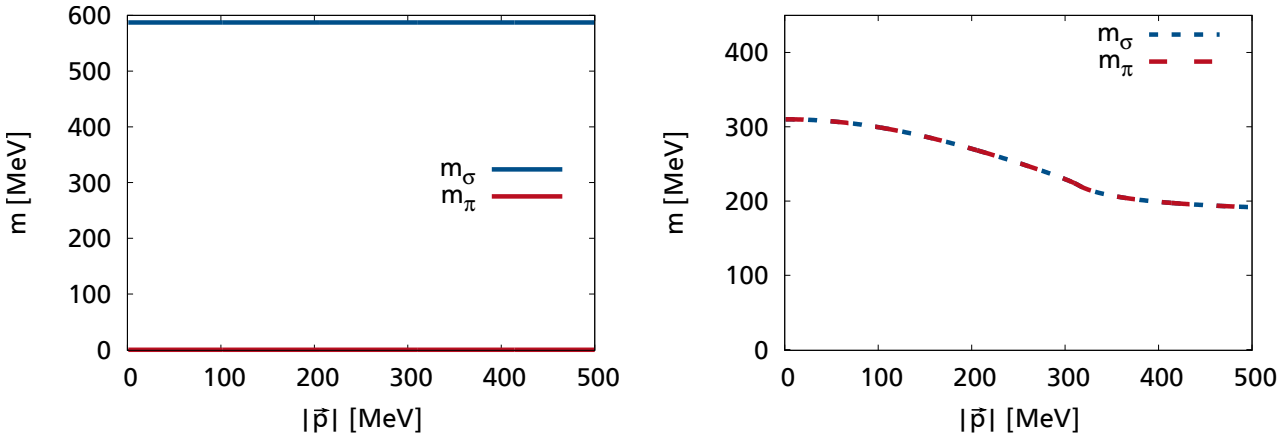

Figure 3.4.: Dispersion relations for the mesons in the broken phase at $\mu = 310$ MeV (left) and in the restored phase $\mu = 350$ MeV (right).

To calculate meson properties, as we did in the last section, we need an expression for the propagators of the theory, which cannot be obtained from the grand potential. Nonetheless the grand potential is an important quantity and it is needed for example to determine the favored solution of the gap equation, where multiple solutions are possible.

We start from the mean-field approximation, which is equivalent to the Hartree-Fock approximation we used in the previous section. Central here are the expectation values of the interaction terms of our model Lagrangian (3.1)

$$S(x) = \langle\overline{\psi}\psi\rangle, \qquad P_a(x) = \langle\overline{\psi}i\gamma_5\tau_a\psi\rangle. \tag{3.39}$$

These expectation values can in principle be space, as well as time dependent. Now we expand the fields around their expectation values, with fluctuations δS and δP_a

$$\overline{\psi}\psi = S(x) + \delta S, \qquad \overline{\psi}i\gamma_5\tau_a\psi = P_a(x) + \delta P_a. \tag{3.40}$$

Up to now this is exact and would remain so if we treated S and P as auxiliary fields, similar to a Hubbard-Stratonovich transformation [69, 70]. The approximation happens in the next step, where we look at the interaction terms of the Lagrangian and neglect quadratic contributions from the fluctuations

$$\left(\overline{\psi}\psi\right)^2 \approx -S^2(x) + 2S(x)\overline{\psi}\psi, \tag{3.41}$$

$$\left(\overline{\psi}i\gamma_5\tau_a\psi\right)^2 \approx -P_a^2(x) + 2P_a(x)\overline{\psi}i\gamma_5\tau^a\psi. \tag{3.42}$$

In the rest of this section we will focus only on spatially modulated condensates and not take into account the possible time dependence. In addition we will only consider diagonal contributions in flavor space, so that the expectation values simplify to $S(x) = S(\vec{x})$ and $P_a(x) = P(\vec{x})\delta_{a3}$.

Making these replacements in the interaction terms of the Lagrangian, yields the mean-field Lagrangian

$$\mathcal{L}_{MF} = \overline{\psi}\mathcal{S}^{-1}\psi - \mathcal{V}, \tag{3.43}$$

with the abbreviations

$$\mathcal{S}^{-1} = i\partial\!\!\!/ - m + 2G_S\left[S(\vec{x}) + i\gamma_5\tau_3 P(\vec{x})\right], \tag{3.44}$$

$$\mathcal{V} = G_S\left(S^2(\vec{x}) + P^2(\vec{x})\right). \tag{3.45}$$

The first part is the inverse propagator and the second part is a potential.

The grand potential per volume is given by

$$\Omega = -\frac{T}{V}\log\mathcal{Z}, \tag{3.46}$$

with temperature T, volume V and the partition function $\mathcal{Z}$ given in the path integral formalism

$$\mathcal{Z}_{MF} = \int \mathcal{D}\overline{\psi}\int \mathcal{D}\psi \exp\left\{\int_{[0,1/T]\times V} d^4x_E\,\left(\mathcal{L}_{MF} + \mu\psi^\dagger\psi\right)\right\}, \tag{3.47}$$

where we have to integrate over Euclidean space-time in the exponent.

Thanks to the mean-field approximation, the exponent of the partition function is bi-linear in the fields and we can perform the path integral, which yields for the grand potential

$$\Omega_{MF} = -\frac{T}{V}\mathrm{Tr}\log\left(\frac{\mathcal{S}^{-1}}{T}\right) + \frac{T}{V}\int_{[0,1/T]\times V} d^4x_E\,\mathcal{V}. \tag{3.48}$$

This lends itself to the definition of a kinetic and a condensate (potential) part of the grand potential

$$\Omega_{kin} = -\frac{T}{V}\mathrm{Tr}\log\left(\frac{\mathcal{S}^{-1}}{T}\right), \tag{3.49}$$

$$\Omega_{cond} = \frac{T}{V}\int_{[0,1/T]\times V} d^4x_E\,\mathcal{V}, \tag{3.50}$$

$$\Omega_{MF} = \Omega_{kin} + \Omega_{cond}, \tag{3.51}$$

where the trace in the kinetic part is over Euclidean space-time, Dirac, color and flavor space.

In order to proceed, we write the inverse propagator as

$$\mathcal{S}^{-1} = \gamma^0\left(i\partial_0 - \mathcal{H}(\vec{x})\right), \tag{3.52}$$

with the Dirac-Hamilton operator of the theory

$$\mathcal{H}(\vec{x}) = \gamma_0\left(-i\gamma_k\partial^k + m - 2G_S\left[S(\vec{x}) + i\gamma_5\tau_3 P(\vec{x})\right]\right). \tag{3.53}$$

With the time derivatives separated, employing the Matsubara formalism again, we can write the kinetic part of the grand potential as a function of the eigenvalues E_ν of the Hamiltonian

$$\Omega_{kin} = -\frac{1}{V}\sum_\nu\left(\frac{E_\nu - \mu}{2} + T\log\left[1 + \exp\left\{\frac{-E_\nu - \mu}{T}\right\}\right]\right) \tag{3.54}$$

We can decompose this Hamiltonian in its flavor components, where the two expressions only differ in a sign stemming from τ_3

$$\mathcal{H} = \mathcal{H}_+ \otimes \mathcal{H}_-, \tag{3.55}$$

$$\mathcal{H}_\pm = \gamma_0\left(-i\gamma_k\partial^k + m - 2G_S\left[S(\vec{x}) \pm i\gamma_5 P(\vec{x})\right]\right). \tag{3.56}$$

Due to isospin symmetry, those two Hamiltonians have the same eigenvalues, which allows us to treat only one of them. Here we take without loss of generality $\mathcal{H}_+$, and we pick up a factor $N_f = 2$ in front of the overall expression.

Now we introduce a mass function

$$M(\vec{x}) = m - 2G_S\left[S(\vec{x}) + iP(\vec{x})\right], \tag{3.57}$$

which allows us to write the Hamiltonian in chiral representation of the Dirac matrices as

$$\mathcal{H}_+(\vec{x}) = \begin{pmatrix} i\sigma_k\partial^k & M(\vec{x}) \\ M^*(\vec{x}) & -i\sigma_k\partial^k \end{pmatrix}. \tag{3.58}$$

The potential part can then be written as

$$\mathcal{V} = \frac{|M(\vec{x}) - m|^2}{4G_S}. \tag{3.59}$$

We will focus only on periodical modulations as mass functions

$$M(\vec{x}) = M(\vec{x} + \vec{n}_i), \qquad i = 1, 2, 3, \tag{3.60}$$

which allows a Fourier decomposition of the form

$$M(\vec{x}) = \sum_{\vec{q}_k} M_{\vec{q}_k} e^{i\vec{q}_k\vec{x}}. \tag{3.61}$$

Analogous to condensed matter physics, the vectors $\vec{n}_i$ span the unit cell of a crystal and the vectors $\vec{q}_k$ are the components of the reciprocal lattice, which we will call wave vectors. In principle there are infinitely many wave vectors possible, we can however define a basis of the reciprocal lattice with just three vectors

$$\vec{b}_i = \epsilon_{ijk}\frac{\vec{n}_j \times \vec{n}_k}{\vec{n}_i \cdot (\vec{n}_j \times \vec{n}_k)}. \tag{3.62}$$

In order to get the eigenvalues of the Hamiltonian we perform a Fourier decomposition, with the definition described in Appendix A.3

$$\mathcal{H}_{\vec{p}_m,\vec{p}_{m'}} = \int d^3x e^{-i\vec{p}_m\vec{x}}\mathcal{H}_+(\vec{x})e^{i\vec{p}_{m'}\vec{x}} \tag{3.63}$$

$$= \begin{pmatrix} -\vec{\sigma}\vec{p}_m\delta_{\vec{p}_m,\vec{p}_{m'}} & \sum_{\vec{q}_k} M_{\vec{q}_k}\delta_{\vec{p}_m,\vec{p}_{m'}+\vec{q}_k} \\ \sum_{\vec{q}_k} M^*_{\vec{q}_k}\delta_{\vec{p}_m,\vec{p}_{m'}-\vec{q}_k} & \vec{\sigma}\vec{p}_m\delta_{\vec{p}_m,\vec{p}_{m'}} \end{pmatrix}. \tag{3.64}$$

Here we see some of the differences that occur in the inhomogeneous model compared to the homogeneous one. In the homogeneous case, we only have $\vec{q}_k = 0$ and we can calculate the eigenvalues in Dirac space, since the Hamiltonian is diagonal in momentum space. The sum over the eigenvalues is only a sum over the momenta.

For the case $\vec{q}_k \neq 0$ this simple procedure is not possible. Different momenta are coupled via the Kronecker deltas in the mass terms, which makes this a non-trivial matrix in momentum space.

In general we can decompose the momenta into a momentum vector in the first Brillouin zone (B.Z.) $\vec{k}_i$ and elements of the reciprocal lattice vectors $\vec{q}_i$

$$\vec{p}_i = \vec{k}_i + \vec{q}_i. \tag{3.65}$$

This means two momenta in the Hamiltonian can only be coupled if they have the same momenta in the first Brillouin zone $\vec{k}_m = \vec{k}_{m'}$, which allows for a decomposition of the Hamiltonian into a direct sum

$$\mathcal{H} = \sum_{\vec{k} \in B.Z.} \mathcal{H}(\vec{k}). \tag{3.66}$$

Now we can take the kinetic part of the grand potential and take the continuum limit in the fashion

$$\frac{1}{V}\sum_{\nu} f(E_\nu) \to \int_{B.Z.} \frac{d^3k}{(2\pi)^3} \sum_{\lambda} f(E_\lambda(\vec{k})), \tag{3.67}$$

where $E_\lambda(\vec{k})$ are the eigenvalues of the Hamiltonians $\mathcal{H}(\vec{k})$. Therefore we can write Equation (3.54) as

$$\Omega_{kin} = -N_f N_c \int_{B.Z.} \frac{d^3k}{(2\pi)^3} \sum_{\lambda} \left(\frac{E_\lambda(\vec{k}) - \mu}{2} + T \log\left[1 + \exp\left\{ \frac{-E_\lambda(\vec{k}) - \mu}{T} \right\} \right] \right). \tag{3.68}$$

In all cases we consider in this work, the eigenvalues come in pairs $\pm|E_\lambda|$, which allows to make the additional simplification

$$\Omega_{kin} = -N_f N_c \int_{B.Z.} \frac{d^3k}{(2\pi)^3} \sum_{\lambda>0} \left(E_\lambda(\vec{k}) + T \log\left[1 + e^{-\frac{E_\lambda(\vec{k})-\mu}{T}} \right] + T \log\left[1 + e^{-\frac{E_\lambda(\vec{k})+\mu}{T}} \right] \right), \tag{3.69}$$

where the notation $\lambda > 0$ indicates that we only sum over positive eigenvalues.

By applying the Fourier decomposition of the mass function to the condensate part of the thermodynamic potential we get

$$\Omega_{cond} = \frac{1}{4G_S} \sum_{\vec{q}_k} \left| M_{\vec{q}_k} - m\delta_{\vec{q}_k,0} \right|^2. \tag{3.70}$$

3.3.1 Gap Equation from the Grand Potential

As discussed in the beginning, we can derive the gap equations from the grand potential.

In general all mass amplitudes $M_{\vec{q}_k}$ and the basis vectors of the reciprocal lattice $\vec{b}_k$ have to fulfill thermodynamic stability conditions

$$\frac{\partial \Omega_{MF}}{\partial M_{\vec{q}_k}} = 0, \qquad \frac{\partial \Omega_{MF}}{\partial M^*_{\vec{q}_k}} = 0, \qquad \frac{\partial \Omega_{MF}}{\partial \vec{b}_k} = 0. \tag{3.71}$$

In addition the solutions of these equations should be minima. We do not want to give a detailed derivation of the gap equations from the grand potential for a general case, since this is not the focus of this work. Interested readers will find a discussion in greater detail in [65] and [71].

Oftentimes it is not possible or numerically not feasible to evaluate the gap equations. In these cases one can instead minimize the grand potential, which tends to be a numerically more robust algorithm for handling the parameter determination in the inhomogeneous case.

3.3.2 Different Modulations

In this section we will give a quick overview of different modulations that have been proposed. The results for the homogeneous modulation and the chiral density wave are needed anyway and the other modulations give us an insight on how to judge our results.

Homogeneous Mass Function

In the homogeneous case the results are straightforward. Since we only have $\vec{q}_k = 0$, the Brillouin zone is infinite in size and the sum over the eigenvalues is reduced to a sum over the Dirac space eigenvalues, which are

$$E_\lambda = \pm\sqrt{\vec{k}^2 + M^2} =: \pm E_k, \tag{3.72}$$

where each of those is two times degenerate. The grand potential is then given by

$$\Omega_{MF} = \Omega_{kin} + \Omega_{cond}, \tag{3.73}$$

$$\Omega_{kin} = -2N_f N_c \int \frac{d^3k}{(2\pi)^3} \left(E_k + T \log\left[1 + e^{-\frac{E_k - \mu}{T}}\right] + T \log\left[1 + e^{-\frac{E_k + \mu}{T}}\right]\right), \tag{3.74}$$

$$\Omega_{cond} = \frac{(M-m)^2}{4G_S}. \tag{3.75}$$

The results for this have already been shown in the previous sections and we will not reiterate them here.

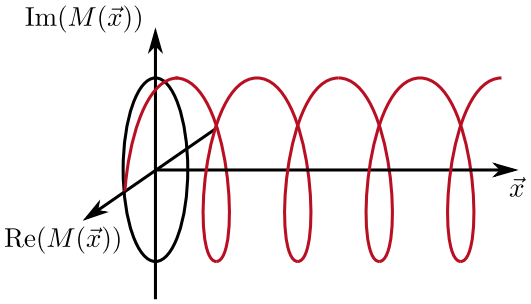

Sketch of the chiral density wave

The chiral density wave (CDW) modulation is the one we want to focus mostly in this work. This mass function has the great advantage that one can calculate the eigenvalues analytically. We will only discuss some aspects here and go into more detail in the next three chapters. For now we just give the definition

$$M(\vec{x}) = Me^{i\vec{q}\vec{x}} \tag{3.76}$$

and calculate the grand potential. The eigenvalues are given by [72]

$$E_{\pm}^2(\vec{k}) = \vec{k}^2 + M^2 + \frac{1}{4}\vec{q}^2 \pm \sqrt{(\vec{k}\cdot\vec{q})^2 + \frac{1}{4}\vec{q}^2 M^2}. \tag{3.77}$$

Like for the homogeneous modulation we can replace the integral over the Brillouin zone with an integral over the whole three-momentum space and calculate the thermodynamic potential straightforwardly. We minimize the grand potential with respect to M and $|\vec{q}| =: q$, which takes care of all free parameters in the model at a given temperature and chemical potential. This is also the most practical way of calculating the parameters, although we will derive the gap equation for M in the next chapter, the minimization process for M and q is both faster and more reliable against small numerical errors.

As a result we show the parameters at vanishing temperature versus chemical potential on the left in Figure 3.5.

The amplitude stays constant at a vacuum value of $M_{vac} = 300$ MeV at low chemical potential, which is due to the silver blaze property [67], and starts to slowly melt away starting at $\mu = 300$ MeV while the wave number is zero. This corresponds to the homogeneous broken phase, the chiral symmetry is broken spontaneously while the spatial symmetry is intact. At $\mu = 311$ MeV we find a first order phase transition at which the wave number jumps to a finite value and increases with higher chemical potentials. The amplitude on the other hand drops to a lower value and continues to decrease. This is the inhomogeneous or inhomogeneous broken phase, where the chiral symmetry, as well as the rotational and translational symmetry are broken. At a second critical chemical potential $\mu = 345$ MeV the mass amplitude reaches zero and the wave number is not a useful quantity anymore, this is a second order phase transition. The chiral symmetry is restored and so is the spatial symmetry.

The right side of Figure 3.5 shows the phase diagram for the CDW modulation. The homogeneous phase transition line is given in red for comparison. We see a similar behavior to the one

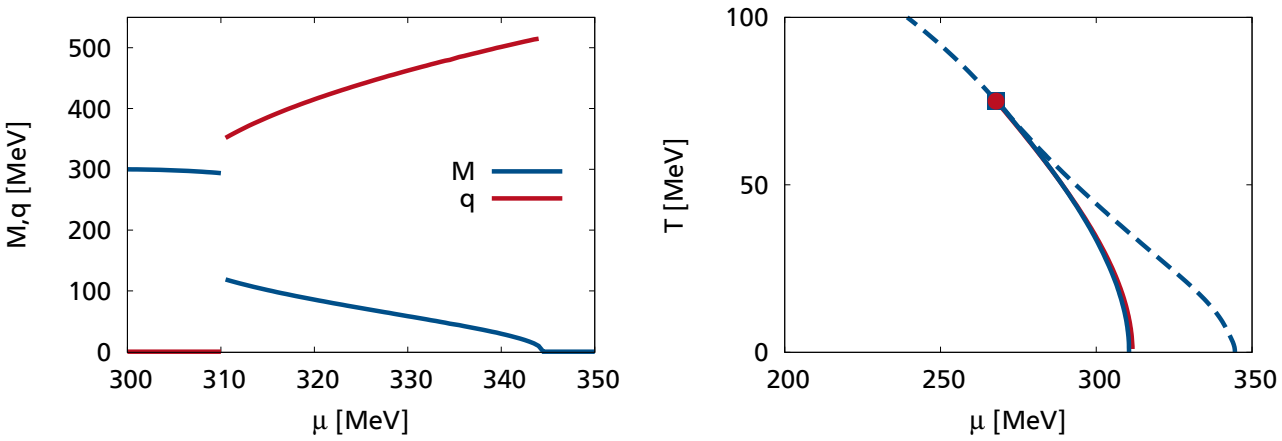

Figure 3.5.: Parameters of the CDW modulation over μ at vanishing temperature (left) and the phase diagram of the CDW modulation (right). Dashed lines indicate second-order phase transitions, while solid lines indicate first-order phase transitions. The square represents the point where the two second order and the first order line meet. The first-order transition from the homogeneous calculations, as well as its critical point are given in red for reference.

described above for a large temperature range, but the chemical potential ranges, where the inhomogeneous phase is favored decreases with increasing temperature. Both phase boundaries of the inhomogeneous phase eventually coincide at the point where we found the critical end point in our homogeneous calculations and at higher temperatures no inhomogeneous solutions can be found.The homogeneous first-order transition is completely covered by the inhomogeneous phase.

Sinusoidal Modulation

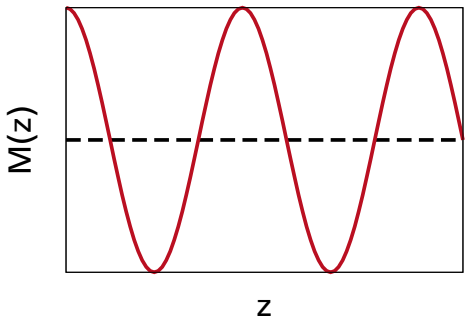

Sketch of the sinusoidal modulation

The next modulation we want to discuss briefly is the sinusoidal modulation. Instead of the single plane wave we used as a mass function in the previous section, we use two waves, to construct a real solution for the mass function

$$M(\vec{x}) = M\cos(\vec{q}\vec{x}) = \frac{M}{2}\left(e^{i\vec{q}\vec{x}} + e^{-i\vec{q}\vec{x}}\right). \tag{3.78}$$

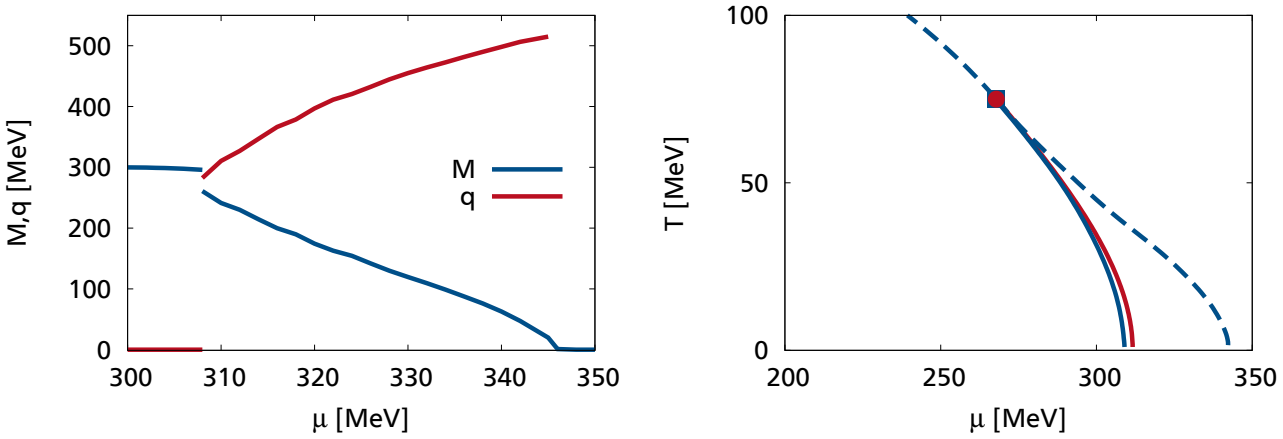

Figure 3.6.: Parameters of the sinusoidal modulation over μ at vanishing temperature (left) and the phase diagram of the sinusoidal modulation (right). Dashed lines indicate second-order phase transitions, while solid lines indicate first-order phase transitions. The square represents the point where the two second order and the first order line meet. The first-order transition from the homogeneous calculations, as well as its critical point are given in red for reference.

This is actually the simplest real mass function we can write down. For this modulation no analytic expression for the eigenvalues is known, so we have to diagonalize the Hamiltonian numerically. This is a rather involved procedure, which we will not show here, since it is not relevant for the main part of this work, but the interested reader can find details in [65, 73, 56, 71].

The results are similar to the chiral density wave modulation. In Figure 3.6 on the left we see the same qualitative behavior as before, although the first-order phase transition is less pronounced. On the right of Figure 3.6 we can see, that the general shape of the phase diagram remains the same, but the onset of the inhomogeneous phase is at lower chemical potentials when comparing to the CDW modulation. The second-order phase transition between the inhomogeneous chirally broken phase and the restored phase is at the same temperatures and chemical potentials, which is an expected behavior that has been shown in [54].

Solitonic Modulation

Lastly, we want to discuss the so called solitonic modulation. Its mass function is given by

$$M(z) = \Delta\nu \frac{\mathrm{sn}(\Delta z|\nu)\mathrm{cn}(\Delta z|\nu)}{\mathrm{dn}(\Delta z|\nu)}, \tag{3.79}$$

where sn, dn and cn are Jacobi elliptic functions.

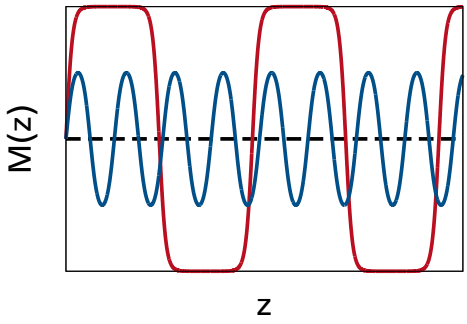

Sketch of the solitonic modulation for parameters $\nu = 0.99999$ (red) and $\nu = 0.5$ (blue)

This rather peculiar modulation was first found as the exact solution for the $1+1$-dimensional Gross-Neveu model [74] and it was shown, that it is a self consistent solution for the $3+1$-dimensional NJL model as well [75]. The main strength of this solution is, that it can assume different shapes of modulations, see the sketch above. For this modulation there is no analytic expression for the eigenvalues known, however one can derive a density of states that allows to transform the momentum integrals in the grand potential into a single energy integral

$$\Omega_{kin,soliton}(T,\mu) = -N_f N_c \int_0^\infty dE \rho_{soliton}(E)\left[f_{vac}(E) + f_{med}(E;T,\mu)\right]. \tag{3.80}$$

The density of states is given in terms of the complete and incomplete elliptic integrals of first and second kind

$$\begin{aligned}\rho_{soliton}(E) = \frac{E\Delta}{\pi^2}\Bigg\{&\theta(\sqrt{\tilde{\nu}}\Delta - E)\left[\mathbf{E}(\tilde{\vartheta}|\tilde{\nu}) + \left(\frac{\mathbf{E}(\nu)}{\mathbf{K}(\nu)} - 1\right)\mathbf{F}(\tilde{\vartheta}|\tilde{\nu})\right] \\ &+ \theta(E - \sqrt{\tilde{\nu}}\Delta)\theta(\Delta - E)\left[\mathbf{E}(\tilde{\nu}) + \left(\frac{\mathbf{E}(\nu)}{\mathbf{K}(\nu)} - 1\right)\mathbf{K}(\tilde{\nu})\right] \\ &+ \theta(E-\Delta)\left[\mathbf{E}(\vartheta|\tilde{\nu}) + \left(\frac{\mathbf{E}(\nu)}{\mathbf{K}(\nu)} - 1\right)\mathbf{F}(\vartheta|\tilde{\nu}) + \frac{\sqrt{(E^2-\Delta^2)(E^2-\tilde{\nu}\Delta^2)}}{E\Delta}\right]\Bigg\},\end{aligned} \tag{3.81}$$

where $\tilde{\nu} = 1-\nu$, $\tilde{\theta} = \arcsin(E/(\sqrt{\tilde{\nu}}\Delta))$ and $\theta = \arcsin(\Delta/E)$.

The parameters here are different from the ones we used in the other modulations, but we can relate Δ and ν to the mass amplitude and the overall frequency of the modulation q by the following relations

$$M = \Delta\nu, \qquad q = \frac{2\pi}{L}, \qquad L = \frac{2\mathbf{K}(\nu)}{\Delta}, \tag{3.82}$$

where L is the period of the modulation.

For this modulation we see a slightly different behavior than for the other ones. In Figure 3.7 on the left, we see that for vanishing temperature the transition between the homogeneous broken and the inhomogeneous phase is second order, instead of first and the mass amplitude is higher, although close to the sinusoidal modulation. On the right side of Figure 3.7 we see that the nature of the phase transitions holds true for the whole temperature range, the first-order transition from the previous sections gives way for a second-order transition between the homogeneous broken and the inhomogeneous phase. The transition to the restored phase remains of second order. The point where the three second-order lines meet coincides with the critical point from the homogeneous calculations and is called a *Lifschitz Point*.

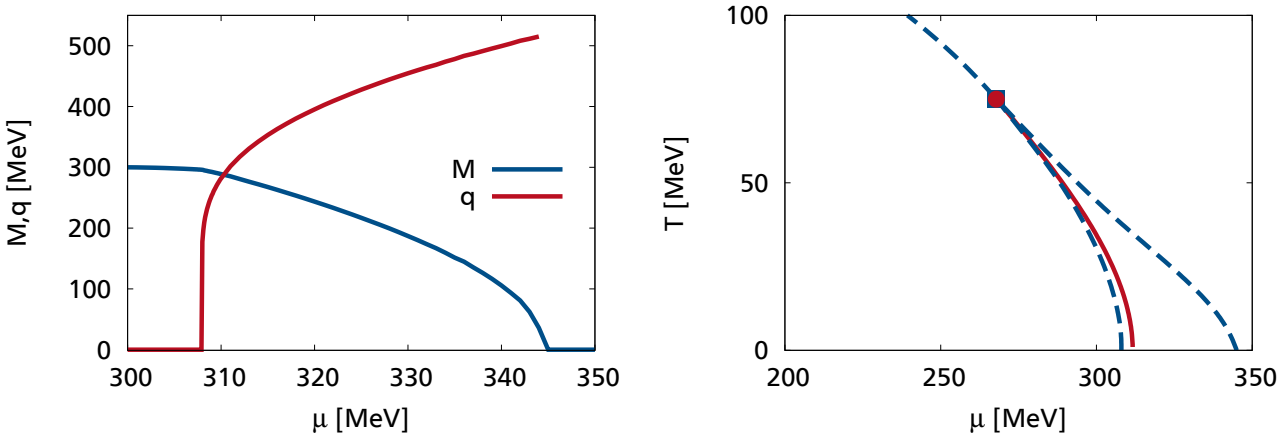

Figure 3.7.: Parameters of the solitonic modulation over μ at vanishing temperature (left) and the phase diagram of the solitonic modulation (right). Dashed lines indicate second-order phase transitions and the square represents the Lifschitz point. The first-order transition from the homogeneous calculations, as well as its critical point are given in red for reference.

Comparison of the Different Modulations

Now that we have seen the results of three different inhomogeneous modulations and the homogeneous one, it is time to compare them to each other. The inhomogeneous calculations show qualitatively largely similar behavior, with the exception of the order of the phase transition from the homogeneous broken to the inhomogeneous region. However as we have already seen in the comparison of the CDW to the sinusoidal modulation, this discrepancy is reduced by taking more Fourier coefficients into account (here two instead of one) and even more so for a larger number of coefficients [71].

We can compare the free energies of the different modulations, see Figure 3.8 where we plotted the values of the grand potentials relative to the restored phase. The first thing to note is that the solitonic modulations are favored, but the sinusoidal modulations are not far off. This can be understood by the fact, that only close to the transition to the homogeneous broken phase the solitonic mass function assumes shapes that are not well reproduced by a single cosine and only there this modulation is favored by a significant margin.

The chiral density wave however is disfavored by a larger amount compared to the other two. Nonetheless it is still favored over the homogeneous modulation in roughly the same parameter region as the other modulations and shows the qualitative behavior we are interested in. Its simplicity and the fact that the eigenvalues and, as we will see in the next section, the propagators can be calculated analytically makes it the ideal testing ground for more complicated calculations like the ones we attempt in this work.

3.4 Regularization

After having seen integrals with divergences throughout this chapter, some words on the regularization are in order. The NJL model is not renormalizable. Therefore we have to apply a regularization scheme, which influences our results. We will fit the parameters to physical

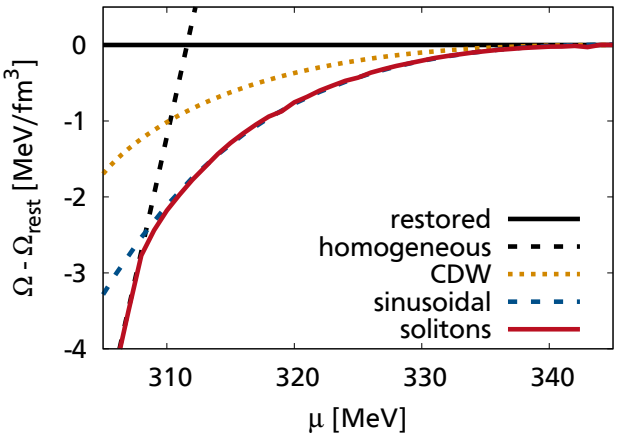

Figure 3.8.: Comparison of the free energies of different modulations at $T = 0$ with respect to the restored energy.

observables, so at least qualitatively the results should still be reasonable. A more detailed prescription on parameter fitting is given in [42].

Most integrals, though not all, can be separated into a divergent vacuum part and a convergent medium part. If this is the case and it is not otherwise stated we only regularize the vacuum part and leave the medium part unaltered.

During the decades that the model has been in use, different regularization schemes have been used, all with their own advantages and disadvantages. We will give an overview of the options one can choose from and afterwards go into more details concerning the scheme we chose.

3.4.1 Different Regularization Schemes

Three-Momentum Cutoff

The simplest and probably most widely used regularization scheme is the sharp three momentum cutoff. After the Matsubara sum has been performed, the absolute value of the spatial momentum is limited by a sharp cutoff, $|\vec{p}| \leq \Lambda$. In practice this means

$$\int \frac{d^3k}{(2\pi)^3} f(\vec{k}) = \int d\Omega \int_0^\infty dk\, k^2 f(k,\Omega) \to \int d\Omega \int_0^\Lambda dk\, k^2 f(k,\Omega), \tag{3.83}$$

where $d\Omega$ contains all angular integrations.

This procedure has the advantage, that no complicated functions are introduced to handle the divergences, this even allows for an analytical solution of some of the occurring integrals. The disadvantages, which disqualify this scheme for our calculations are quite severe. This regularization scheme breaks Lorentz invariance. For mesons this means, that in the vacuum we have an unphysical dependence of the meson masses on the external momentum. In the inhomogeneous calculations this regularization scheme would restrict the number of coupled momenta in an unphysical way and render our results useless.

Four-Momentum Cutoff

To circumvent the problem of the three-momentum cutoff one could instead try to restrict the full four-momentum with a sharp cutoff. This can only be done by performing a Wick rotation on the integrals and transforming them to Euclidean space. The Euclidean momentum can then be limited by $\sqrt{p_4^2 + \vec{p}^2} \leq \Lambda$, where $p_0 = ip_4$.

This does however not resolve the problems in the inhomogeneous phase, the number of coupled momenta would still be restricted. In addition, it might influence the results at finite temperature and chemical potential in a way that other regularization schemes don't.

We will not use this scheme in this work, a parameter set can be found in [42].

Pauli-Villars Regularization

Instead of a applying a sharp cutoff, the Pauli-Villars regularization scheme [76] allows for a smooth integrand behavior. To do this we subtract a function with the same asymptotic behavior as the original function. The number of regulating functions needed corresponds to the degree of divergence the integral shows.

$$\int \frac{d^3k}{(2\pi)^3} f_0(\vec{k}) \to \int \frac{d^3k}{(2\pi)^3} \sum_{j=0}^{N_{PV}} c_j^{PV} f_j(\vec{k}). \tag{3.84}$$

This scheme has the advantage of delivering a smooth integrand, which can be integrated over the whole momentum / energy range, which renders cutoff effects in the inhomogeneous phase unproblematic.

This is our regularization scheme of choice and we will go into more details on how to apply it in the next section.

Proper Time Regularization

The Schwinger proper time regularization [77] can be introduced by replacing the logarithm in Equation (3.48) with an exponential representation

$$\log A \to -\int_0^\infty \frac{d\tau}{\tau} f(\tau) e^{-\tau A}, \tag{3.85}$$

where $f(\tau)$ acts as a blocking function to regulate the integrals. Different blocking functions are possible, the simplest would be to simply use a lower bound $f(\tau) = \theta(\tau - 1/\Lambda^2)$.

Another possibility is to use the blocking function

$$f(\tau) = 1 - 3e^{-\tau\Lambda^2} + 3e^{-2\tau\Lambda^2} - e^{-3\tau\Lambda^2}, \tag{3.86}$$

which produces the Pauli-Villars regularization we will discuss in the next section.

3.4.2 Details on the Pauli-Villars Regularization Scheme

The regularization scheme of choice in this work is the Pauli-Villars regularization scheme [76].

In the homogeneous model it is common to regularize the masses, making the replacement

$$\int \frac{d^3k}{(2\pi)^3} f(\vec{k}, M) = \int \frac{d^3k}{(2\pi)^3} \sum_{j=0}^{N_{PV}} c_j^{PV} f(\vec{k}, \sqrt{M^2 + j\Lambda^2}). \tag{3.87}$$

The coefficients c_j^{PV} have to fulfill the conditions

$$\sum_{j=0}^{N_{PV}} c_j^{PV} = \sum_{j=0}^{N_{PV}} j c_j^{PV} = \cdots = \sum_{j=0}^{N_{PV}} j^{N_PV-1} c_j^{PV} = 0. \tag{3.88}$$

For the integrals shown in this work, in the homogeneous case, this is equivalent to regularizing the occurring energies $E_{\vec{k}} = \sqrt{\vec{k}^2 + M^2}$, since this is the only place the masses show up in the integrals.

In the inhomogeneous phase, regularizing the energies is usually the only choice. Since the mass is a function, it is not clear how to actually regularize it, since regularizing only the amplitude can lead to unwanted effects, such as an inability to determine a value for the wave number or artifacts in the restored phase, where the mass amplitude is zero, but additional amplitudes are generated by the regulators. For this reason, the integrals in the inhomogeneous models for the gap equation and the grand potential are regularized in the following way

$$\int \frac{d^3k}{(2\pi)^3} f(E_{\vec{k}}) = \int \frac{d^3k}{(2\pi)^3} \sum_{j=0}^{N_{PV}} c_j^{PV} f(\sqrt{E_{\vec{k}}^2 + j\Lambda^2}). \tag{3.89}$$

This regularization of energies diverges a bit from the original concept of Pauli and Villars, but can further be justified by the blocking function we gave in the previous section for the proper time regularization scheme.

The minimum number of regulators needed to render the integrals convergent is determined by the degree of divergence in the occurring integrals. While for the integrals found in this work two regulators $c_j^{PV} = \{1, -2, 1\}$ would be sufficient, to be comparable to previous works, we choose to use three regulating functions, resulting in coefficients $c_j^{PV} = \{1, -3, 3, -1\}$.

Now we have to fix two remaining parameters, the coupling constant G_S and the cutoff Λ. If we worked away from the chiral limit we would also have to fit the bare quark mass m. To obtain physically meaningful results we fit these parameters to physical observables in the vacuum.

The first observable we fit to is a pion decay constant of $f_\pi = 88$ MeV, which differs from the result one might find in most literature, since it is the value specifically calculated for the chiral limit [78].

Second we fit to the a constituent quark mass in vacuum of $M = 300$ MeV. This of course is not an observable in the classical sense, in most works one might find a fit to the chiral condensate $\langle\overline{\psi}\psi\rangle$. That however would yield rather small vacuum quark masses for the Pauli-Villars regularization scheme.

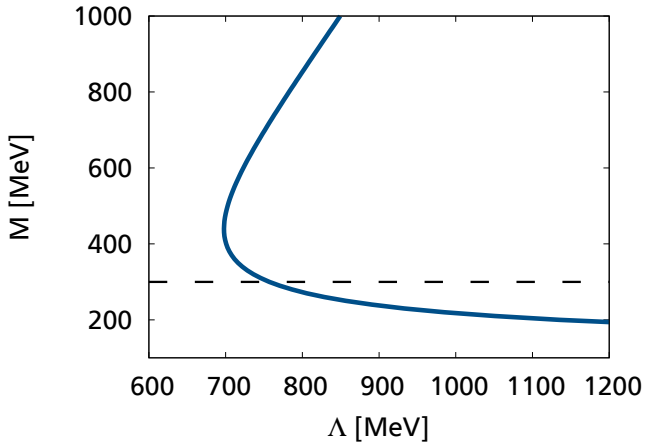

Figure 3.9.: Constituent quark mass M over the value of the Pauli-Villars cutoff Λ for three regulators and fixed coupling constant. The desired value of the mass of $M = 300$ MeV in vacuum is indicated by the dashed black line.

The resulting parameters used throughout this work are then given as

$$\Lambda = 757.048\,\text{MeV}, \qquad G_S = 6.00214/\Lambda^2. \tag{3.90}$$

The regularization recipe we describe here is widely used for the calculations of the inhomogeneous NJL model and of course works just as well in the homogeneous model, which allows us to compare to previous works. All calculations in this work are done with these parameters and most are done with the replacement described in Equation (3.89). For the inhomogeneous mesons in Chapter 6 the situation is not quite as simple and warrants a separate discussion which can be found in that chapter.

4 Inhomogeneous Propagators and the Chiral Density Wave

In this chapter we give an overview of the properties of the quark propagator in the inhomogeneous phase in the NJL model. In particular there are some aspects to take into account that lack in most other theories.

In the previous section we saw the general Hamiltonian, Equation (3.64), and from that the inverse propagator in momentum space can be derived as

$$S^{-1}(p,p') = \gamma^0 \left(p_0 (2\pi)^4 \delta^{(4)} \left(p - p' \right) - H(p,p') \right), \tag{4.1}$$

as stated in Equation (3.52). Here we treat the matrix structure from Section 3.3 as functional arguments

$$H_{p,p'} \to H(p,p'), \tag{4.2}$$

which fits more consistently with the definitions of operations in Appendix A. Just as the Hamiltonian the inverse propagator is a matrix in momentum space and since quite often the propagator is needed instead of the inverse propagator, this poses the problem to invert an infinite continuous matrix. To understand this a bit better we will highlight some of the consequences.

The most important differences to the homogeneous ansatz lies in the matrix structure itself, the momentum arguments correspond to incoming and outgoing momenta. This means, in contrast to homogeneous modulations we can have different incoming and outgoing momenta, as shown in Figure 4.1. This stems from broken translational invariance. This can be explained

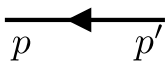

Figure 4.1.: Diagrammatic representation of a dressed propagator in the inhomogeneous phase

by the ansatz we made. In mean-field approximation, as the name suggests, interactions are handled via a background field and since the condensates are momentum dependent in the inhomogeneous phase, so is the background field. This allows a propagating quark to pick up or store momentum in the background field. One should note however that the absolute value of momentum is not arbitrary, but only elements of the reciprocal lattice can be exchanged, as can easily be seen by looking at the off diagonal structure in the Hamiltonian (3.64). This allows us to formulate a rule for the incoming and outgoing momenta

$$p' - p = \vec{q}_k, \qquad \vec{q}_k \in \text{R.L.} \tag{4.3}$$

As mentioned before, we can write down the Hamiltonian with the description given in Section 3.3, but for most quantities we have to invert the resulting inverse propagator. In most cases the propagator can only be evaluated numerically after applying a cutoff on the matrix structure of

the Hamiltonian. This is a very involved procedure and in addition to being computationally expensive, quite prone to errors, especially for more complex calculations like the polarization loops we discuss later in this work.

The elegant way, if it is possible, is to find an analytical representation of the diagonal Hamiltonian, together with the transformations (eigenvectors). This is what we will show in the next section for the chiral density wave.

4.1 Chiral Transformations

A great advantage of the chiral density wave (CDW) modulation is the fact, that eigenvalues of the Hamiltonian can be calculated analytically. If we define the condensates as

$$\langle\overline{\psi}\psi\rangle = -\frac{M}{2G_S}\cos(\vec{q}\vec{x}), \qquad \langle\overline{\psi}i\gamma^5\tau^3\psi\rangle = -\frac{M}{2G_S}\sin(\vec{q}\vec{x}), \tag{4.4}$$

dividing the amplitude by $2G_S$ compared to the definition given in Section 3.3.2. We can write the Hamiltonian in coordinate space as, see Appendix C.1 for details,

$$H(x) = -i\gamma_0\gamma^i\partial_i + \gamma_0 M\exp(i\gamma^5\tau^3\vec{q}\vec{x}), \tag{4.5}$$

which fulfills the eigenvalue relation

$$H(x)\psi(x) = E\psi(x), \tag{4.6}$$

with eigenvalues E and eigenstates $\psi(x)$. Due to the explicit $\vec{x}$ dependence in the second summand of the Hamiltonian the Fourier transformation would yield a non-trivial matrix in momentum space (compare also A.3) which requires more elaborate techniques to arrive at the eigenvalues. We can perform a unitary transformation on the fields [72]

$$\psi(x) = U(x)\psi'(x), \qquad U(x) = \exp\left(-\frac{1}{2}i\gamma^5\tau^3\vec{q}\vec{x}\right), \tag{4.7}$$

which leads to a new eigenvalue relation, with transformed fields and a transformed Hamiltonian, but the same eigenvalues as before

$$H(x)U(x)\psi'(x) = EU(x)\psi'(x) \tag{4.8}$$

$$\Rightarrow \qquad H'(x)\psi'(x) = E\psi'(x), \tag{4.9}$$

where we defined the transformed Hamiltonian as

$$H'(x) = U^\dagger(x)H(x)U(x). \tag{4.10}$$

This transformed Hamiltonian

$$H'(x) = -i\gamma_0\gamma^i\partial_i - \frac{1}{2}\gamma_0\gamma^5\tau^3\gamma^i q_i + \gamma_0 M \tag{4.11}$$

has no explicit dependence on $\vec{x}$ and the eigenvalues can easily be determined to be

$$E_{\pm}^2(\vec{k}) = \vec{k}^2 + M^2 - \frac{\vec{q}^2}{4} \pm \sqrt{(\vec{k}\cdot\vec{q})^2 + \frac{\vec{q}^2 M^2}{4}}. \tag{4.12}$$

We can perform a Fourier transformation on the transformation matrices, see Appendix C.1

$$\begin{aligned} U(k,k') = \frac{1}{2}\Big[&(\mathbb{1}+\gamma^5\tau^3)(2\pi)^4\delta^{(4)}\left(k-k'-q/2\right) \\ &+(\mathbb{1}-\gamma^5\tau^3)(2\pi)^4\delta^{(4)}\left(k-k'+q/2\right)\Big], \end{aligned} \tag{4.13}$$

$$\begin{aligned} U^\dagger(k,k') = \frac{1}{2}\Big[&(\mathbb{1}+\gamma^5\tau^3)(2\pi)^4\delta^{(4)}\left(k-k'+q/2\right) \\ &+(\mathbb{1}-\gamma^5\tau^3)(2\pi)^4\delta^{(4)}\left(k-k'-q/2\right)\Big] \end{aligned} \tag{4.14}$$

and apply them on the Hamiltonian in momentum space

$$\begin{aligned} H(p,p') = \gamma_0\Big[&-\gamma^i p_i(2\pi)^4\delta^{(4)}\left(p-p'\right) \\ &+\frac{M}{2}\left((\mathbb{1}+\gamma_5)(2\pi)^4\delta^{(4)}\left(p-p'-q\right)+(\mathbb{1}-\gamma_5)(2\pi)^4\delta^{(4)}\left(p-p'+q\right)\right)\Big] \end{aligned} \tag{4.15}$$

to get the transformed propagator in momentum space

$$H'(p,p') = \left[-\gamma_0\gamma^i p_i - \frac{1}{2}\gamma_0\gamma^5\tau^3\gamma^i q_i + \gamma_0 M\right](2\pi)^4\delta^{(4)}\left(p-p'\right), \tag{4.16}$$

where we see, that it is indeed a diagonal matrix in momentum space. Alternatively, one could take the transformed propagator in coordinate space, Equation (4.11), and perform the Fourier transformation.

4.2 Transformed Propagator

We start from the inverse propagator in momentum space, which is

$$\begin{aligned} S^{-1}(p,p') &= \gamma^0\left(p_0(2\pi)^4\delta^{(4)}\left(p-p'\right) - H(\vec{p},\vec{p}')\right) \\ &= \not{p}(2\pi)^4\delta^{(4)}\left(p-p'\right) \\ &\quad -\frac{M}{2}\left[(\mathbb{1}+\gamma_5)(2\pi)^4\delta^{(4)}\left(p-p'-q\right)+(\mathbb{1}-\gamma_5)(2\pi)^4\delta^{(4)}\left(p-p'+q\right)\right] \end{aligned} \tag{4.17}$$

and replace the Hamiltonian by the transformed one

$$S^{-1}(p,p') = \gamma^0\left(p_0(2\pi)^4\delta^{(4)}\left(p-p'\right) - \int\frac{d^4k}{(2\pi)^4}\int\frac{d^4k'}{(2\pi)^4}\,U(p,k)H'(\vec{k},\vec{k}')U^\dagger(k',p)\right) \tag{4.18}$$

$$= \int\frac{d^4k}{(2\pi)^4}\int\frac{d^4k'}{(2\pi)^4}\,U^\dagger(p,k)\gamma^0\left(k_0(2\pi)^4\delta^{(4)}\left(k-k'\right) - H'(\vec{k},\vec{k}')U^\dagger(k',p)\right), \tag{4.19}$$

where we picked up an additional dagger from the commutator with γ_0. Now we can make the definition

$$S^{-1}(p,p') =: \int \frac{d^4k}{(2\pi)^4} \int \frac{d^4k'}{(2\pi)^4} U^\dagger(p,k) S'^{-1}(k,k') U^\dagger(k',p'), \tag{4.20}$$

with the transformed inverse propagator

$$S'^{-1}(p,p') = \left[\not{p} + \frac{1}{2}\gamma^5\tau^3 \not{q} - M \right] (2\pi)^4 \delta^{(4)}\left(p-p'\right). \tag{4.21}$$

Now we want to invert this expression, with the definition of the inverse in accordance with Appendix A

$$\int \frac{d^4k}{(2\pi)^4} S^{-1}(p,k) S(k,p') = (2\pi)^4 \delta^{(4)}\left(p-p'\right) \mathbb{1}_{D,f,c}. \tag{4.22}$$

Since this propagator is diagonal in momentum space we can invert it analytically in Dirac and flavor space. A lengthy but straightforward calculation yields

$$S'(p,p') = \frac{A(p) + \gamma^5\tau^3 B(p) + \not{C}(p) + \gamma^5\tau^3 \not{D}(p) + \gamma^5\tau^3\gamma^\mu\gamma^\nu E_{\mu\nu}}{N(p)} (2\pi)^4 \delta^{(4)}\left(p-p'\right) \tag{4.23}$$

$$=: S'(p)(2\pi)^4 \delta^{(4)}\left(p-p'\right), \tag{4.24}$$

with the abbreviations

$$\begin{aligned}
A(p) &= M\left(p^2 - \frac{1}{4}q^2 - M^2\right), \\
B(p) &= -M(p\cdot q), \\
\not{C}(p) &= \not{p}\left(p^2 + \frac{1}{4}q^2 - M^2\right) - \frac{1}{2}(p\cdot q)\not{q}, \\
\not{D}(p) &= -\frac{1}{2}\left(p^2 + \frac{1}{4}q^2 + M^2\right)\not{q} + (p\cdot q)\not{p}, \\
E_{\mu\nu}(p) &= M p_\mu q_\nu, \\
N(p) &= \left(p^2 + \frac{1}{4}q^2 - M^2\right)^2 + q^2M^2 - (p\cdot q)^2.
\end{aligned}$$

This expression has a rich Dirac structure, which is the trade off we have to make to get a diagonal propagator. As for the untransformed propagator, we can get it from the transformed propagator and the transformation matrices via the relation

$$S = \left(S^{-1}\right)^{-1} = \left(U^\dagger S'^{-1} U^\dagger\right)^{-1} = \left(U^\dagger\right)^{-1} S' \left(U^\dagger\right)^{-1} = U S' U, \tag{4.25}$$

where we omitted the integrals and momentum dependencies and just treated everything as a matrix in accordance with Appendix A.

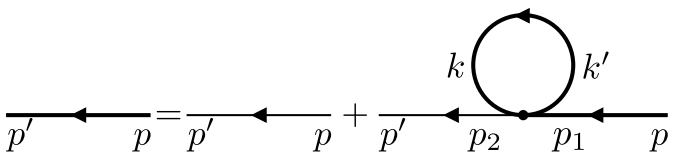

Figure 4.2.: Diagrammatic representation of the gap equation.

4.3 Gap Equation

To see why this formulation of the propagators is useful we look at the gap equation. This equation, given in diagrammatic form in Figure 4.2, is formally a Dyson equation or more commonly referred to in the context of the NJL model, the Hartree equation. It is a self consistent equation that allows to calculate the constituent quark mass.

Reading from the diagram we can write

$$iS(p',p) = iS_0(p',p) + \int \frac{d^4p_1}{(2\pi)^4} \int \frac{d^4p_2}{(2\pi)^4}\, iS_0(p',p_2)\,(-i\Sigma(p_2,p_1))\, iS(p_1,p), \tag{4.26}$$

with the self-energy given as

$$\begin{aligned}\Sigma(p_2,p_1) = -2iG_S \int \frac{d^4k}{(2\pi)^4} \int \frac{d^4k'}{(2\pi)^4} \Big[&\mathbb{1}\mathrm{Tr}\big(\mathbb{1} iS(k,k')\big) \\ &+ i\gamma^5\tau^3\mathrm{Tr}\big(i\gamma_5\tau_3 iS(k,k')\big)\Big](2\pi)^4\delta^{(4)}\big(p_2-k+k'-p_1\big).\end{aligned} \tag{4.27}$$

Since the bare propagator is diagonal in momentum space

$$S_0(p,p') = S_0(p)(2\pi)^4\delta^{(4)}\big(p-p'\big) \tag{4.28}$$

Equation (4.26) simplifies slightly

$$iS(p',p) = iS_0(p')(2\pi)^4\delta^{(4)}\big(p'-p\big) + \int \frac{d^4p_1}{(2\pi)^4}\, iS_0(p')\big(-i\Sigma(p',p_1)\big) iS(p_1,p). \tag{4.29}$$

Using the rules for continuous matrix multiplication we can invert this equation to an even simpler form (see Appendix C.2 for more details)

$$S^{-1}(p',p) = S_0^{-1}(p')(2\pi)^4\delta^{(4)}\big(p'-p\big) - \Sigma(p',p). \tag{4.30}$$

The key point is to derive a value for the mass amplitude and to do that we can directly put in the untransformed inverse propagator from Equation (4.17) on the left, as well as the bare propagator on the right and only have to worry about the self-energy. We take Equation (4.27) and insert Equation (4.25) and after integrating out all occurring delta-functions we arrive at

$$\begin{aligned}\Sigma(p',p) = iG_S\Big[&(\mathbb{1}-\gamma_5\tau_3)(2\pi)^4\delta^{(4)}\big(p'-p-q\big) \\ &+ (\mathbb{1}+\gamma_5\tau_3)(2\pi)^4\delta^{(4)}\big(p'-p+q\big)\Big]\int \frac{d^4k}{(2\pi)^4}\,\mathrm{Tr}S'(k).\end{aligned} \tag{4.31}$$

Now we compare the momentum, Dirac and Flavor components of the different summands in Equation (4.30) to arrive at the equation for M, which yields

$$M = 2iG_S \int \frac{d^4k}{(2\pi)^4} \mathrm{Tr} S'(k). \tag{4.32}$$

The trace can be evaluated with Equation (4.23). Without loss of generality we restrict the modulation in the z-direction, so

$$q = 2Q\vec{e}_z. \tag{4.33}$$

The factor 2 here is purely conventional to make the expression better readable. The trace yields

$$\begin{aligned} \mathrm{Tr} S'(k) &= 4N_f N_c \frac{A(k)}{N(k)} && (4.34)\\ &= 4N_f N_c \frac{M\left(k^2+Q^2-M^2\right)}{\left(k^2-Q^2-M^2\right)^2+4Q^2M^2-4(k_zQ)^2} && (4.35)\\ &= 4N_f N_c M \frac{k_0^2-\frac{1}{2}\left(E_+^2(\vec{k})+E_-^2(\vec{k})\right)+2Q^2}{\left(k_0^2-E_+^2(\vec{k})\right)\left(k_0^2-E_-^2(\vec{k})\right)}. && (4.36) \end{aligned}$$

In the last step we expressed some of the quantities in terms of the energies (see Equation (4.12)), which for the modulation in z-direction looks like

$$E_\pm = \sqrt{k_z^2+\vec{k}_\perp^2+M^2+Q^2 \pm 2Q\sqrt{k_z^2+M^2}}, \tag{4.37}$$

where in addition we separated the momenta in the direction of the modulation k_z and a two vector perpendicular to the modulation $\vec{k}_\perp = (k_x, k_y)^T$.

In order to calculate the masses in the medium we employ the Matsubara formalism in Equation (4.36). We make the replacement

$$i\int \frac{d^4k}{(2\pi)^4} f(k_0,\vec{k}) \to -T\sum_{m=-\infty}^{\infty}\int \frac{d^3k}{(2\pi)^3} f(i\omega_m+\mu,\vec{k}), \tag{4.38}$$

with temperatures T, chemical potential μ and the fermionic Matsubara frequencies $\omega_m = (2m+1)\pi T$. The sum can be evaluated by using the residue theorem, which is detailed in Appendix C.3. The end result is

$$\begin{aligned} M = 2G_S N_f N_c M \int \frac{d^3k}{(2\pi)^3} \frac{1}{\sqrt{k_z^2+M^2}} \Bigg[& \frac{\sqrt{k_z^2+M^2}+Q}{E_+(\vec{k})}\left(1-n_F(E_+(\vec{k})+\mu)-n_F(E_+(\vec{k})-\mu)\right) \\ & + \frac{\sqrt{k_z^2+M^2}-Q}{E_-(\vec{k})}\left(1-n_F(E_-(\vec{k})+\mu)-n_F(E_-(\vec{k})-\mu)\right)\Bigg], \end{aligned} \tag{4.39}$$

with the Fermi distribution

$$n_F(z) = \left[1+\exp\left(\frac{z}{T}\right)\right]^{-1}. \tag{4.40}$$

The vacuum part of this expression, the part independent of the Fermi distributions, is divergent and we will treat it with the regularization procedure described in Section 3.4.

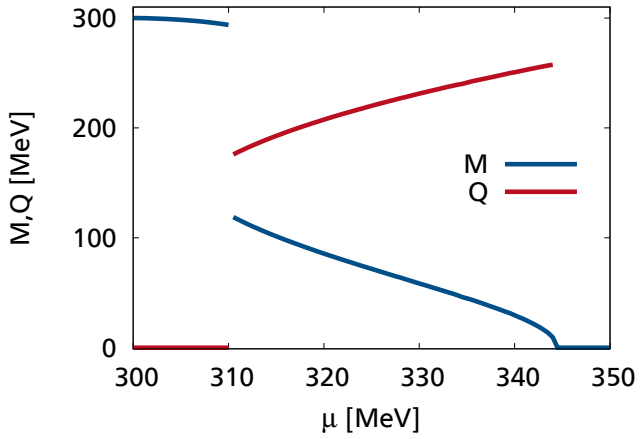

Figure 4.3.: Mass amplitude M in blue and wave number Q in red for vanishing temperature.

4.3.1 Results

As mentioned before the gap equation only determines the amplitude M, but not the wave number Q. To determine the wave number we have to minimize the thermodynamic potential Ω from Equation (3.51). Doing so results in Figure 4.3 which shows the mass amplitude M and the wave number Q versus the chemical potential μ at vanishing temperature. The resulting picture closely resembles the one shown in Section 3.3.2 from the previous chapter, as it should. Since we have already discussed the results there, we will not reiterate them here. The only difference between Figures 4.3 and 3.5 (left) stems from a different definition of q and Q. In the last chapter we took $q = |\vec{q}|$, which is the definition that matches the other modulations. In this chapter and the following ones however, we defined $\vec{q} = 2Q\vec{e}_z$, which is purely conventional. The only reason to do so is to cancel out the factors $1/2$ commonly appearing in front of $\vec{q}$ and to better differentiate to the four-momentum q.

5 Nambu-Goldstone Modes

In this chapter we derive the types of collective excitations that can arise from the symmetries of the model with a chiral density modulation, the *Nambu-Goldstone modes*.

The ground work for the Goldstone theorem was done by Nambu [64] in the context of superconductors and was refined by Goldstone [15], who later extended the theorem to quantum field theories [79].

The theorem states, that whenever a Lagrangian is invariant under a continuous symmetry, but the ground state is not, a massless, spinless particle appears in the spectrum. This is spontaneous symmetry breaking and there are many examples in nature that can be described with the Goldstone theorem.

One prominent example of Goldstone bosons are the pions, which are generated by the spontaneous breakdown of chiral symmetry in the QCD vacuum. In nature it is only an approximate symmetry, since the mass of the light quarks does not vanish, pions have a finite mass. However in our ansatz, we take the bare quark masses to be zero, which makes the chiral symmetry exact and our pions massless. Another example of a Goldstone boson is the phonon, a quasiparticle which can be related to crystal vibrations in condensed matter physics. It is generated by the breakdown of rotational and translational symmetry.

In this work, we have the spontaneous breakdown of chiral symmetry as well as rotational and translational symmetry, so we expect to find massless pions and phonons.

5.1 Identifying the Goldstone Modes

In this section, which is largely based on [62], we want to concentrate on the two kinds of symmetries that are spontaneously broken in the inhomogeneous phase, the rotational/translational symmetry and the chiral symmetry. For the chiral density wave consider the scalar and pseudoscalar condensate separately

$$\phi_S = M\cos(qz) \propto \langle\overline{\psi}\psi\rangle, \qquad \phi_P = M\sin(qz) \propto \langle\overline{\psi}i\gamma_5\tau_3\psi\rangle. \tag{5.1}$$

If we want to investigate small (collective) deviations in space, we shift the space dependency by a small amount u

$$\phi_S = M\cos(q(z+u)), \qquad \phi_P = M\sin(q(z+u)). \tag{5.2}$$

By applying the standard addition theorems and assuming u to be small ($u \ll 1/q$), we find the condensates to be

$$\phi_S = M\cos(qz) - Mqu\sin(qz) + \mathcal{O}(u^2), \tag{5.3}$$
$$\phi_P = M\sin(qz) + Mqu\cos(qz) + \mathcal{O}(u^2). \tag{5.4}$$

For the chiral symmetry we combine the transformations from $SU_V(2)$ and $SU_A(2)$, which act on the quark fields as follows

$$SU_V(2): \quad \psi \to e^{-i\vec{\tau}\vec{\alpha}/2}\psi, \qquad \overline{\psi} \to \overline{\psi}e^{i\vec{\tau}\vec{\alpha}/2}, \tag{5.5}$$

$$SU_A(2): \quad \psi \to e^{-i\gamma_5\vec{\tau}\vec{\beta}/2}\psi, \qquad \overline{\psi} \to \overline{\psi}e^{-i\gamma_5\vec{\tau}\vec{\beta}/2}. \tag{5.6}$$

Here $\vec{\alpha}$ and $\vec{\beta}$ are arbitrary (but small) 3 vectors, relating to the rotations in vector and axial-vector space. This leads to overall rotations

$$\overline{U} = e^{i\vec{\tau}(\vec{\alpha}-\gamma_5\vec{\beta})} = 1 + \frac{i}{2}\vec{\tau}(\vec{\alpha}-\gamma_5\vec{\beta}) + \mathcal{O}(\vec{\alpha}^2, \vec{\beta}^2), \tag{5.7}$$

$$U = e^{-i\vec{\tau}(\vec{\alpha}+\gamma_5\vec{\beta})} = 1 - \frac{i}{2}\vec{\tau}(\vec{\alpha}+\gamma_5\vec{\beta}) + \mathcal{O}(\vec{\alpha}^2, \vec{\beta}^2), \tag{5.8}$$

where we approximated to leading order in $\vec{\alpha}$ and $\vec{\beta}$. These transformations act on the combined chiral condensates

$$\phi = \phi_S + i\gamma^5\vec{\tau}\vec{\phi}_P, \tag{5.9}$$

where we should note, that for the moment we do not restrict ourselves to only the π_3 contribution. Applying the transformations on this expression and continue to only consider leading order leads to

$$\overline{U}\phi U = \phi_S + i\gamma^5\vec{\tau}\vec{\phi}_P + \frac{i}{2}\vec{\alpha}\left([\vec{\tau}, \phi_S] + [\vec{\tau}, i\gamma^5\vec{\tau}\vec{\phi}_P]\right) - \frac{i}{2}\vec{\beta}\left(\{\gamma_5\vec{\tau}, \phi_S\} + \{\gamma_5\vec{\tau}, i\gamma^5\vec{\tau}\vec{\phi}_P\}\right) \tag{5.10}$$

$$= \phi_S + i\gamma^5\vec{\tau}\vec{\phi}_P - \frac{1}{2}\gamma^5\alpha_a(2i\varepsilon_{abc}\tau_c)(\phi_P)_b - i\gamma_5\vec{\tau}\vec{\beta}\phi_S + \vec{\beta}\vec{\phi}_P. \tag{5.11}$$

We can separate this in the two condensates

$$\phi_S \to \phi_S + \vec{\beta}\vec{\phi}_P, \tag{5.12}$$

$$\vec{\phi}_P \to \vec{\phi}_P - \vec{\alpha} \times \vec{\phi}_P - \vec{\beta}\phi_S. \tag{5.13}$$

Now we want to combine the two different transformations. For better readability we write everything in a four component vector $\phi = (\phi_S, \vec{\phi}_P)$. The standard CDW is

$$\phi_0 = M \begin{pmatrix} \cos(qz) \\ 0 \\ 0 \\ \sin(qz) \end{pmatrix} \tag{5.14}$$

and after we applied the transformations we find

$$\phi = \phi_0 + M \begin{pmatrix} (-qu + \beta_3)\sin(qz) \\ -\alpha_2\sin(qz) - \beta_1\cos(qz) \\ \alpha_1\sin(qz) - \beta_2\cos(qz) \\ (qu - \beta_3)\cos(qz) \end{pmatrix}. \tag{5.15}$$

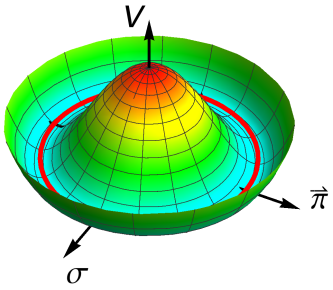

Figure 5.1.: Illustration of the Mexican hat potential in σ and $\vec{\pi}$ plane

From the first and last component of this vector we can see that the chiral density wave is invariant under simultaneous rotation by the angle β_3 and a spatial translation along the z-Axis, if the condition $qu - \beta_3 = 0$ is satisfied. Since the spontaneous breaking of symmetries only depends on the sum, only one NG boson is required to describe both translational symmetry breaking and chiral symmetry breaking in the inhomogeneous phase. Without loss of generality, we can concentrate only on $\beta_3 \neq 0$ and set $u = 0$ for the rest of the discussion, which resembles the uncharged pion in the homogeneous case.

In the second and third component of ϕ we still have a dependence on the components of the two vectors $\vec{\alpha}$ and $\vec{\beta}$, however it can be shown that these are linearly dependent [80, 81, 82] and it suffices only to take the components of $\vec{\beta}$ into account, since only those are present in the homogeneous broken phase.

Overall this means that we only find three independent NG modes in the CDW phase, which can be described by $\vec{\beta}$.

5.2 Understanding the Pion Vertex

In Section 3.2.2 we have already shown how to calculate mesons in the NJL model for the homogeneous case. In the next chapter we will extend the formalism to the inhomogeneous phase, where due to the non-diagonal momentum space structure the calculations will be much more complicated. In this section we want to take the opportunity to give a simpler picture of the steps necessary to calculate the Goldstone modes in the inhomogeneous phase.

In the homogeneous ansatz we made a choice, to have the massive direction parallel to the chiral condensate $\langle\overline{\psi}\psi\rangle$. When looking at the mean-field Lagrangian (3.43) in a slightly different notation

$$\mathcal{L} = \overline{\psi}\left(i\partial\!\!\!/ + \Gamma_M \phi_M\right)\psi - \frac{1}{4G_S}\phi_M^2, \tag{5.16}$$

with implicit summation over $M \in \{\sigma, \vec{\pi}\}$, it is obvious, that we could have chosen any of the ϕ_M to be the massive direction. It also shows, that the vertices $\Gamma_\sigma = \mathbb{1}$ and $\Gamma_{\vec{\pi}} = i\gamma_5\vec{\tau}$ are associated with the condensates $\phi_\sigma \propto \langle\overline{\psi}\psi\rangle$ and $\phi_{\vec{\pi}} \propto \langle\overline{\psi}i\gamma_5\vec{\tau}\psi\rangle$ respectively.

We can illustrate this with the Mexican hat potential in Figure 5.1, where we show the potential as a function of ϕ_σ and the compactified $\phi_{\vec{\pi}}$ condensate. Our choice of a minimum in the σ direction is not unique, we could have taken any direction marked by the red line and it would still be a minimum of the potential. All states along the red line have the same energy level, but they represent different ground states. This is exactly the premise of the Goldstone theorem.

By choosing the massive direction to be aligned with ϕ_σ, the other three condensates $\phi_{\vec{\pi}}$ are associated with the Goldstone modes. This explains why the σ-meson, we calculated with the σ-vertex, Γ_σ, is massive while the others are massless. In the vector picture of the previous section, we chose our condensates in the following way

$$\phi_\sigma = \begin{pmatrix} M \\ 0 \\ 0 \\ 0 \end{pmatrix}, \qquad \phi_{\pi_1} = \begin{pmatrix} 0 \\ 1 \\ 0 \\ 0 \end{pmatrix}, \qquad \phi_{\pi_2} = \begin{pmatrix} 0 \\ 0 \\ 1 \\ 0 \end{pmatrix}, \qquad \phi_{\pi_3} = \begin{pmatrix} 0 \\ 0 \\ 0 \\ 1 \end{pmatrix}. \tag{5.17}$$

We can see, that these are all orthogonal vectors, which is also what we see in the simple Mexican hat potential, where the massless modes are in the perpendicular direction to the massive mode.

In the inhomogeneous ansatz, particularly for the chiral density wave, the story changes. Instead of having one fixed direction, we have chosen our ansatz in a way, that the massive direction changes in position space. While at $z = 0$ the massive direction coincides with the ϕ_σ condensate, at $z = \pi/2q$ it coincides with ϕ_{π_3}. This means the Goldstone mode has to be a linear combination of the two condensates.

To get an intuitive idea of how this might look like, we go back to the vector notation and write our condensate as

$$\phi_{CDW} = M \begin{pmatrix} \cos(qz) \\ 0 \\ 0 \\ \sin(qz) \end{pmatrix}. \tag{5.18}$$

Following the logic laid out for the homogeneous case, we can deduce that the Goldstone modes have to be perpendicular to our ansatz and we find

$$\phi_{\pi_1} = \begin{pmatrix} 0 \\ 1 \\ 0 \\ 0 \end{pmatrix}, \qquad \phi_{\pi_2} = \begin{pmatrix} 0 \\ 0 \\ 1 \\ 0 \end{pmatrix}, \qquad \phi_{\bar{\pi}} = \begin{pmatrix} -\sin(qz) \\ 0 \\ 0 \\ \cos(qz) \end{pmatrix}. \tag{5.19}$$

The first two are the same charged pions as before, but the third is something new, we named it $\bar{\pi}$. It is space dependent as we expected.

We can write down the corresponding vertex

$$\Gamma_{\bar{\pi}} = -\mathbb{1}\sin(qz) + i\gamma_5\tau_3\cos(qz). \tag{5.20}$$

This should be the vertex of the third Goldstone boson and in fact in the next chapter we will show that it is.

6 Mesons in the Inhomogeneous Phase

In Section 3.2.2 we have already discussed how to describe mesons in the NJL model. The same techniques are applicable here, with the additional difficulty of the momentum dependence of the propagators. In explicit diagrammatic form the Bethe-Salpeter equation is given by

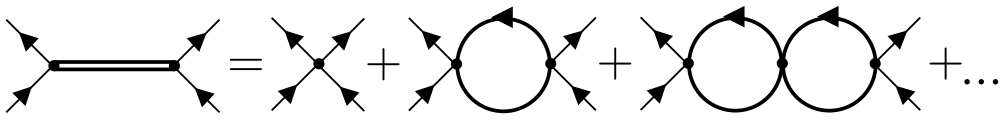

After the resummation, which is described in Appendix D.1, is complete we write down the Bethe-Salpeter equation as

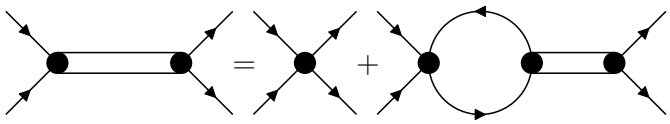

or written in terms of the scattering matrix $\hat{T}$

$$i\hat{T} = i\hat{K} + i\hat{K}\left(-i\hat{J}\right)i\hat{T}, \tag{6.1}$$

with the bare scattering kernel $\hat{K}$ and the polarization loop $\hat{J}$. These quantities are matrices in momentum space and meson type, which is spanned by the vertices. We will denote both spaces by collective indices which we will label with Greek symbols starting from α. It should be noted that in contrast to the homogeneous case, the incoming and outgoing vertices may differ. We can separate internal and external structure of the scattering kernel by writing

$$\hat{K} = \Gamma_\alpha K_{\alpha\beta} \bar{\Gamma}_\beta \tag{6.2}$$

and the same separation is possible for the scattering matrix

$$\hat{T} = -\Gamma_\alpha D_{\alpha\beta} \bar{\Gamma}_\beta \tag{6.3}$$

where we will call $D_{\alpha\beta}$ the *generalized meson propagator*. If we put this together we find

$$-\Gamma_\alpha D_{\alpha\beta}\bar{\Gamma}_\beta = \Gamma_\alpha K_{\alpha\beta}\bar{\Gamma}_\beta - \Gamma_\alpha K_{\alpha\gamma}\bar{\Gamma}_\gamma \hat{J} \Gamma_\delta D_{\delta\beta}\bar{\Gamma}_\beta. \tag{6.4}$$

We define

$$J_{\alpha\beta} := \bar{\Gamma}_\alpha \hat{J} \Gamma_\beta, \tag{6.5}$$

which allows us to write

$$-D_{\alpha\beta} = K_{\alpha\beta} - K_{\alpha\gamma} J_{\gamma\delta} D_{\delta\beta}. \tag{6.6}$$

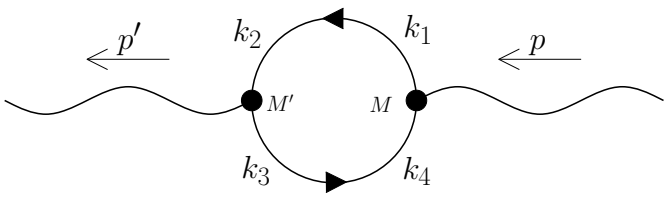

Figure 6.1.: Polarization loop in the inhomogeneous phase

Let us take a look at the individual contributions to this equation. $D_{\alpha\beta}$ is unknown and is the matrix to be determined. $K_{\alpha\beta}$, the scattering kernel, can be written as

$$K_{\alpha\beta} \equiv K_{M'M}(p',p) = 2G_S\delta_{M'M}(2\pi)^4\delta^{(4)}\left(p'-p\right), \tag{6.7}$$

with incoming momentum p and outgoing momentum p'.

The polarization loop is a more involved object, which diagrammatically is given in Figure 6.1, corresponding to $-iJ_{M'M}(p',p)$. We should note that in contrast to the scattering kernel, this object has a non-diagonal structure in momentum space, as well as in meson type. To understand this structure we can evaluate the diagram to

$$J_{M'M}(p',p) = i\left(\prod_{j=1}^{4}\int\frac{d^4k_j}{(2\pi)^4}\right)\mathrm{tr}\Big[\left(\bar{\Gamma}_{M'}(p')\right)_{k_3,k_2} iS(k_2,k_1)\left(\Gamma_M(p)\right)_{k_1,k_4} iS(k_4,k_3)\Big]. \tag{6.8}$$

The vertices we introduced here have a more complicated structure than those found in most works and Chapter 3.2.2, which stems from the additional momentum dependence of our problem. This is just a different notation, which will come in handy later. The vertices are defined by the diagrams

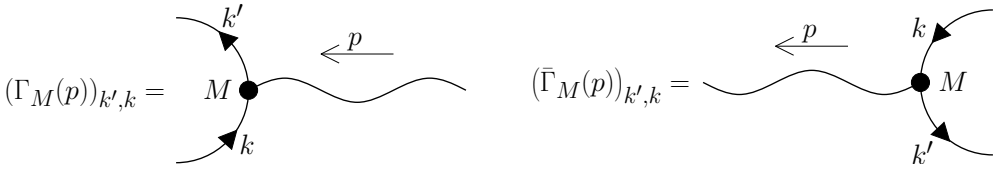

which translates from the interactions of the Lagrangian to be

$$\left(\Gamma_\sigma(p)\right)_{k',k} = \mathbb{1}(2\pi)^4\delta^{(4)}\left(k'-k-p\right), \qquad \left(\bar{\Gamma}_\sigma(p)\right)_{k',k} = \mathbb{1}(2\pi)^4\delta^{(4)}\left(k'-k+p\right), \tag{6.9}$$

$$\left(\Gamma_\pi(p)\right)_{k',k} = i\gamma_5\tau_3(2\pi)^4\delta^{(4)}\left(k'-k-p\right), \quad \left(\bar{\Gamma}_\pi(p)\right)_{k',k} = i\gamma_5\tau_3(2\pi)^4\delta^{(4)}\left(k'-k+p\right). \tag{6.10}$$

Since the polarization loop is non-diagonal in momentum space, so is Equation (6.6), which makes the evaluation of the generalized meson propagator difficult. What we want to do is find a unitary transformation that diagonalizes the equation in momentum space. We call these transformations

$$W_{\alpha\beta} \equiv W_{MM'}(p',p), \qquad W^\dagger_{\alpha\gamma}W_{\gamma\beta} = \delta_{\alpha\beta}. \tag{6.11}$$

6.1 Transformations on the Bethe-Salpeter Equation

Thanks to the unitarity of the transformation we can insert them as identities in Equation (6.6)

$$-D_{\alpha\beta} = K_{\alpha\beta} - K_{\alpha\gamma} W^{\dagger}_{\gamma\delta} W_{\delta\epsilon} J_{\epsilon\zeta} W^{\dagger}_{\zeta\eta} W_{\eta\theta} D_{\theta\beta} \tag{6.12}$$

$$-D_{\alpha\beta} = K_{\alpha\beta} - K_{\alpha\gamma} W^{\dagger}_{\gamma\delta} J'_{\delta\epsilon} W_{\epsilon\zeta} D_{\zeta\beta}, \tag{6.13}$$

where we defined

$$J'_{\alpha\beta} = W_{\alpha\gamma} J_{\gamma\delta} W^{\dagger}_{\delta\beta}. \tag{6.14}$$

To proceed, we multiply this equation with W from the left and $W^{\dagger}$ from the right and define

$$D'_{\alpha\beta} := W_{\alpha\gamma} D_{\gamma\delta} W^{\dagger}_{\delta\beta}, \tag{6.15}$$

$$K'_{\alpha\beta} := W_{\alpha\gamma} K_{\gamma\delta} W^{\dagger}_{\delta\beta} = K_{\alpha\beta}, \tag{6.16}$$

where the last equality stems from the fact that the scattering kernel is proportional to unity in meson type and momentum space. The BSE reduces to

$$-D'_{\alpha\beta} = K'_{\alpha\beta} - K'_{\alpha\gamma} J'_{\gamma\delta} D'_{\delta\beta}, \tag{6.17}$$

which closely resembles the equation before the transformation. By construction, all quantities in this equation are diagonal in momentum space. This yields a self-consistent equation for the transformed generalized meson propagator, which we will evaluate in the transformed space and can transform back after the evaluation is complete. To solve this equation we write

$$-D'_{\alpha\beta} = K'_{\alpha\beta} - K'_{\alpha\gamma} J'_{\gamma\delta} D'_{\delta\beta} \tag{6.18}$$

$$-\delta_{\alpha\delta} D'_{\delta\beta} + K'_{\alpha\gamma} J'_{\gamma\delta} D'_{\delta\beta} = K'_{\alpha\beta} \tag{6.19}$$

$$-\left(\delta_{\alpha\delta} - K'_{\alpha\gamma} J'_{\gamma\delta}\right) D'_{\delta\beta} = K'_{\alpha\beta} \tag{6.20}$$

$$D'_{\alpha\beta} = -\left(\mathbb{1} - \underline{K'}\,\underline{J'}\right)^{-1}_{\alpha\gamma} K'_{\gamma\beta}. \tag{6.21}$$

Since the expressions on the right hand side are all diagonal in momentum space, the left hand side and therefore the transformed generalized meson propagator has to be diagonal as well. The only remaining matrix structure is in the meson type (σ, π), which is just a 2x2-matrix, which can be diagonalized or inverted easily.

The components of the matrix we have to invert in the previous equation are given by

$$\delta_{M'M} - 2G_S \sum_N \int \frac{d^4k'}{(2\pi)^4}\, \delta_{M'N} (2\pi)^4 \delta^{(4)}\left(p' - k'\right) J'_{NM}(k') \tag{6.22}$$

$$= \delta_{M'M} - 2G_S J'_{M'M}(p'), \tag{6.23}$$

or in matrix form for meson type

$$2G_S \begin{pmatrix} \frac{1}{2G_S} - J'_{\sigma\sigma}(p') & -J'_{\sigma\pi}(p') \\ -J'_{\pi\sigma}(p') & \frac{1}{2G_S} - J'_{\pi\pi}(p') \end{pmatrix}. \tag{6.24}$$

So the inverse is

$$\frac{1}{2G_S}\frac{1}{\left(\frac{1}{2G_S}-J'_{\sigma\sigma}(p')\right)\left(\frac{1}{2G_S}-J'_{\pi\pi}(p')\right)-J'_{\sigma\pi}(p')J'_{\pi\sigma}(p')}\begin{pmatrix}\frac{1}{2G_S}-J'_{\pi\pi}(p') & J'_{\sigma\pi}(p')\\ J'_{\pi\sigma}(p') & \frac{1}{2G_S}-J'_{\sigma\sigma}(p')\end{pmatrix}. \quad (6.25)$$

Overall we find the transformed generalized meson propagator

$$\underline{D}'(p')=-\frac{1}{\left(\frac{1}{2G_S}-J'_{\sigma\sigma}(p')\right)\left(\frac{1}{2G_S}-J'_{\pi\pi}(p')\right)-J'_{\sigma\pi}(p')J'_{\pi\sigma}(p')}\begin{pmatrix}\frac{1}{2G_S}-J'_{\pi\pi}(p') & J'_{\sigma\pi}(p')\\ J'_{\pi\sigma}(p') & \frac{1}{2G_S}-J'_{\sigma\sigma}(p')\end{pmatrix}. \quad (6.26)$$

Alternatively, we can look at the inverse of the above expression, since in the end we are interested in its poles

$$\underline{D'}^{-1}(p')=-\begin{pmatrix}\frac{1}{2G_S}-J'_{\sigma\sigma}(p') & -J'_{\sigma\pi}(p')\\ -J'_{\pi\sigma}(p') & \frac{1}{2G_S}-J'_{\pi\pi}(p')\end{pmatrix}. \quad (6.27)$$

Now, the instrumental thing is to find the transformations and evaluate the components of the polarization loop, which we will do in the next sections.

6.2 Transformation of the Polarization Loop

In order to diagonalize the polarization loop in momentum space, we use the unitary transformation W. In the polarization loop, it only acts on the momentum and meson type dependence of the vertices. The polarization loop transforms as

$$W_{\alpha\gamma}J_{\gamma\delta}W^{\dagger}_{\delta\beta}=J'_{\alpha\beta}\equiv J'_{M'M}(p')(2\pi)^4\delta^{(4)}\left(p'-p\right), \quad (6.28)$$

where we defined

$$\begin{aligned}&J'_{M'M}(p')(2\pi)^4\delta^{(4)}\left(p'-p\right) \quad (6.29)\\ &\quad=i\left(\prod_{j=1}^{4}\int\frac{d^4k_j}{(2\pi)^4}\right)\mathrm{tr}\Big[\left(\bar{\Gamma}'_{M'}(p')\right)_{k_3,k_2}iS(k_2,k_1)\left(\Gamma'_M(p)\right)_{k_1,k_4}iS(k_4,k_3)\Big],\end{aligned}$$

with the new vertices

$$\Gamma'_\alpha=\Gamma_\beta W^{\dagger}_{\beta\alpha},\qquad \bar{\Gamma}'_\alpha=W_{\alpha\beta}\bar{\Gamma}_\beta. \quad (6.30)$$

Although not obvious from the equation, from the definition of the transformations, the polarization loop is now diagonal in momentum space, but it can still have a non-diagonal structure for the meson type. In the end, we want to diagonalize the polarization loop completely, but for now we focus only on the momentum space since we have a clear procedure to do so and work out the meson type structure later. More details of these transformations are laid out in Appendix D.2, together with the explicit form of the transformed vertices.

To find the transformations that are described in Equation (6.28) appears to be a difficult task, but since we already have some insight in how we want to proceed, we can make our life easier. To evaluate the polarization loop in Equation (6.8) we will introduce the same transformed propagators as we did in the Chapter 4, namely

$$S(p',p) = \int \frac{d^4k'}{(2\pi)^4} \int \frac{d^4k}{(2\pi)^4} U(p',k')S'(k')(2\pi)^4\delta^{(4)}\left(k'-k\right)U(k,p). \tag{6.31}$$

Using this knowledge and applying it to the polarization loop above allows us to treat the propagators as diagonal in momentum space, with the trade-off of modifying the vertices, so that they are non diagonal

$$J_{M'M}(p',p) = i\left(\prod_{j=1}^{4}\int \frac{d^4k_j}{(2\pi)^4}\right)\mathrm{tr}\Big[\left(\bar{\Gamma}_{M'}(p')\right)_{k_3,k_2} iS(k_2,k_1)\left(\Gamma_M(p)\right)_{k_1,k_4} iS(k_4,k_3)\Big] \tag{6.32}$$

$$\begin{aligned} &= i\left(\prod_{j=1}^{4}\int \frac{d^4k_j}{(2\pi)^4}\right)\left(\prod_{l=1}^{4}\int \frac{d^4r_l}{(2\pi)^4}\right)\times \\ &\quad\times \mathrm{tr}\Big[\left(\bar{\Gamma}_{M'}(p')\right)_{k_3,k_2} iU(k_2,r_2)S'(r_2,r_1)U(r_1,k_1) \\ &\quad\quad\times \left(\Gamma_M(p)\right)_{k_1,k_4} iU(k_4,r_4)S'(r_4,r_3)U(r_3,k_3)\Big] \end{aligned} \tag{6.33}$$

$$\begin{aligned} &= i\left(\prod_{j=1}^{4}\int \frac{d^4k_j}{(2\pi)^4}\right)\left(\prod_{l=1}^{4}\int \frac{d^4r_l}{(2\pi)^4}\right)\times \\ &\quad\times \mathrm{tr}\Big[U(r_3,k_3)\left(\bar{\Gamma}_{M'}(p')\right)_{k_3,k_2} iU(k_2,r_2)S'(r_2)(2\pi)^4\delta^{(4)}(r_2-r_1) \\ &\quad\quad\times U(r_1,k_1)\left(\Gamma_M(p)\right)_{k_1,k_4} iU(k_4,r_4)S'(r_4)(2\pi)^4\delta^{(4)}\left(r_4-r_3\right)\Big] \end{aligned} \tag{6.34}$$

$$\begin{aligned} &= i\left(\prod_{j=1}^{4}\int \frac{d^4r_j}{(2\pi)^4}\right)\times \\ &\quad\times \mathrm{tr}\Big[\left(\bar{\Gamma}''_{M'}(p')\right)_{r_3,r_2} iS'(r_2)(2\pi)^4\delta^{(4)}(r_2-r_1) \\ &\quad\quad\times \left(\Gamma''_M(p)\right)_{r_1,r_4} iS'(r_4)(2\pi)^4\delta^{(4)}\left(r_4-r_3\right)\Big] \end{aligned} \tag{6.35}$$

$$= i\int \frac{d^4r_2}{(2\pi)^4}\int \frac{d^4r_4}{(2\pi)^4}\,\mathrm{tr}\Big[\left(\bar{\Gamma}''_{M'}(p')\right)_{r_4,r_2} iS'(r_2)\left(\Gamma''_M(p)\right)_{r_2,r_4} iS'(r_4)\Big], \tag{6.36}$$

where we defined new vertices under the internal transformations U

$$\left(\Gamma''_M(p)\right)_{r,r'} = \int \frac{d^4k}{(2\pi)^4}\int \frac{d^4k'}{(2\pi)^4}\,U(r,k)\left(\Gamma_M(p)\right)_{k,k'}U(k',r'), \tag{6.37}$$

$$\left(\bar{\Gamma}''_M(p)\right)_{r,r'} = \int \frac{d^4k}{(2\pi)^4}\int \frac{d^4k'}{(2\pi)^4}\,U(r,k)\left(\bar{\Gamma}_M(p)\right)_{k,k'}U(k',r'). \tag{6.38}$$

It is noteworthy that the transformations U only act on the internal momenta of the polarization loop, the ones indicated by the subscripts in the vertices. The transformations W, which we want to act on the vertices, only act on the external momenta, to make the vertices diagonal in momentum space.

If we take the polarization loop now, the double primed vertices are the only thing not diagonal in momentum space. Since the original vertices had diagonal momentum space structure, one possibility is a transformation that counteracts the U transformations. If we can find a transformation that has the following properties

$$\left(\Gamma'_M(p)\right)_{k',k} = \sum_N \int \frac{d^4s}{(2\pi)^4} \left(\Gamma_N(s)\right)_{k',k} W^\dagger_{NM}(s,p) \tag{6.39}$$

$$\stackrel{!}{=} \int \frac{d^4r'}{(2\pi)^4} \int \frac{d^4r}{(2\pi)^4} U^\dagger(k',r') \left(\Gamma_M(p)\right)_{r',r} U^\dagger(r,k), \tag{6.40}$$

$$\left(\bar\Gamma'_M(p)\right)_{k',k} = \sum_N \int \frac{d^4s}{(2\pi)^4} W_{MN}(p,s) \left(\bar\Gamma_M(s)\right)_{k',k} \tag{6.41}$$

$$\stackrel{!}{=} \int \frac{d^4r'}{(2\pi)^4} \int \frac{d^4r}{(2\pi)^4} U^\dagger(k',r') \left(\bar\Gamma_M(p)\right)_{r',r} U^\dagger(r,k), \tag{6.42}$$

the desired structure will emerge naturally from the unitarity of the transformations U. This implies, that the doubly primed vertices should relate to the original ones

$$\left(\bar\Gamma''_{M'}(p')\right)_{r',r} = \left(\bar\Gamma_{M'}(p')\right)_{r',r}, \qquad \left(\Gamma''_M(p)\right)_{r',r} = \left(\Gamma_M(p)\right)_{r',r}. \tag{6.43}$$

The transformed vertices read in terms of the original ones, suppressing the internal momenta for the moment, since they do not change

$$\Gamma'_\sigma(p) = \frac{1}{2}\left[\Gamma_\sigma(p-q) + \Gamma_\sigma(p+q) - i\Gamma_\pi(p-q) + i\Gamma_\pi(p+q)\right], \tag{6.44}$$

$$\bar\Gamma'_\sigma(p') = \frac{1}{2}\left[\bar\Gamma_\sigma(p'-q) + \bar\Gamma_\sigma(p'+q) + i\bar\Gamma_\pi(p'-q) - i\bar\Gamma_\pi(p'+q)\right], \tag{6.45}$$

$$\Gamma'_\pi(p) = \frac{1}{2}\left[i\Gamma_\sigma(p-q) - i\Gamma_\sigma(p+q) + \Gamma_\pi(p-q) + \Gamma_\pi(p+q)\right], \tag{6.46}$$

$$\bar\Gamma'_\pi(p') = \frac{1}{2}\left[-i\bar\Gamma_\sigma(p'-q) + i\bar\Gamma_\sigma(p'+q) + \bar\Gamma_\pi(p'-q) + \bar\Gamma_\pi(p'+q)\right], \tag{6.47}$$

which makes the problem of finding the appropriate transformations W a simple task of solving a linear system of equations

$$\left(\bar\Gamma'_M(p)\right)_{k',k} = \sum_N \int \frac{d^4r}{(2\pi)^4} W_{MN}(p,r) \left(\bar\Gamma_N(r)\right)_{k',k}, \tag{6.48}$$

$$\left(\Gamma'_M(p)\right)_{k',k} = \sum_N \int \frac{d^4r}{(2\pi)^4} \left(\Gamma_N(r)\right)_{k',k} W^\dagger_{NM}(r,p). \tag{6.49}$$

The resulting transformations in components are

$$W_{\sigma\sigma}(p',k) = W_{\pi\pi}(p',k) = \frac{1}{2}\left[(2\pi)^4\delta^{(4)}\left(p'+q-k\right) + (2\pi)^4\delta^{(4)}\left(p'-q-k\right)\right], \tag{6.50}$$

$$W_{\sigma\pi}(p',k) = \left(W_{\pi\sigma}(p',k)\right)^* = \frac{i}{2}\left[-(2\pi)^4\delta^{(4)}\left(p'+q-k\right) + (2\pi)^4\delta^{(4)}\left(p'-q-k\right)\right] \tag{6.51}$$

and

$$W^{\dagger}_{\sigma\sigma}(k,p) = W^{\dagger}_{\pi\pi}(k,p) = \frac{1}{2}\left[(2\pi)^4\delta^{(4)}(p+q-k) + (2\pi)^4\delta^{(4)}(p-q-k)\right], \tag{6.52}$$

$$W^{\dagger}_{\sigma\pi}(k,p) = \left(W^{\dagger}_{\pi\sigma}(k,p)\right)^* = \frac{i}{2}\left[-(2\pi)^4\delta^{(4)}(p+q-k) + (2\pi)^4\delta^{(4)}(p-q-k)\right]. \tag{6.53}$$

The unitarity of these transformations can easily be checked

$$WW^{\dagger} \equiv \sum_N \int \frac{d^4k}{(2\pi)^4}\, W_{M'N}(p',k) W^{\dagger}_{NM}(k,p) = \delta_{M'M}(2\pi)^4\delta^{(4)}\left(p'-p\right). \tag{6.54}$$

We can apply these transformations on the polarization loop

$$J'_{M'M}(p',p) = \sum_{N'N} \int \frac{d^4r'}{(2\pi)^4} \int \frac{d^4r}{(2\pi)^4}\, W_{M'N'}(p',r') J_{N'N}(r',r) W^{\dagger}_{NM}(r,p) \tag{6.55}$$

$$= i\left(\prod_{j=1}^{4} \int \frac{d^4k_j}{(2\pi)^4}\right) \mathrm{tr}\left[\left(\bar{\Gamma}'_{M'}(p')\right)_{k_3,k_2} iS(k_2,k_1)\left(\Gamma'_M(p)\right)_{k_1,k_4} iS(k_4,k_3)\right] \tag{6.56}$$

and we will see in Section 6.3 that we obtain the desired result.

6.3 Evaluating the Polarization Loop

In this section we try to compress a very lengthy and complex calculation into a compact form. For this reason a lot of abbreviations have been used. Although they are explained when they first appear, in Appendix D.4 we give a complete list in one page for the reader's convenience.

We want to start from the expression of the transformed polarization loop, which resembles the general one as given in equation (6.8), although with the transformed vertices

$$J'_{M'M}(p',p) = i\left(\prod_{j=1}^{4} \int \frac{d^4k_j}{(2\pi)^4}\right) \mathrm{tr}\left[\left(\bar{\Gamma}'_{M'}(p')\right)_{k_3,k_2} iS(k_2,k_1)\left(\Gamma'_M(p)\right)_{k_1,k_4} iS(k_4,k_3)\right]. \tag{6.57}$$

Now we insert the transformations for the propagators (4.25) and find that

$$\int \frac{d^4k_3}{(2\pi)^4} \int \frac{d^4k_2}{(2\pi)^4}\, U(r_3,k_3)\left(\bar{\Gamma}'_{M'}(p')\right)_{k_3,k_2} U(k_2,r_1) = \left(\bar{\Gamma}_{M'}(p')\right)_{r_3,r_1}, \tag{6.58}$$

$$\int \frac{d^4k_1}{(2\pi)^4} \int \frac{d^4k_4}{(2\pi)^4}\, U(r_1,k_1)\left(\Gamma'_M(p)\right)_{k_1,k_4} U(k_4,r_3) = \left(\Gamma_M(p)\right)_{r_1,r_3}. \tag{6.59}$$

After evaluating all possible remaining delta-functions, which in detail can be found in Appendix D.3, and integrals in the polarization loop, the expression yields

$$J'_{M'M}(p',p) = i\int \frac{d^4k}{(2\pi)^4}\, \mathrm{tr}\left[\Gamma_{M'} iS'(k+p')\Gamma_M iS'(k)\right](2\pi)^4\delta^{(4)}\left(p'-p\right) \tag{6.60}$$

$$=: J'_{M'M}(p')(2\pi)^4\delta^{(4)}\left(p'-p\right), \tag{6.61}$$

where Γ_M and $\Gamma_{M'}$ are the vertices without any momentum dependence, namely just $\mathbb{1}$ and $i\gamma_5\tau_3$. We see, that this expression is indeed diagonal in momentum space, as signified by the delta-function, just as we intended. As mentioned earlier, this expression is not diagonal in the meson type, due to the more complicated Dirac structure compared to the homogeneous case, mixed traces do not vanish. We are left with the task to evaluate four different traces, which with our knowledge of the structure of the propagator (4.23) is straightforward. For the sake of readability we choose a matrix notation for the full polarization loop, so that

$$\underline{J}'(p') = \begin{pmatrix} J'_{\sigma\sigma}(p') & J'_{\sigma\pi}(p') \\ J'_{\pi\sigma}(p') & J'_{\pi\pi}(p') \end{pmatrix}. \tag{6.62}$$

After careful evaluation of the four traces, details in Appendix D.3, we find

$$\underline{J}'(p') = i \int \frac{d^4k}{(2\pi)^4} \frac{4}{N(k+p')N(k)} \begin{pmatrix} -(f_{ABE} + f_{CD}) & -ig_{CD} \\ ig_{CD} & f_{ABE} - f_{CD} \end{pmatrix}, \tag{6.63}$$

with

$$f_{ABE} = A(k+p')A(k) + B(k+p')B(k) + E^{\mu}_{\ \nu}(k+p')E_{\mu}^{\ \nu}(k), \tag{6.64}$$
$$f_{CD} = C^{\mu}(k+p')C_{\mu}(k) - D^{\mu}(k+p')D_{\mu}(k), \tag{6.65}$$
$$g_{CD} = C^{\mu}(k+p')D_{\mu}(k) - D^{\mu}(k+p')C_{\mu}(k). \tag{6.66}$$

This lends itself to a redefinition of the functions in the transformed polarization loop as

$$\underline{J}'(p') = \begin{pmatrix} J'_{\sigma\sigma}(p') & -iJ'_X(p') \\ iJ'_X(p') & J'_{\pi\pi}(p') \end{pmatrix}. \tag{6.67}$$

In addition we will write some of the lengthy expressions, that are not necessary at a given point in the calculations as $\underline{j_i}$ and give them increasing numbers every time something has changed. They can be found in Appendix D.4, the first one is

$$\underline{j_1}(k,p) = \begin{pmatrix} -(f_{ABE} + f_{CD}) & -ig_{CD} \\ ig_{CD} & f_{ABE} - f_{CD} \end{pmatrix}. \tag{6.68}$$

It is useful to note, that the denominators of all elements of the polarization loop matrix are the same, which means they can be evaluated in a similar fashion. The next step is to evaluate the above expressions in the medium. This is done by introducing the Matsubara formalism, as we did in Section 4.3 and replace the zero components of the momenta

$$k_0 \to i\omega_n + \mu, \qquad \omega_n = (2n+1)\pi T, \tag{6.69}$$
$$p'_0 \to i\omega_m, \qquad \omega_m = 2m\pi T, \tag{6.70}$$

where we use fermionic Matsubara frequencies for the internal momentum and bosonic Matsubara frequencies for the external momenta. To evaluate the Matsubara sum we make use of the residue theorem, similar to the gap equation, where we described the method in more

detail in Appendix C.3. The resulting Fermi distributions are periodic in the bosonic Matsubara frequencies which allows to set

$$n_F(i\omega_m + x) = \frac{1}{1+\exp\left((i\omega_m + x)/T\right)} = \frac{1}{1+\exp\left(x/T\right)} = n_F(x). \tag{6.71}$$

We make an analytic continuation from the bosonic Matsubara frequencies to p_0' and apply a partial fraction decomposition in p_0'. Finally we arrive at

$$\underline{J}'(p') = \sum_{\pm\pm\pm\pm} \int \frac{d^3k}{(2\pi)^3} \frac{1 - n_F(E_{k,\pm}+\mu) - n_F(E_{k,\pm}-\mu)}{-E_{p,\pm} \pm (E_{k,\pm} \pm p_0')} \underline{j_2}_{\pm,\pm,\pm}(\vec{k},\vec{p}'). \tag{6.72}$$

Here we abridged the eigenvalues of the Hamiltonian, see equation (4.12) for readability

$$E_{k,\pm} := E_{\pm}(\vec{k}), \qquad E_{p,\pm} := E_{\pm}(\vec{k}+\vec{p}') \tag{6.73}$$

and the complicated function $\underline{j_2}(\vec{k},\vec{p})$, which is still a matrix in meson type and can be found in more detail in Appendix D.4. Taking care of the different possible signs inside the eigenvalues $(\pm,\pm)$, the different signs from the residues $(\pm)$ and the sign from the partial fraction decomposition $(\pm)$, we have 16 different expressions we have to sum over, which is expressed by the sum $\sum_{\pm\pm\pm\pm}$ in front of the integral. The integrand still has poles over the integration range, which gives rise to an imaginary part. We can identify the location of the poles, for example in terms of $k_\perp$ when working in cylindrical coordinates

$$k_\perp\Big|_{\text{pole}} = \frac{-(p_3^2 + \epsilon_{k,\pm}^2 - \epsilon_{p,\pm}^2)p_\perp \cos\theta \pm \sqrt{p_0^2\left((p_3^2+\epsilon_{k,\pm}^2-\epsilon_{p,\pm}^2)^2 - 4\epsilon_{k,\pm}^2(p_0^2 - p_\perp^2\cos^2\theta)\right)}}{2(p_0^2 - p_\perp^2\cos^2\theta)}, \tag{6.74}$$

with

$$\epsilon_{k,\pm} = E_{k,\pm}(k_\perp = 0), \qquad \epsilon_{p,\pm} = E_{p,\pm}(k_\perp = p_\perp = 0). \tag{6.75}$$

The numerically most reliable way to proceed is to calculate the imaginary part of the polarization loop and get the real part via the Kramers-Kronig relation [83, 84]

$$\mathrm{Re}\left(\underline{J}'(p_0,\vec{p})\right) = \frac{1}{\pi}\mathrm{PV}\int_{-\infty}^{\infty} d\omega \frac{\mathrm{Im}\left(\underline{J}'(\omega,\vec{p})\right)}{\omega - p_0}, \tag{6.76}$$

where PV$(\cdot)$ stands for the Cauchy principal value. To calculate the imaginary part we use the Sokhotski-Plemelj theorem [85, 86], which for our case states

$$\lim_{\varepsilon\to 0} \mathrm{Im}\left(\frac{1}{x \pm i\varepsilon}\right) = \mp\pi\delta(x). \tag{6.77}$$

6.3.1 Evaluating the Imaginary Part

As mentioned above, we want to calculate the polarization loop via its imaginary part. We start off from equation (6.72). We emphasize the complex nature of this expression, by adding an imaginary constant $i\epsilon$ to p_0', which we will sent to zero later on

$$\underline{J}'(p') = \sum_{\pm\pm\pm\pm} \int \frac{d^3k}{(2\pi)^3} \frac{1}{-E_{p,\pm} \pm (E_{k,\pm} \pm p_0' \pm i\epsilon)} \underline{j_3}_{\pm\pm\pm}(\vec{k}, \vec{p}'). \tag{6.78}$$

The imaginary part of this expression can be deduced from the aforementioned Sokhotski-Plemelj theorem

$$\begin{aligned} \mathrm{Im}\left(\underline{J}'(p')\right) &= \lim_{\epsilon\to 0} \sum_{\pm\pm\pm\pm} \int \frac{d^3k}{(2\pi)^3} \mathrm{Im}\left(\frac{1}{-E_{p,\pm} \pm (E_{k,\pm} \pm p_0' \pm i\epsilon)} \underline{j_3}_{\pm\pm\pm}(\vec{k}, \vec{p}') \right) && (6.79) \\ &= -\pi \sum_{\pm\pm\pm\pm} \sigma_{\pm\pm} \int \frac{d^3k}{(2\pi)^3} \underline{j_3}_{\pm\pm\pm}(\vec{k}, \vec{p}') \delta\left(-E_{p,\pm} \pm (E_{k,\pm} \pm p_0')\right), && (6.80) \end{aligned}$$

where σ_x denotes the sign of the argument x. Since in this case $\pm$ and $\pm$ are just signs on their own, we can write them in front of the expression and write the integral over momentum space in cylindrical coordinates

$$\begin{aligned} \mathrm{Im}\left(\underline{J}'(p')\right) = -\pi \sum_{\pm\pm\pm\pm} \int_{-\infty}^{\infty} \frac{dk_z}{(2\pi)^3} \int_0^{\infty} dk_\perp \, k_\perp \int_{-\pi}^{\pi} d\theta \, (\pm\pm \underline{j_3}_{\pm\pm\pm}(k_z, k_\perp, \cos\theta, \vec{p}')) \\ \times \delta\left(-E_{p,\pm} \pm (E_{k,\pm} \pm p_0')\right). \end{aligned} \tag{6.81}$$

To evaluate the delta distribution we want to substitute the different integration variables with the two different energies. In order to do so an intermediate step is helpful where we substitute $\cos\theta$

$$\int_{-\pi}^{\pi} d\theta \, f(\cos\theta) = 2 \int_{-1}^{1} dc \frac{f(c)}{\sqrt{1-c^2}} =: 2 \int_{-1}^{1} dc f(c) g(c). \tag{6.82}$$

To keep track of the integration boundaries we introduce θ-functions to limit them and allow us to expand the integration domain to the whole real line for all variables. In addition we want to introduce θ-functions that constrain our energies $E_{k,\pm}$ and $E_{p,\pm}$ to positive values. This of course is always implied, but the additional functions help greatly to keep track of this fact and this method of notation is less error prone. The imaginary part of the polarization loop reads

$$\begin{aligned} \mathrm{Im}\left(\underline{J}'(p')\right) = -2\pi \sum_{\pm\pm\pm\pm} \int_{-\infty}^{\infty} \frac{dk_z}{(2\pi)^3} \int_{-\infty}^{\infty} dk_\perp \, k_\perp \int_{-\infty}^{\infty} dc \, [\pm\pm \underline{j_3}_{\pm\pm\pm}(k_z, k_\perp, c, \vec{p}') g(c)] \\ \times \delta\left(-E_{p,\pm} \pm (E_{k,\pm} \pm p_0')\right) \theta(E_{k,\pm}) \theta(E_{p,\pm}) \theta(c+1) \theta(1-c) \theta(k_\perp). \end{aligned} \tag{6.83}$$

Now we want to substitute c with $E_{p,\pm}$ and $k_\perp$ with $E_{k,\pm}$ in the following way

$$\begin{aligned} E_{k,\pm} &= \sqrt{k_\perp^2 + \epsilon_{k,\pm}^2}, & E_{p,\pm} &= \sqrt{k_\perp^2 + {p'_\perp}^2 + 2k_\perp p'_\perp c + \epsilon_{p,\pm}^2}, \\ dk_\perp &= \frac{E_{k,\pm}}{k_\perp} dE_{k,\pm}, & dc &= \frac{E_{p,\pm}}{k_\perp p'_\perp} dE_{p,\pm}, \\ k_\perp &= \sqrt{E_{k,\pm}^2 - \epsilon_{k,\pm}^2}, & c &= \frac{E_{p,\pm}^2 - k_\perp^2 - {p'_\perp}^2 - \epsilon_{p,\pm}^2}{2k_\perp p'_\perp} \\ & & &= \frac{E_{p,\pm}^2 - E_{k,\pm}^2 - {p'_\perp}^2 + \epsilon_{k,\pm}^2 - \epsilon_{p,\pm}^2}{2p'_\perp \sqrt{E_{k,\pm}^2 - \epsilon_{k,\pm}^2}}, \end{aligned} \tag{6.84}$$

with the shorthand notation

$$\epsilon_{k,\pm} := E_{k,\pm}(k_\perp = 0) = \sqrt{k_z^2 + Q^2 + M^2 \pm 2Q\sqrt{k_z^2 + M^2}}, \tag{6.85}$$

$$\epsilon_{p,\pm} := E_{p,\pm}(k_\perp = p'_\perp = 0) = \sqrt{(k_z + p'_z)^2 + Q^2 + M^2 \pm 2Q\sqrt{(k_z + p'_z)^2 + M^2}}. \tag{6.86}$$

All of this results in rather lengthy expressions, more suited for the Appendix D.5. The next step is to evaluate the integral over $E_{p,\pm}$ in order to eliminate the δ-function. After that we can rearrange the θ-functions and separate the integral over $E_{k,\pm}$. This results in

$$\begin{aligned} \mathrm{Im}\left(\underline{J}'(p')\right) = -2 \sum_{\pm\pm} \int_{-\infty}^{\infty} dk_z \underline{j_4}_{\pm\pm}(k_z, (p'_0, \vec{p}\,')) \\ \times \left[\sum_{\pm\pm} \int dE_{k,\pm} (\pm\pm\pm\pm) \frac{1 - n_F(E_{k,\pm} - \mu) - n_F(E_{k,\pm} + \mu)}{\sqrt{-4p_3^2\left((E_{k,\pm} \pm \alpha)^2 - \beta^2\right)}} \Xi_{\pm\pm}(E_{k,\pm}) \right]. \end{aligned} \tag{6.87}$$

The abbreviations introduced here, are

$$p_3^2 = {p'_0}^2 - {p'_\perp}^2, \tag{6.88}$$

$$\alpha = \frac{p'_0}{2p_3^2}(p_3^2 + \Delta\epsilon), \tag{6.89}$$

$$\beta = \sqrt{\frac{{p'_\perp}^2}{4p_3^2}\left[\frac{(p_3^2 + \Delta\epsilon)^2}{p_3^2} - 4\epsilon_{k,\pm}^2\right]}, \tag{6.90}$$

$$\Delta\epsilon = \epsilon_{k,\pm}^2 - \epsilon_{p,\pm}^2 \tag{6.91}$$

and Ξ containing all the remaining θ-functions

$$\begin{aligned} \Xi_{\pm\pm}(E_{k,\pm}) = \theta(\mp)\Big[\theta(p_3^2)\theta(\mp p'_0)\theta(p_3^2 - (\epsilon_{k,\pm} + \epsilon_{p,\pm})^2)\chi_{[\mp\alpha-\beta, \mp\alpha+\beta]}(E_{k,\pm})\Big] \\ + \theta(\pm)\Big[\theta(p_3^2)\Big\{\theta(\pm p'_0)\theta(\epsilon_{p,\pm} - \epsilon_{k,\pm} - |p_3|) \\ + \theta(\mp p'_0)\theta(\epsilon_{k,\pm} - \epsilon_{p,\pm} - |p_3|)\Big\}\chi_{[\mp\alpha-\beta, \mp\alpha+\beta]}(E_{k,\pm}) \\ + \theta(-p_3^2)\chi_{[\mp\alpha+\beta, \infty]}(E_{k,\pm})\Big]. \end{aligned} \tag{6.92}$$

We can perform the vacuum part of the inner integral in equation (6.87) analytically

$$\begin{aligned}
&\sum_{\pm\pm}\int dE_{k,\pm}(\pm\pm\pm\pm)\frac{1}{\sqrt{-4p_3^2\left((E_{k,\pm}\pm\alpha)^2-\beta^2\right)}}\Xi_{\pm\pm}(E_{k,\pm})\\
&=-\sigma(p_0')\frac{\pm\pm\pi}{2\sqrt{p_3^2}}\theta(p_3^2)\Big[\theta(\epsilon_{k,\pm}-\epsilon_{p,\pm}-\sqrt{p_3^2})-\theta(\epsilon_{p,\pm}-\epsilon_{k,\pm}-\sqrt{p_3^2})\\
&\qquad-\theta(p_3^2-(\epsilon_{k,\pm}+\epsilon_{p,\pm})^2)\Big].
\end{aligned}\tag{6.93}$$

The vacuum part has no contributions from $p_3^2<0$.
In the special case of $T=0$ we can solve the integrals for the medium part as well. The Fermi distributions reduce to

$$n_F(E_{k,\pm}-\mu)+n_F(E_{k,\pm}+\mu)\overset{T\to 0}{=}\theta(\mu-E_{k,\pm}),\tag{6.94}$$

which allows us to perform the integral

$$\sum_{\pm\pm}\int dE_{k,\pm}(\pm\pm\pm\pm)\frac{\theta(\mu-E_{k,\pm})}{\sqrt{-4p_3^2\left((E_{k,\pm}\pm\alpha)^2-\beta^2\right)}}\Xi_{\pm\pm}(E_{k,\pm})\tag{6.95}$$

$$=\theta(-p_3^2)\sum_{\pm}\frac{(\pm\pm\pm)}{2\sqrt{-p_3^2}}\log\left(\frac{\pm\alpha+\mu+\sqrt{(\pm\alpha+\mu)^2-\beta^2}}{\beta}\right)\theta(\pm\alpha+\mu-\beta)\tag{6.96}$$

$$\begin{aligned}
&+\theta(p_3^2)\sum_{\pm\pm}\frac{(\pm\pm\pm\pm)}{2\sqrt{p_3^2}}\Big[\frac{\pi}{2}\left[\theta(\mu\pm\alpha+\beta)+\theta(\mu\pm\alpha-\beta)\right]\\
&\qquad+\arctan\left(\frac{\mu\pm\alpha}{\sqrt{\beta^2-(\mu\pm\alpha)^2}}\right)\theta(\beta^2-(\mu\pm\alpha)^2)\Big]\\
&\times\Big[\theta(\pm)\left(\theta(\mp p_0)\theta(\epsilon_{k,\pm}-\epsilon_{p,\pm}-|p_3|)+\theta(\pm p_0)\theta(\epsilon_{p,\pm}-\epsilon_{k,\pm}-|p_3|)\right)\\
&\quad+\theta(\mp)\theta(\mp p_0)\theta(p_3^2-(\epsilon_{k,\pm}+\epsilon_{p,\pm})^2)\Big]
\end{aligned}$$

The details on how to arrive at the integrals is given in Appendix D.6.

6.3.2 Regularization of the Polarization Loop

As we already mentioned in Section 3.4, we have to do a little more work, to properly regularize the integrals in the polarization loop. The straightforward idea to just regularize the mass would render the integral finite, but since it is not applicable to the gap equation, it would leave us with inconsistent results. The regularization of the energies, which we applied for the gap equation, is also difficult, since we chose $E_{k,\pm}$ and $E_{p,\pm}$ as integration variables, when we evaluated the imaginary part.

Instead we chose to regularize the energies before the substitution. This effectively regularizes the reduced energies, so that we end up with

$$\epsilon_{k,\pm}\to\epsilon_{k,\pm,j}=\sqrt{\epsilon_{k,\pm}^2+j\Lambda^2},\qquad \epsilon_{p,\pm}\to\epsilon_{p,\pm,j}=\sqrt{\epsilon_{p,\pm}^2+j\Lambda^2}.\tag{6.97}$$

In addition we have found, that in order to stay consistent with the homogeneous numerical results only the energy integral, Equation (6.93), should be regularized.

This ensures that all limits we can show analytically, directly from the traces and the four-momentum representation of the propagators, which is shown in the following sections, are respected by our regularization scheme.

6.4 Diagonalization in Meson Type

So far we have diagonalized the polarization loop in momentum space, but left the non-diagonal structure in the meson type as it is. However this is a simple two by two matrix structure which we can easily diagonalize analytically, but the expressions for the polarization loop become more involved. So instead we do this after having calculated the polarization loop in its form from the previous section.

We start from the form given in Equation (6.67), where we introduce an additional shorthand for better readability

$$\underline{J}'(p') = \begin{pmatrix} J'_{\sigma\sigma}(p') & -iJ'_X(p') \\ iJ'_X(p') & J'_{\pi\pi}(p') \end{pmatrix} =: \begin{pmatrix} \sigma & -ix \\ ix & \pi \end{pmatrix}. \tag{6.98}$$

The eigenvalues are simply the eigenvalues of the two by two matrix and in matrix form

$$\underline{J}''(p') = \frac{1}{2}\begin{pmatrix} \sigma+\pi-\sqrt{(\pi-\sigma)^2+4x^2} & 0 \\ 0 & \sigma+\pi+\sqrt{(\pi-\sigma)^2+4x^2} \end{pmatrix}, \tag{6.99}$$

where $\underline{J}'' = V^\dagger \underline{J}' V$. The transformations V are given by the normalized eigenvectors and can be written as

$$V = \begin{pmatrix} \frac{i}{2x}\frac{\pi-\sigma+\sqrt{(\pi-\sigma)^2+4x^2}}{\sqrt{1+\frac{1}{4x^2}\left(\pi-\sigma+\sqrt{(\pi-\sigma)^2+4x^2}\right)^2}} & \frac{i}{2x}\frac{\pi-\sigma-\sqrt{(\pi-\sigma)^2+4x^2}}{\sqrt{1+\frac{1}{4x^2}\left(\pi-\sigma-\sqrt{(\pi-\sigma)^2+4x^2}\right)^2}} \\ \frac{1}{\sqrt{1+\frac{1}{4x^2}\left(\pi-\sigma+\sqrt{(\pi-\sigma)^2+4x^2}\right)^2}} & \frac{1}{\sqrt{1+\frac{1}{4x^2}\left(\pi-\sigma-\sqrt{(\pi-\sigma)^2+4x^2}\right)^2}} \end{pmatrix}. \tag{6.100}$$

Since the transformations are again unitary, we can easily write down the transformed Bethe-Salpeter equation

$$-D''_{\alpha\beta} = K''_{\alpha\beta} - K''_{\alpha\gamma} J''_{\gamma\delta} D''_{\delta\beta}, \tag{6.101}$$

where we defined

$$D''_{\alpha\beta} = V^\dagger_{\alpha\gamma} D'_{\gamma\delta} V_{\delta\beta}, \tag{6.102}$$

$$K''_{\alpha\beta} = V^\dagger_{\alpha\gamma} K'_{\gamma\delta} V_{\delta\beta} = K_{\alpha\beta}. \tag{6.103}$$

Alternatively we can start directly from the inverted generalized meson propagator in Equation (6.27)

$$\underline{D}''^{-1}(p') = \underline{V}^\dagger \underline{D}'^{-1}(p') \underline{V} = \underline{V}^\dagger \begin{pmatrix} \frac{1}{2G_S}-\sigma & ix \\ -ix & \frac{1}{2G_S}-\pi \end{pmatrix} V \tag{6.104}$$

$$= \frac{1}{2G_S} - \frac{1}{2}\begin{pmatrix} \sigma+\pi-\sqrt{(\pi-\sigma)^2+4x^2} & 0 \\ 0 & \sigma+\pi+\sqrt{(\pi-\sigma)^2+4x^2} \end{pmatrix}. \tag{6.105}$$

We write the eigenvalues as

$$D''^{-1}_{\pm}(p') = \frac{1}{2G_S} - \frac{1}{2}\Big[J'_{\sigma\sigma}(p') + J'_{\pi\pi}(p') \pm \sqrt{(J'_{\sigma\sigma}(p') - J'_{\pi\pi}(p'))^2 - 4J'^2_X(p')}\Big]. \tag{6.106}$$

Ultimately, these eigenvalues give us the poles for the generalized meson propagator and we will use them in our numerical calculations in the next sections.

6.5 Homogeneous Limit

Since all these expressions are quite complicated, one should consider the limit to the homogeneous expressions to make sure no errors have been made. This limit is reached by sending Q to zero.

We can start directly from the traces in Equation (6.63). The off-diagonal traces vanish, since for $Q = 0$ $D_\mu(k)$, from the definition of the propagator (4.23), vanishes. The mesons decouple and we can write

$$J'_{\sigma\sigma}(p') = 4N_f N_c \int \frac{d^4k}{(2\pi)^4} \frac{k^2 + k\cdot p' + M^2}{(k^2 - M^2)((k+p')^2 - M^2)}, \tag{6.107}$$

$$J'_{\pi\pi}(p') = -4N_f N_c \int \frac{d^4k}{(2\pi)^4} \frac{k^2 + k\cdot p' - M^2}{(k^2 - M^2)((k+p')^2 - M^2)}, \tag{6.108}$$

which is the same result we got from the homogeneous traces, compare Appendix B.2.1.

This shows that the starting point obeys the limits to the homogeneous phase and in the next sections we will use this limit as a test to show our derivations and numerical calculations are correct.

6.6 Calculating the Goldstone Boson

To calculate the Goldstone boson, we are interested in the on-shell energies, for which the generalized meson propagator we constructed in this chapter exhibits a pole. The condition is

$$D'^{-1}(p'_0, \vec{p}' = 0) = 0. \tag{6.109}$$

For the Goldstone mode it should be $p'_0 = 0$ everywhere where the chiral symmetry is broken. We take the limit

$$\lim_{p'\to 0} D'^{-1}(p') = \lim_{p'\to 0} \begin{pmatrix} \frac{1}{2G_S} - J'_{\sigma\sigma}(p') & iJ'_X(p') \\ -iJ'_X(p') & \frac{1}{2G_S} - J'_{\pi\pi}(p') \end{pmatrix} = \begin{pmatrix} \frac{1}{2G_S} - J'_{\sigma\sigma}(0) & 0 \\ 0 & \frac{1}{2G_S} - J'_{\pi\pi}(0) \end{pmatrix}. \tag{6.110}$$

The first thing to note here is that the off-diagonal meson type components vanish, so we do not have to concern us with mixing of flavors for this discussion. As mentioned in the previous chapter, the $\pi\pi$-component should give us the Goldstone boson, so we will focus on that.

We can write down the expression

$$\frac{1}{2G_S} - J'_{\pi\pi}(0) = \frac{1}{2G_S} + 4iN_f N_c \int \frac{d^4k}{(2\pi)^4} \frac{k^2 - M^2 + Q^2}{(k^2 - Q^2 - M^2)^2 + 4Q^2M^2 - 4(k_z Q)^2} = 0. \tag{6.111}$$

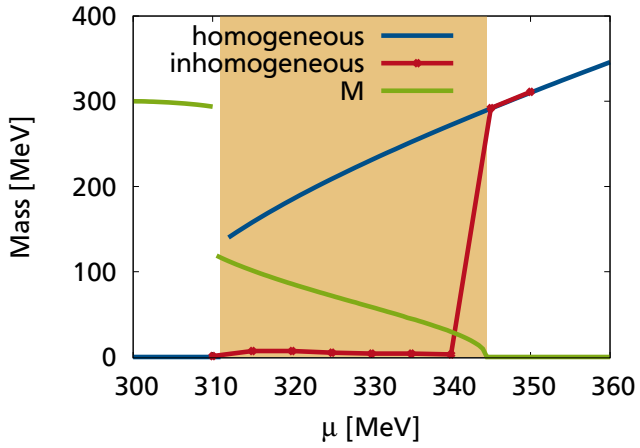

Figure 6.2.: Mass of the Goldstone boson as a function of chemical potential at vanishing temperature. The homogeneous solution, which is given by the neutral pion, is blue, while the inhomogeneous solution is red. In green the mass amplitude of the quark is given for reference and the inhomogeneous region is shaded orange.

This formula is familiar, it closely resembles the trace in the gap equation in the form of Equation (4.35). We can rewrite this as

$$4iN_fN_c\int\frac{d^4k}{(2\pi)^4}\frac{k^2-M^2+Q^2}{(k^2-Q^2-M^2)^2+4Q^2M^2-4(k_zQ)^2}=i\frac{1}{M}\int\frac{d^4k}{(2\pi)^4}\,\mathrm{tr}[S'(k)]. \tag{6.112}$$

Rewriting the condition in Equation (6.111) yields

$$\frac{1}{2G_S}-i\frac{1}{M}\int\frac{d^4k}{(2\pi)^4}\,\mathrm{tr}[S'(k)]=0 \tag{6.113}$$

$$1-2iG_S\frac{1}{M}\int\frac{d^4k}{(2\pi)^4}\,\mathrm{tr}[S'(k)]=0, \tag{6.114}$$

which is just the gap equation, compare Equation (4.32), divided by the mass amplitude M. This means the condition is fulfilled wherever the gap equation yields a non-trivial solution. Therefore whenever the chiral symmetry is spontaneously broken, we have a massless mode, described by the $J'_{\pi\pi}$ component.

This is exactly what is stated in the Goldstone theorem, therefore we have found the Goldstone boson.

After having shown this, we want to use it as a benchmark for our numerics. We calculated the left side of Equation (6.109) as a function of p'_0 at vanishing external three momentum and present the first zero crossing in Figure 6.2 as a function of μ for vanishing temperatures. The red dots and line indicate the inhomogeneous solution, while the blue line shows the homogeneous solution for m_π as a reference. Here we see the expected behavior. In the homogeneous broken phase, our solution is degenerate with the one from the homogeneous ansatz and both are zero. In the inhomogeneous broken phase the solution remains zero, with some errors, but it is clearly distinct from the homogeneous ansatz, that is already in the restored phase. In the restored phase, the inhomogeneous solution is degenerate with the homogeneous ansatz once more and the pion acquires mass.

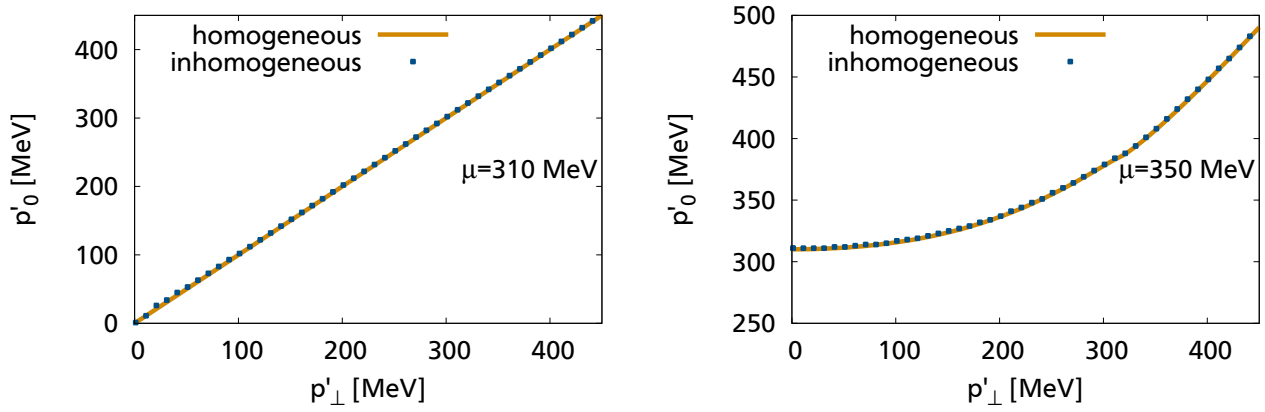

Figure 6.3.: Dispersion relation as a function of $p'_\perp$ in the chirally broken homogeneous phase (left) and the restored phase (right). Solutions from the inhomogeneous ansatz are given in blue and the homogeneous solution is given in orange for reference.

Overall, the results from the inhomogeneous calculations as described in this chapter are in very good agreement with what we would expect from the analytical limits we can take, which inspires confidence, that we have indeed found the Goldstone boson and our framework is capable to reproduce its properties.

6.7 Dispersion Relation of the Goldstone Boson

The dispersion relation is given as

$$p'_0(p'_\perp, p'_z), \tag{6.115}$$

which is defined by the poles in the diagonalized meson propagator

$$D''^{-1}(p'_0, p'_\perp, p'_z) \stackrel{!}{=} 0, \tag{6.116}$$

given by Equation (6.105). In particular we are interested in the eigenvalue with the positive sign, so for all pictures in this section the defining equation for p'_0 is

$$D''^{-1}_{+}(p') = \frac{1}{2G_S} - \frac{1}{2}\left[J'_{\sigma\sigma}(p') + J'_{\pi\pi}(p') + \sqrt{(J'_{\sigma\sigma}(p') - J'_{\pi\pi}(p'))^2 - 4J'^2_X(p')}\right] = 0. \tag{6.117}$$

For the dispersion relations there are two interesting cases. The first one is with momentum perpendicular to the modulation, the second one with momentum parallel to the modulation.

6.7.1 Dispersion Relation in the Perpendicular Direction

We will start with the former case. Since we cannot set the momentum in z-direction exactly zero for implementation reasons, we set it to $p_z = 1$ MeV, which should suffice. One thing to note here, is that our results show the off-diagonal meson type components J'_X are very small

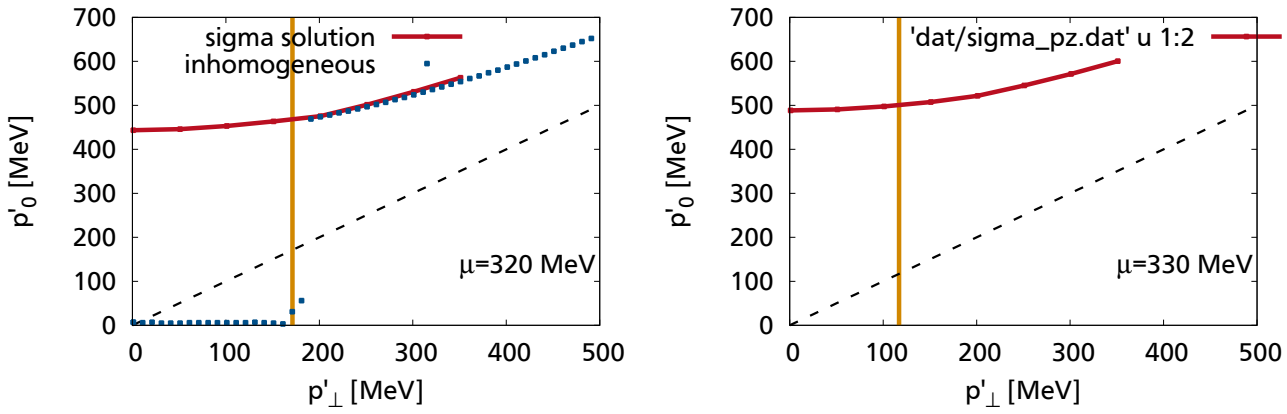

Figure 6.4.: Dispersion relation as a function of $p'_\perp$ for two inhomogeneous solutions, $\mu = 320$ MeV (left) and $\mu = 330$ MeV (right). The solution is given in blue, while the orange lines indicate two times the mass amplitude M. The black dashed line indicates $p_3^2 = 0$. The solution for the other eigenvalue $D_-''^{-1}$ is given in red.

compared to the diagonal ones. In all calculations they are more than three orders of magnitude smaller. We can show analytically, that for $p'_z = 0$, the integrand of J'_X over k_z is an odd function, which renders the integral zero. For this reason, it is sufficient to only take

$$D_+''^{-1} = \frac{1}{2G_S} - J'_{\pi\pi}(p'_0, p'_\perp, p'_z = 0) \tag{6.118}$$

into account.

In Figure 6.3 we show the dispersion relations in the homogeneous broken and restored phase. This yields exactly what we expect and the results match the homogeneous ones quite nicely. It shows, that we can retain the homogeneous limits we have discussed in Section 6.5. Since there is no preferred direction in the homogeneous limit, the dispersion relations as a function of p'_z look exactly the same.

For the inhomogeneous phase, we show two plots for $\mu = 320$ MeV and $\mu = 330$ MeV in Figure 6.4. Both exhibit similar behavior. From the plot it looks like the energy remains zero until a threshold, which is roughly twice the mass amplitude, then p'_0 starts growing. This behavior is unexpected. Previous works [62] have estimated a fourth-power dependency on the perpendicular momenta, but even within our margin of error, this does not seem likely. Rather it looks like a threshold opening at $p'_\perp = 2M$. Another unexpected feature is the discontinuity in the dispersion relation. At larger perpendicular momentum the solution jumps to a much higher value. There we can see that we obtain roughly the same solution we get from the other eigenvalue, by the condition $D_-''^{-1}(p'_0, p'_\perp, p'_z = 0) = 0$.

This behavior is shown for more values of the chemical potential in Figure 6.5, where the first value above zero is marked in blue and the first value above the jump is marked in red. The orange line indicates twice the mass amplitude and we can see that within the error bars the blue line agrees.

To better understand what is happening we take a closer look at the inverse generalized meson propagator as a function of p'_0. In Figure 6.6 on the right we have given examples of perpendicular momenta from all three types of solution regions, where the solution for p'_0 is zero, where it is small and where it is large.

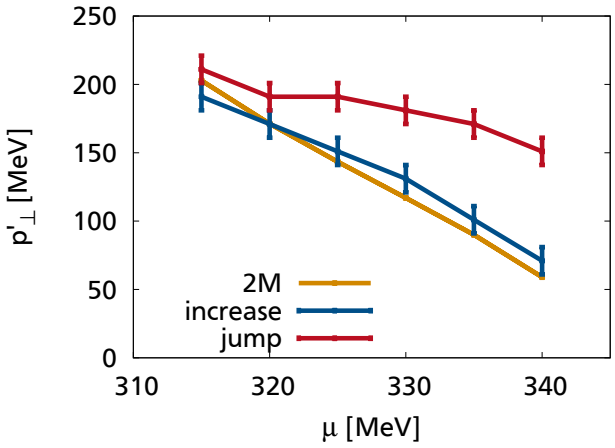

Figure 6.5.: Changes in the dispersion relation. The onset of finite values is given in blue, the location of the discontinuity is given in red, twice the mass amplitude is given in orange.

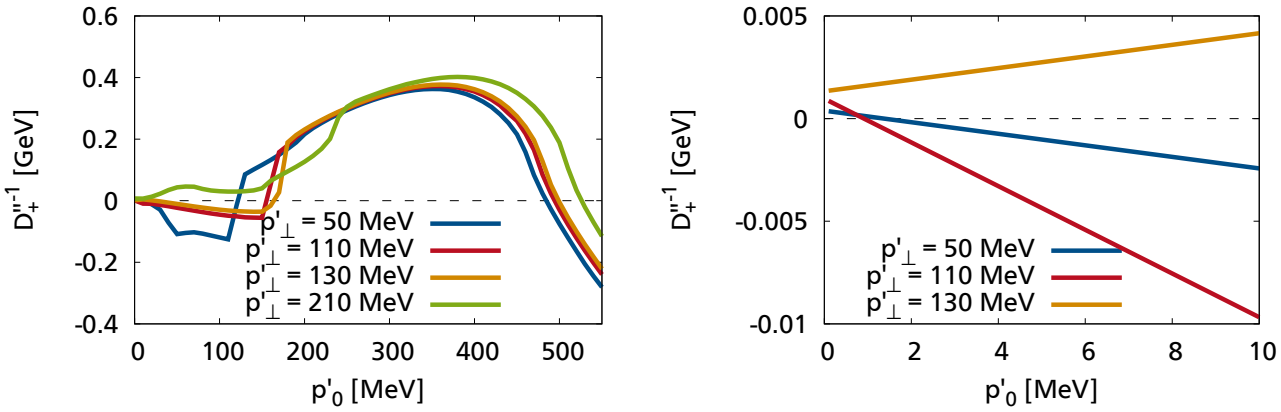

Figure 6.6.: The inverse generalized meson propagator as a function of p_0' for different values of the perpendicular momentum at a chemical potential of 330 MeV. Different ranges of p_0' are given left and right.

For small $p_\perp'$ we find the solution close to zero and with increasing p_0' there are more solutions to be found, especially the slope to negative values is of interest. As we increase the perpendicular momentum, the propagator at $p_0' = 0$ rises, so that the zero crossing comes at higher energies. At the same time the region of negative values for low p_0' assumes lower absolute values. At a certain point, the slope does not assume any values smaller than zero anymore and we find no further solutions at low p_0'. Instead the lowest lying solution is roughly at $p_0' \approx 500$ MeV. There is a solution in that region for all values of the perpendicular momentum, but only at high enough $p_\perp'$ is it the lowest lying one. This large solution coincides with the solution for the other eigenvalue, the one related to the sigma meson.

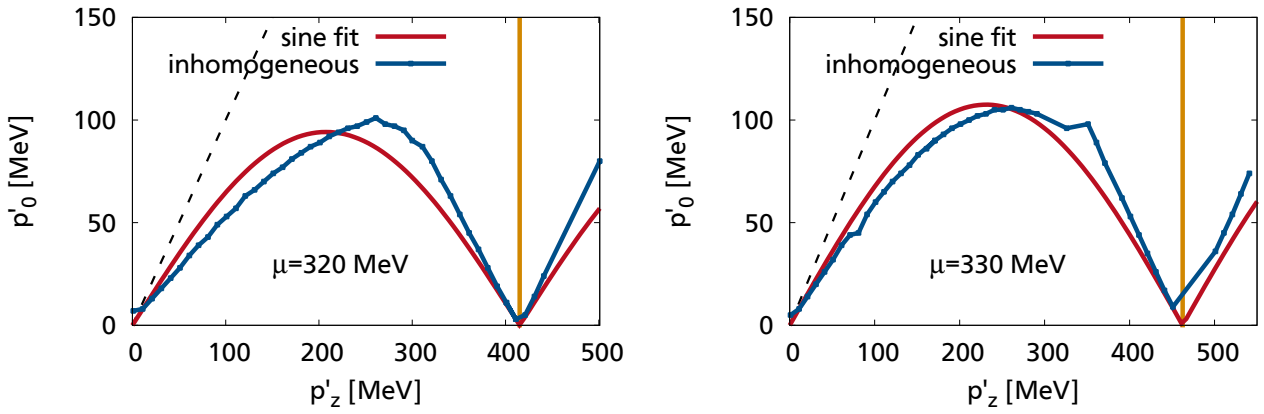

Figure 6.7.: Dispersion relation as a function of p_z' for two inhomogeneous solutions, $\mu = 320$ MeV (left) and $\mu = 330$ MeV (right). The solution is given in blue, while the orange lines here indicate two times the wave number Q. The red line gives a sinusoidal fit, as we would expect for a phonon in a one-dimensional chain. The black dashed line indicates $p^2 = 0$.

6.7.2 Dispersion Relation in the Parallel Direction

For the dispersion relation in direction of the modulation, it is instructive to repeat some findings from phonons in a regular crystal. The details can be found in every condensed matter text book, see for example [87].

We consider a classical, one-dimensional, mono-atomic chain, where the fluctuations are along the chain. In the low temperature limit one considers a quadratic nearest-neighbor potential, akin to masses connected with springs. Solving the equations of motion one arrives at a dispersion relation

$$\omega(k) = \sqrt{\frac{\kappa}{M}} \left| \sin\left(\frac{ka}{2}\right) \right|, \tag{6.119}$$

with a spring constant κ, the mass M and the lattice spacing a, which for our case would be $a = \pi/Q$.

Since we already mentioned in Chapter 5 the phonon and the pion we calculated in this chapter are equivalent, we can expect to see some similarities. In fact Figure 6.7 shows a behavior, that might be periodic in the first Brillouin zone, which is indicated by the orange line. The blue lines are our results and the red lines are a fit of the amplitude in Equation (6.119). The fits do not agree perfectly with our results, however, given that the fit is motivated by a classical approach and only has one parameter, the similarities are noteworthy.

In condensed matter theory the sound velocity can be derived from the linear slope of the sine wave close to momentum zero. Since sound waves have long wavelength compared to the lattice spacing, which is true for conventional crystals and certainly for our case, this is a good approximation. It is the limit where group and phase velocity are equal. For our case we find

$$c_S = \frac{\pi}{Q}\sqrt{\frac{\kappa}{M}}. \tag{6.120}$$

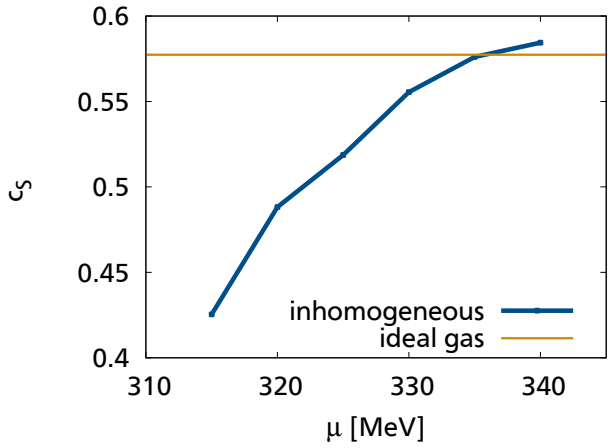

Figure 6.8.: Speed of sound in the direction of the Modulation in the chiral density wave as a function of chemical potential. The ideal gas value for neutron stars is given in orange.

Instead of taking the sine fit we have shown in the previous figures and plugging the results into this equation, we take a different approach. We take a few values of the dispersion relation close to $p_z' = 0$ and fit a linear slope to them. The results are given in Figure 6.8. This can only be an approximation, since we started from a non-relativistic ansatz, but nonetheless we can see that causality is not violated and our results are within the same order of magnitude of the ideal gas solution, which is of the order $c_S = c/\sqrt{3}$. For a broader discussion of the speed of sound in neutron stars see [88]. We see that with rising chemical potential, and therefore rising wave number and decreasing mass amplitude, the speed of sound is increasing.

6.8 Backward Transformation of the BSE

After having derived an expression for the transformed generalized meson propagator, one might want to go back to the original expression in Equation (6.6). We have only worked with the transformed expressions so far, since they contained all information we were interested in. If the full generalized meson propagator is needed however, one has to reverse the transformations. In this section, we want to give the reversed expressions and discuss some of its features.

The reversion of the transformation is straightforward via the definition of D'

$$D_{\alpha\beta} = W^{\dagger}_{\alpha\gamma} D'_{\gamma\delta} W_{\delta\beta}. \tag{6.121}$$

On the other hand, since we are only interested in the poles of the generalized meson propagator, it is easier to directly invert the inverse expression

$$D^{-1}_{\alpha\beta} = W^{\dagger}_{\alpha\gamma} D'^{-1}_{\gamma\delta} W_{\delta\beta}, \tag{6.122}$$

or with explicit momentum and meson type dependence

$$D^{-1}_{M'M}(p',p) = \sum_{N'N}\int \frac{d^4k'}{(2\pi)^4}\int \frac{d^4k}{(2\pi)^4}\, W^{\dagger}_{M'N'}(p',k')D'^{-1}_{N'N}(k')(2\pi)^4\delta^{(4)}\left(k'-k\right)W_{NM}(k,p) \tag{6.123}$$

$$= \sum_{N'N}\int \frac{d^4k'}{(2\pi)^4}\, W^{\dagger}_{M'N'}(p',k')D'^{-1}_{N'N}(k')W_{NM}(k',p) \tag{6.124}$$

$$= -\sum_{N'N}\int \frac{d^4k'}{(2\pi)^4}\, W^{\dagger}_{M'N'}(p',k')\begin{pmatrix} \frac{1}{2G_S} - J'_{\sigma\sigma}(k') & iJ'_X(k') \\ -iJ'_X(k') & \frac{1}{2G_S} - J'_{\pi\pi}(k') \end{pmatrix}_{N'N} W_{NM}(k',p). \tag{6.125}$$

Component by component we find

$$\begin{aligned}\left(\underline{D}\right)^{-1}_{\sigma\sigma} = {} & \frac{1}{4}\left[J'_{\sigma\sigma}(p'-q) - J'_{\pi\pi}(p'-q)\right](2\pi)^4\delta^{(4)}\left(p'-p-2q\right) \\ & + \frac{1}{4}\left[J'_{\sigma\sigma}(p'+q) - J'_{\pi\pi}(p'+q)\right](2\pi)^4\delta^{(4)}\left(p'-p+2q\right) \\ & + \frac{1}{4}\Big[-\frac{1}{G_S} + J'_{\sigma\sigma}(p'-q) + J'_{\pi\pi}(p'-q) + 2J'_X(p'-q) \\ & \quad -\frac{1}{G_S} + J'_{\sigma\sigma}(p'+q) + J'_{\pi\pi}(p'+q) - 2J'_X(p'+q)\Big](2\pi)^4\delta^{(4)}\left(p'-p\right),\end{aligned} \tag{6.126}$$

$$\begin{aligned}\left(\underline{D}\right)^{-1}_{\pi\pi} = {} & \frac{1}{4}\left[J'_{\pi\pi}(p'-q) - J'_{\sigma\sigma}(p'-q)\right](2\pi)^4\delta^{(4)}\left(p'-p-2q\right) \\ & + \frac{1}{4}\left[J'_{\pi\pi}(p'+q) - J'_{\sigma\sigma}(p'+q)\right](2\pi)^4\delta^{(4)}\left(p'-p+2q\right) \\ & + \frac{1}{4}\Big[-\frac{1}{G_S} + J'_{\sigma\sigma}(p'-q) + J'_{\pi\pi}(p'-q) + 2J'_X(p'-q) \\ & \quad -\frac{1}{G_S} + J'_{\sigma\sigma}(p'+q) + J'_{\pi\pi}(p'+q) - 2J'_X(p'+q)\Big](2\pi)^4\delta^{(4)}\left(p'-p\right),\end{aligned} \tag{6.127}$$

$$\begin{aligned}\left(\underline{D}\right)^{-1}_{\sigma\pi} = {} & -\frac{i}{4}\left[J'_{\pi\pi}(p'-q) - J'_{\sigma\sigma}(p'-q)\right](2\pi)^4\delta^{(4)}\left(p'-p-2q\right) \\ & - \frac{i}{4}\left[J'_{\sigma\sigma}(p'+q) - J'_{\pi\pi}(p'+q)\right](2\pi)^4\delta^{(4)}\left(p'-p+2q\right) \\ & - \frac{i}{4}\Big[J'_{\sigma\sigma}(p'-q) + J'_{\pi\pi}(p'-q) + 2J'_X(p'-q) \\ & \quad -J'_{\sigma\sigma}(p'+q) - J'_{\pi\pi}(p'+q) + 2J'_X(p'+q)\Big](2\pi)^4\delta^{(4)}\left(p'-p\right),\end{aligned} \tag{6.128}$$

$$\begin{aligned}\left(\underline{D}\right)^{-1}_{\pi\sigma} = {} & \frac{i}{4}\left[J'_{\pi\pi}(p'-q) - J'_{\sigma\sigma}(p'-q)\right](2\pi)^4\delta^{(4)}\left(p'-p-2q\right) \\ & + \frac{i}{4}\left[J'_{\sigma\sigma}(p'+q) - J'_{\pi\pi}(p'+q)\right](2\pi)^4\delta^{(4)}\left(p'-p+2q\right) \\ & - \frac{i}{4}\Big[J'_{\sigma\sigma}(p'-q) + J'_{\pi\pi}(p'-q) + 2J'_X(p'-q) \\ & \quad -J'_{\sigma\sigma}(p'+q) - J'_{\pi\pi}(p'+q) + 2J'_X(p'+q)\Big](2\pi)^4\delta^{(4)}\left(p'-p\right).\end{aligned} \tag{6.129}$$

These expressions are rather lengthy and we won't give numerical results for them. However there are a some things to learn from them.

First of all, the full momentum dependence of the inverse general meson propagator. It only has components for incoming and outgoing momenta that are the same or if they differ by $2q$. We can also see that for the homogeneous broken case, at $q = 0$, the propagator gives the homogeneous solution, since J'_X vanishes. For the restored phase, $J'_{\sigma\sigma}$ and $J'_{\pi\pi}$ are degenerate, from which we can read, that the inverse generalized meson propagator is diagonal in momentum space.

These expressions could be useful as inputs for future calculations, where the full momentum dependence of the generalized meson propagator is needed.

7 Conclusion and Outlook

In this work we have investigated a space dependent chiral condensate in the two-flavor Nambu–Jona-Lasinio model. The goal was to find and calculate the Nambu-Goldstone modes in the inhomogeneous phase, where in addition to the chiral symmetry, rotational and translational symmetry is broken as well.

We have summarized some of the main aspects of our model so far in Chapter 3. Starting from these formalisms we aimed to introduce a way to calculate quantities, that depend on the propagator of the theory and which can not be derived from the grand potential directly. The difficulty here is that propagators exchange momenta with the background field, which renders them non-trivial matrices in momentum space, with differing incoming and outgoing momenta. This makes the treatment for the general case quite difficult, so we focused on one specific modulation for the mass function, the chiral density wave (CDW), a one-dimensional plane wave as our modulation of choice.

From a method originally conceived to diagonalize the Hamiltonian of our model to obtain analytical eigenvalues, we extended this formalism to allow us to diagonalize the inverse propagator in momentum space. The diagonal structure of the transformed inverse propagator in momentum space allows us to calculate its inverse, the fully transformed propagator for the CDW, analytically, which we found to have a much richer Dirac structure than the homogeneous propagator.

Then we put our calculations to the test by calculating the gap equation from the Feynman diagram, which allowed us to compare our results to the gap equation derived from stationary conditions in the grand potential. We found our results in agreement with previous works for this test case.

The next step was to identify the number and type of Goldstone modes in the inhomogeneous phase with the CDW modulation. One can show, that there are three Goldstone modes to consider and that the fluctuations in direction of the modulation is equivalent to the meson, which in the homogeneous case would correspond to the uncharged pion. We gave a physical argument how to build the vertex of this meson, which has a spatial dependence to consider. Since the massive direction rotates between the scalar and pseudo-scalar condensate, so does its perpendicular direction.

Afterwards we calculated the meson in earnest, starting from the Bethe-Salpeter equation with fully dressed inhomogeneous propagators. Like for most quantities in the inhomogeneous phase the generalized meson propagator is non-diagonal in momentum space and we introduced transformations on the whole equation to diagonalize all expressions. The key quantity in this calculation was the polarization loop, which was diagonalized in momentum space by these transformations as well. We showed that transformations that diagonalized the polarization loop, diagonalize the whole equation and armed with this knowledge found a way to determine the necessary transformation. In order to calculate Goldstone modes and dispersion relations, we needed a way to calculate the polarization loop. Due to the more complicated Dirac structure of the inhomogeneous propagators, compared to the homogeneous ones, the expressions in our calculations were much more involved. Nonetheless, most steps found in

homogeneous calculations are applicable for the inhomogeneous case as well, so we managed to give a calculable expression for finite temperature and chemical potential. The expressions for the inhomogeneous generalized meson propagator were non-diagonal in the meson type as well and we gave a quick calculation to diagonalize these expressions. We checked the resulting expressions to be consistent with the homogeneous calculations in the absence of a space-dependent condensate and found them to be in agreement both from an analytical standpoint and our numerical calculations. We gave an analytical proof that we found a Goldstone boson and verified it with numerical calculations. This is in accordance with the physical arguments we gave in the previous chapter and gives confidence in our derivation of the Bethe-Salpeter equation. We moved on to calculate the dispersion relations of the Goldstone boson, where we checked the conformity with the homogeneous results as a first step and found that our results are in agreement again.

We differentiated two cases for the dispersion relation in the inhomogeneous phase, momenta perpendicular to the modulation and momenta parallel to it. For the perpendicular momenta, we can show a decoupling of the meson types. The dispersion relations gave quite unexpected results, the energy of the Goldstone bosons remains zero or very small, below our numerical precision, until a certain threshold of perpendicular momenta, equal to two times the mass amplitude, were reached. In addition we found a jump to a higher energy at larger external momenta, after which the solutions for the two mesons are degenerate. The jump indicates gapped energies, which is not uncommon in dispersion relations for massive particles, but comes as a surprise for a massless boson.

For external momenta in direction of the modulation we see a different behavior, the dispersion relation starts to rise, while staying below the diagonal that would indicate a zero overall squared four-momentum. At a certain external momentum, the curve starts declining and seems to show a periodic behavior with a period of twice the wave number, which indicates periodicity in the first Brillouin zone. We see no jump in the dispersion relation. This behavior is reminiscent of a classical phonon from condensed matter physics. We fitted the dispersion relation from a classical phonon model to our results and saw reasonable agreement. We then went on to determine the speed of sound from the phonon dispersion relation, which yielded results in a reasonable range, between 45% and 60% of the speed of light.

Overall we have shown how to calculate propagators for the full inhomogeneous phase, which allows the access to much more observables than before. These techniques have already been used to calculate expectation values in the inhomogeneous phase with success in [89]. Together with this work, one is able to examine the stability of the one-dimensional inhomogeneous phase by determining the long range correlations. As stated by Landau and Peierls [61], one-dimensional crystals should be unstable against thermal fluctuations, so it would be interesting to investigate, how this manifests for our model. First studies close to the Lifschitz point have shown an algebraic decay of the long range order [63], but we still do not know how this would look like at lower temperatures, with less fluctuations.

In addition, building up on this work, one should be able to derive transport properties in the inhomogeneous phase. This might be especially interesting for neutron starts, where it has already been shown, that a inhomogeneous phase has minimal influence on the mass - radius relation [90], but other effects, like the cooling of neutron stars, might be influenced much stronger. Transport properties are also interesting, in order to determine the presence of an inhomogeneous phase in upcoming experiments searching for the first-order phase transition in the QCD phase diagram at FAIR.

A more long time goal would be to do the investigations shown in this work for a more realistic, real valued modulation of the mass function. There one would expect more Goldstone modes and the calculations for the phonon have to be done in a different framework. In addition, one would likely have to invert the inverse propagator numerically, which allows much less control over its components. This in turn would not only complicate the calculations, but also make some of the steps we have done in this work impossible. It allows for much less control over the regularization as well.

One of the big goals is to calculate inhomogeneous condensates in a functional renormalization group framework. This would allow for fluctuations. Some steps have been undertaken in a quark meson model to calculate the inhomogeneous phase [58], but as of now, all of them are closely related to mean-field calculations. This is where our work could come in handy. One possibility to arrive at an FRG framework would involve starting out from the mean-field meson dispersion relations, which we have calculated, or have shown how to calculate in this work.

A Definitions and Conventions

A.1 Conventions

Throughout this work we use natural units $\hbar = c = k_B = 1$.
Unless otherwise stated Greek letters $\mu, \nu, \ldots$ indicate Lorentz indices, running from 0 to 3, while Latin letters $i, j, \ldots$ are spatial indices, running from 1 to 3.
We make use of the Einstein sum convention with the Minkowski metric

$$g_{\mu\nu} = \mathrm{diag}(1, -1, -1, -1), \tag{A.1}$$

which leads to the following scalar products for four vectors

$$x^\mu y_\mu = x_0 y_0 + x^i y_i = x_0 y_0 - \vec{x} \cdot \vec{y}. \tag{A.2}$$

If an explicit representation of Dirac matrices is given we use the Weyl representation

$$\gamma^0 = \begin{pmatrix} 0 & \mathbb{1} \\ \mathbb{1} & 0 \end{pmatrix}, \quad \gamma^k = \begin{pmatrix} 0 & \sigma^k \\ -\sigma^k & 0 \end{pmatrix}, \quad \gamma^5 = \begin{pmatrix} -\mathbb{1} & 0 \\ 0 & \mathbb{1} \end{pmatrix}, \tag{A.3}$$

where σ^k are the Pauli matrices

$$\sigma^1 = \begin{pmatrix} 0 & 1 \\ 1 & 0 \end{pmatrix}, \quad \sigma^2 = \begin{pmatrix} 0 & -i \\ i & 0 \end{pmatrix}, \quad \sigma^3 = \begin{pmatrix} 1 & 0 \\ 0 & -1 \end{pmatrix}. \tag{A.4}$$

A.2 Continuous Matrix Multiplications

In this work we repeatedly deal with the multiplications of objects which can be interpreted as matrices in coordinate or momentum space. To have a consistent framework to deal with this kind of operation we define analogously to the discrete matrix multiplication

$$\underline{C} = \underline{A} \cdot \underline{B}, \tag{A.5}$$

$$c_{ij} = \sum_k a_{ik} b_{ki} \tag{A.6}$$

a continuous version by replacing the sum with an integral. For the typical four dimensional case this takes the form

$$C(x, x') = \int d^4y A(x, y) B(y, x'), \tag{A.7}$$

$$C(p, p') = \int \frac{d^4k}{(2\pi)^4} A(p, k) B(k, p'), \tag{A.8}$$

where for the momentum space case we have an additional normalizing factor $(2\pi)^4$ which arises from our definition of the Fourier transformation. All matrices are denoted by having 2 arguments, whereas vectors in continuous space only have 1 argument. We can define a diagonal matrix as

$$D(p,p') = D(p)(2\pi)^4 \delta^{(4)}\left(p-p'\right), \tag{A.9}$$

with the vector $D(p)$. Inverse matrices are defined as follows

$$\underline{A}^{-1} \cdot \underline{A} = \mathbb{1}, \tag{A.10}$$

$$\int d^4y A^{-1}(x,y)A(y,x') = \delta^{(4)}(x-x'), \tag{A.11}$$

$$\int \frac{d^4k}{(2\pi)^4} A^{-1}(p,k)A(k,p') = (2\pi)^4 \delta^{(4)}\left(p-p'\right). \tag{A.12}$$

A.3 Fourier Transformations

In analogy to the standard definitions of Fourier transformations of functions, the Fourier transformation for a vector is straightforward

$$f(p) = \int d^4x e^{-ipx} f(x), \tag{A.13}$$

$$f(x) = \int \frac{d^4p}{(2\pi)^4} e^{ipx} f(p). \tag{A.14}$$

To transform a matrix in coordinate or momentum space we use two integrals and two exponential functions

$$F(p,p') = \int d^4x \int d^4x' e^{ipx} F(x,x') e^{-ip'x'}, \tag{A.15}$$

$$F(x,x') = \int \frac{d^4p}{(2\pi)^4} \int \frac{d^4p'}{(2\pi)^4} e^{-ipx} F(p,p') e^{ip'x'}. \tag{A.16}$$

One special case we have to consider is the transformation of a Hamiltonian of the form

$$H(x) = \partial_x + \Delta e^{iqx}. \tag{A.17}$$

While this might look like a vector in coordinate space, the presence of the derivative changes the situation and a straightforward transformation would not yield correct results. Therefore we treat such objects as diagonal matrices and write

$$H(x,x') = \delta^{(4)}(x-x')\, H(x) \tag{A.18}$$

and perform the transformation as we would for any other matrix

$$H(p,p') = \int d^4x \int d^4x' e^{ipx} H(x,x') e^{-ip'x'} \tag{A.19}$$

$$= \int d^4x \int d^4x' e^{ipx} \delta^{(4)}(x-x') \left[\partial_x + \Delta e^{iqx}\right] e^{-ip'x'} \tag{A.20}$$

$$= \int d^4x e^{ipx} \left[\partial_x + \Delta e^{iqx}\right] e^{-ip'x} \tag{A.21}$$

$$= \int d^4x \left[-ip' e^{i(p-p')x} + \Delta e^{i(p+q-p')x}\right] \tag{A.22}$$

$$= -ip'(2\pi)^4 \delta^{(4)}\left(p-p'\right) + \Delta(2\pi)^4 \delta^{(4)}\left(p+q-p'\right). \tag{A.23}$$

B Gap Equation and Mesons in the Homogeneous Phase

Here we will give some of the details on how to calculate the gap equation and mesons in the homogeneous NJL model. A lot of these calculations are very similar to the inhomogeneous ones, but with much more compact expressions, which makes it easier to understand the concepts going into these calculations.

We will start out with the calculations of the Matsubara sum in the gap equation, before we turn to the polarization loop.

B.1 Matsubara Formalism in the Homogeneous Gap Equation

The integral from Section 3.2.1 that we are interested in is

$$iI_1 = i\int \frac{d^4k}{(2\pi)^4}\,\frac{1}{k^2-M^2+i\varepsilon}, \tag{B.1}$$

or after the introduction of the Matsubara formalism

$$iI_1 = -T\sum_{m=-\infty}^{\infty}\int \frac{d^3k}{(2\pi)^3}\,\frac{1}{(i\omega_m+\mu)^2-E_k^2} \tag{B.2}$$

$$= -T\sum_{m=-\infty}^{\infty}\int \frac{d^3k}{(2\pi)^3}\,\frac{1}{2E_k}\left[\frac{1}{i\omega_m+\mu-E_k}-\frac{1}{i\omega_m+\mu+E_k}\right], \tag{B.3}$$

where in the second step we performed a partial fraction decomposition in the integrand. The sum over the Matsubara frequencies can be interpreted as a sum over residues, which invites to use the residue theorem backward to arrive at

$$iI_1 = \frac{1}{2\pi i}\oint_\Gamma dz\int \frac{d^3k}{(2\pi)^3}\,\frac{1}{2E_k}\,\frac{1}{\exp(z/T)+1}\left[\frac{1}{z+\mu-E_k}-\frac{1}{z+\mu+E_k}\right], \tag{B.4}$$

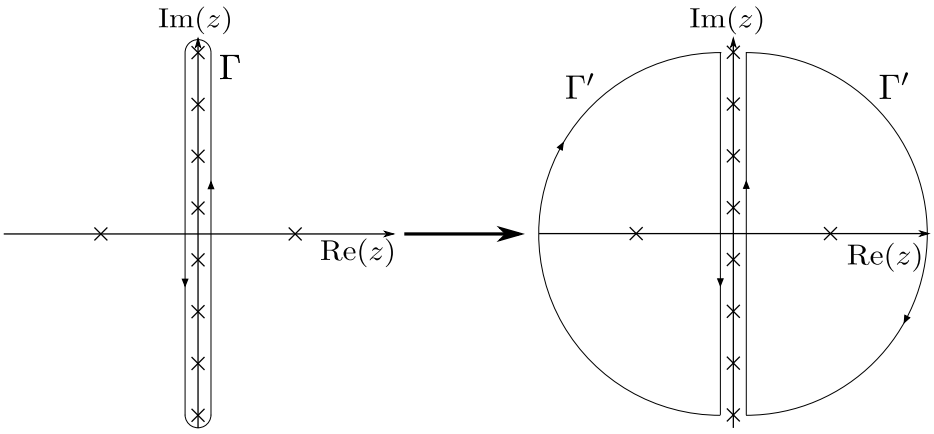

Figure B.1.: Illustration of the integration contours used to derive the integral iI_1.

with the integration contour Γ, illustrated in Figure B.1 on the left and the function chosen so that it has poles, where $z = i\omega_m$. By a transformation of the contour Γ' we can use the residue theorem forward to integrate over the simple poles on the real axis

$$iI_1 = \frac{1}{2\pi i}\oint_{\Gamma'} dz \int \frac{d^3k}{(2\pi)^3}\,\frac{1}{2E_k}\frac{1}{\exp(z/T)+1}\left[\frac{1}{z+\mu-E_k}-\frac{1}{z+\mu+E_k}\right] \tag{B.5}$$

$$= -\int \frac{d^3k}{(2\pi)^3}\,\frac{1}{2E_k}\left[\frac{1}{\exp((E_k-\mu)/T)+1}-\frac{1}{\exp((-E_k-\mu)/T)+1}\right]. \tag{B.6}$$

We introduce Fermi distribution functions

$$n_F(z) = \left[1+\exp\left(\frac{z}{T}\right)\right]^{-1}, \tag{B.7}$$

with the property $n_F(-z) = 1 - n_F(z)$, which allows us to write the integral

$$iI_1 = \int \frac{d^3k}{(2\pi)^3}\left(\frac{1}{2E_k}-\frac{1}{2E_k}\left[n_F(E_k-\mu)+n_f(E_k+\mu)\right]\right). \tag{B.8}$$

B.2 Homogeneous Polarization Loop

For the polarization loop we start of by separating the expression from the trace into two separate integrals, before we perform the Matsubara formalism for the fermionic frequencies.

B.2.1 Separation of the Integrals

From the definition of the polarization loop we obtain the expression for σ

$$J_\sigma(p) = i\int \frac{d^4k}{(2\pi)^4}\,\mathrm{tr}\left[\frac{\not{k}+\not{p}+M}{(k+p)^2-M^2+i\varepsilon}\cdot\frac{\not{k}+M}{k^2-M^2+i\varepsilon}\right] \tag{B.9}$$

$$= i\int \frac{d^4k}{(2\pi)^4}\,\mathrm{tr}\left[\frac{k^2+k\cdot p+2\not{k}M+\not{p}M+M^2}{((k+p)^2-M^2+i\varepsilon)(k^2-M^2+i\varepsilon)}\right] \tag{B.10}$$

$$= 4N_fN_c i\int \frac{d^4k}{(2\pi)^4}\,\frac{k^2+k\cdot p+M^2}{((k+p)^2-M^2+i\varepsilon)(k^2-M^2+i\varepsilon)}. \tag{B.11}$$

By adding and subtracting in the denominator, we get the form

$$J_\sigma(p) = 4N_fN_c\Bigg(i\int \frac{d^4k}{(2\pi)^4}\,\frac{1}{k^2-M^2+i\varepsilon} - i\int \frac{d^4k}{(2\pi)^4}\,\frac{k\cdot p+p^2-2M^2}{((k+p)^2-M^2+i\varepsilon)(k^2-M^2+i\varepsilon)}\Bigg). \tag{B.12}$$

We can show

$$\int \frac{d^4k}{(2\pi)^4}\,\frac{2k\cdot p+p^2}{((k+p)^2-M^2+i\varepsilon)(k^2-M^2+i\varepsilon)} \tag{B.13}$$

$$= \int \frac{d^4k}{(2\pi)^4}\,\frac{-2k\cdot p-p^2}{((k+p)^2-M^2+i\varepsilon)(k^2-M^2+i\varepsilon)} = 0, \tag{B.14}$$

by applying the substitution $k \to -k - p$, which allows us to replace $k \cdot p = -p^2/2$ in the polarization loop

$$J_\sigma(p) = 4N_f N_c \Bigg(i \int \frac{d^4k}{(2\pi)^4} \frac{1}{k^2 - M^2 + i\varepsilon} \tag{B.15}$$
$$- i \int \frac{d^4k}{(2\pi)^4} \frac{p^2/2 - 2M^2}{((k+p)^2 - M^2 + i\varepsilon)(k^2 - M^2 + i\varepsilon)} \Bigg)$$
$$= 4N_f N_c i \int \frac{d^4k}{(2\pi)^4} \frac{1}{k^2 - M^2 + i\varepsilon} \tag{B.16}$$
$$- 2N_f N_c (p^2 - 4M^2) i \int \frac{d^4k}{(2\pi)^4} \frac{1}{((k+p)^2 - M^2 + i\varepsilon)(k^2 - M^2 + i\varepsilon)}$$
$$= 4N_f N_c \; iI_1 - 2N_f N_c (p^2 - 4M^2) i I_2(p), \tag{B.17}$$

where we identified the integral iI_1, which we already discussed in the last section and defined the integral $iI_2(p)$, which we will treat in the upcoming section.

The calculation for the pion polarization loop is analogous and yields

$$J_\pi(p) = 4N_f N_c i I_1 - 2N_f N_c \; p^2 \; iI_2(p). \tag{B.18}$$

B.2.2 Evaluating the Integral $iI_2(p)$

The integral is given by

$$iI_2(p) = i \int \frac{d^4k}{(2\pi)^4} \frac{1}{((k+p)^2 - M^2 + i\varepsilon)(k^2 - M^2 + i\varepsilon)}. \tag{B.19}$$

We start of by introducing the Matsubara formalism, similar to the gap equation. Here however, we have bosonic momenta p, in addition to the fermionic momenta k. We will use the subscript n for the fermionic frequencies $i\omega_n = (2n+1)\pi i T$ and the subscript m for the bosonic ones $i\omega_m = 2\pi m i T$, which both run over the whole set of integers. The integral reads

$$iI_2(i\omega_m, \vec{p}) = -T \sum_{n=-\infty}^{\infty} \int \frac{d^3k}{(2\pi)^3} \frac{1}{((i\omega_n + \mu + i\omega_m)^2 - E_p^2 + i\varepsilon)((i\omega_n + \mu)^2 - E_k^2 + i\varepsilon)}. \tag{B.20}$$

Here in addition to the energies $E_k = \sqrt{\vec{k}^2 + M^2}$, we also defined the energies depending on $\vec{k} + \vec{p}$, $E_p = \sqrt{(\vec{k} + \vec{p})^2 + M^2}$.

Again, we will use the residue theorem backwards, introducing the Fermi distribution $n_F(z)$

$$iI_2(i\omega_m, \vec{p}) = \int \frac{d^3k}{(2\pi)^3} \frac{1}{2\pi i} \oint_\Gamma dz \frac{n_F(z)}{((z + \mu + i\omega_m)^2 - E_p^2 + i\varepsilon)((z+\mu)^2 - E_k^2 + i\varepsilon)}, \tag{B.21}$$

with the integration contour Γ sketched in Figure B.2.

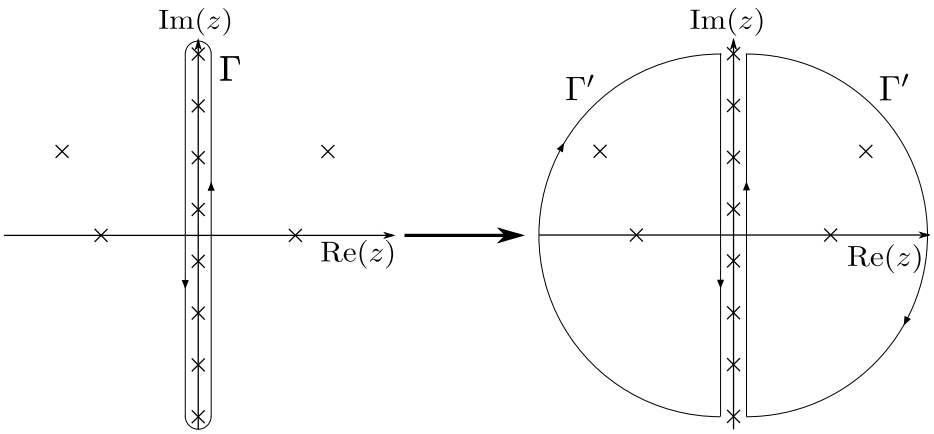

Figure B.2.: Sketch of the integration contours for the integral $iI_2(p)$

We can deform the integration contour to Γ', running over the poles $z_{1,2} = \pm E_k - \mu$ and $z_{3,4} = \pm E_p - \mu + i\omega_m$. Applying the residue theorem again, we get the sum

$$iI_2(i\omega_M, \vec{p}) = -\int \frac{d^3k}{(2\pi)^3} \sum_{i=1}^{4} \mathrm{Res}_{z_i} \frac{n_F(z)}{((z+\mu+i\omega_m)^2 - E_p^2 + i\varepsilon)((z+\mu)^2 - E_k^2 + i\varepsilon)} \tag{B.22}$$

$$\begin{aligned} = -\int \frac{d^3k}{(2\pi)^3} \Bigg[& \frac{n_F(E_k-\mu)}{2E_k(E_k+i\omega_m-E_p)(E_k+i\omega_m+E_p)} \\ & + \frac{n_F(-E_k-\mu)}{-2E_k(-E_k+i\omega_m-E_p)(-E_k+i\omega_m+E_p)} \\ & + \frac{n_F(E_p-i\omega_m-\mu)}{2E_p(E_p-i\omega_m-E_k)(E_p-i\omega_m+E_k)} \\ & + \frac{n_F(-E_p-i\omega_m-\mu)}{-2E_p(-E_p-i\omega_m-E_k)(-E_p-i\omega_m+E_k)} \Bigg]. \end{aligned} \tag{B.23}$$

Now we can use several properties to simplify this expression. First of all, the Fermi distribution is periodic in $2\pi i T k$, $k \in \mathbb{Z}$, and therefore in the bosonic Matsubara frequencies $n_F(z + i\omega_m) = n_F(z)$. Furthermore we can make the substitution $\vec{k} \to -\vec{k} - \vec{p}$ in the third and fourth summands of the integrand, which simplifies the expression to

$$\begin{aligned} iI_2(i\omega_M, \vec{p}) = -\int \frac{d^3k}{(2\pi)^3} \Bigg[& \frac{n_F(E_k-\mu)}{2E_k(E_k+i\omega_m-E_p)(E_k+i\omega_m+E_p)} \\ & - \frac{n_F(-E_k-\mu)}{2E_k(E_k-i\omega_m+E_p)(E_k-i\omega_m-E_p)} \\ & + \frac{n_F(E_k-\mu)}{2E_k(E_k-i\omega_m-E_p)(E_k-i\omega_m+E_p)} \\ & - \frac{n_F(-E_k-\mu)}{2E_k(E_k+i\omega_m+E_p)(E_k+i\omega_m-E_p)} \Bigg]. \end{aligned} \tag{B.24}$$

After performing a partial fraction decomposition and some further simplifications, we can write this expression as

$$iI_2(i\omega_m,\vec{p}) = \int \frac{d^3k}{(2\pi)^3}\,\frac{n_F(-E_k-\mu)-n_F(E_k-\mu)}{4E_kE_p}\times \\ \times\left(\frac{2(E_k-E_p)}{(E_k-E_p)^2-(i\omega_m)^2}-\frac{2(E_k+E_p)}{(E_k+E_p)^2-(i\omega_m)^2}\right) \tag{B.25}$$

and with the abbreviations $s_{k,p}=E_p+E_k$ and $d_{k,p}=E_p-E_k$ and using $n_F(-z)=1-n_F(z)$ again, we find

$$iI_2(i\omega_m,\vec{p}) = \int \frac{d^3k}{(2\pi)^3}\,\frac{1-n_F(E_k+\mu)-n_F(E_k-\mu)}{2E_kE_p}\left(\frac{d_{k,p}}{(i\omega_m)^2-d_{k,p}^2}+\frac{s_{k,p}}{(i\omega_m)^2-s_{k,p}^2}\right). \tag{B.26}$$

We can further simplify this expression to

$$iI_2(i\omega_m,\vec{p}) = \int \frac{d^3k}{(2\pi)^3}\left[\left(\frac{1}{E_k}-\frac{n_F(E_k+\mu)+n_F(E_k-\mu)}{2E_kE_p}s_{k,p}\right)\frac{1}{(i\omega_m)^2-s_{k,p}^2}\right. \\ \left.-\frac{n_F(E_k+\mu)-n_F(E_k-\mu)}{2E_kE_p}\frac{d_{k,p}}{(i\omega_m)^2-d_{k,p}^2}\right]. \tag{B.27}$$

To calculate the masses of mesons we need the retarded version of this integral, which we can obtain, by making the analytic continuation $i\omega_m \to p_0+i\varepsilon$.

This integral still has poles, which makes the numerical evaluation complicated and prone for errors. The most stable and fastest way to evaluate the integral is via it's imaginary part, which is related to the real part via the Kramers-Kronig relation

$$\mathrm{Re}\,(iI_2(p_0,\vec{p})) = \frac{1}{\pi}\mathrm{PV}\int_{-\infty}^{\infty} d\omega\frac{\mathrm{Im}\,(iI_2(\omega,\vec{p}))}{\omega-p_0}. \tag{B.28}$$

To get the imaginary part, we employ the Sokhotski-Plemelj theorem stating

$$\lim_{\varepsilon\to 0}\mathrm{Im}\left(\frac{1}{x\pm i\varepsilon}\right) = \mp\pi\delta(x). \tag{B.29}$$

Now we can use this on the expression in Equation (B.27) after the analytic continuation and write

$$\mathrm{Im}\,(iI_2(p_0,\vec{p})) = -\pi\int \frac{d^3k}{(2\pi)^3}\left[\left(\frac{1}{2E_k\,s_{k,p}}-\frac{n_F(E_k+\mu)+n_F(E_k-\mu)}{4E_kE_p}\right)\big(\delta(p_0-s_{k,p})-\delta(p_0+s_{k,p})\big)\right. \\ \left.-\frac{n_F(E_k+\mu)-n_F(E_k-\mu)}{4E_kE_p}\big(\delta(p_0-d_{k,p})-\delta(p_0+d_{k,p})\big)\right]. \tag{B.30}$$

Since the integral only depends on the energies E_k and E_p and not on the momenta directly, we can substitute the integration variables $k = |\vec{k}|$ and $\cos\theta$, the angle between $\vec{k}$ and $\vec{p}$, which yields

$$\begin{aligned}\mathrm{Im}\,(iI_2(p_0,\vec{p})) = \\ -\frac{1}{16\pi|\vec{p}|}\int_M^\infty dE_k \int_{E_p^-}^{E_p^+} dE_p \Bigg[\left(\frac{2E_p}{s_{k,p}}\right)\big(\delta(p_0-s_{k,p})-\delta(p_0+s_{k,p})\big) \\ -(n_F(E_k+\mu)+n_F(E_k-\mu))\big(\delta(p_0-d_{k,p})-\delta(p_0+d_{k,p})+\delta(p_0-s_{k,p})-\delta(p_0+s_{k,p})\big)\Bigg],\end{aligned} \tag{B.31}$$

where

$$E_p^\pm = \sqrt{M^2+(|\vec{k}|\pm|\vec{p}|)^2} = \sqrt{M^2+\left(\sqrt{E_k^2-M^2}\pm|\vec{p}|\right)^2}. \tag{B.32}$$

The delta functions are all of the form $\delta(p_0 \pm E_k \pm E_p)$ and we can integrate them out by integrating over E_p. For $p^2 = p_0^2 - \vec{p}^2 > 0$ we find

$$\begin{aligned}\mathrm{Im}\,(iI_2(p_0,\vec{p})) = -\frac{1}{16\pi|\vec{p}|}\theta(p^2-4M^2) \\ \Bigg[\theta(p_0)\int_{\frac{p_0}{2}-\sqrt{\Delta}}^{\frac{p_0}{2}+\sqrt{\Delta}} dE_k \left(2\frac{p_0-E_k}{p_0}-(n_F(E_k+\mu)+n_F(E_k-\mu))\right) \\ \theta(-p_0)\int_{-\frac{p_0}{2}-\sqrt{\Delta}}^{-\frac{p_0}{2}+\sqrt{\Delta}} dE_k \left(2\frac{p_0+E_k}{p_0}-(n_F(E_k+\mu)+n_F(E_k-\mu))\right)\Bigg]\end{aligned} \tag{B.33}$$

and for $p^2 = p_0^2 - \vec{p}^2 < 0$

$$\begin{aligned}\mathrm{Im}\,(iI_2(p_0,\vec{p})) = \frac{1}{16\pi|\vec{p}|}\Bigg[\int_{-\frac{p_0}{2}+\sqrt{\Delta}}^{\infty} dE_k\ (n_F(E_k+\mu)+n_F(E_k-\mu)) \\ -\int_{\frac{p_0}{2}+\sqrt{\Delta}}^{\infty} dE_k\ (n_F(E_k+\mu)+n_F(E_k-\mu))\Bigg].\end{aligned} \tag{B.34}$$

Here we defined

$$\sqrt{\Delta} = \frac{|\vec{p}|}{2}\sqrt{\frac{p^2-4M^2}{p^2}}. \tag{B.35}$$

After some additional simplifications we can integrate over the remaining energies, which leads to
$p^2 > 0$:

$$\begin{aligned}\mathrm{Im}\,(iI_2(p_0,\vec{p})) = -\frac{1}{16\pi}\theta(p^2-4M^2)\sigma_{p_0}\Bigg[\sqrt{\frac{p^2-4M^2}{p^2}} \\ +\frac{T}{|\vec{p}|}\log\left(\frac{1+e^{-\frac{1}{T}\left(\left|\frac{p_0}{2}\right|+\sqrt{\Delta}-\mu\right)}}{1+e^{-\frac{1}{T}\left(\left|\frac{p_0}{2}\right|-\sqrt{\Delta}-\mu\right)}}\right)+\frac{T}{|\vec{p}|}\log\left(\frac{1+e^{-\frac{1}{T}\left(\left|\frac{p_0}{2}\right|+\sqrt{\Delta}+\mu\right)}}{1+e^{-\frac{1}{T}\left(\left|\frac{p_0}{2}\right|-\sqrt{\Delta}+\mu\right)}}\right)\Bigg],\end{aligned} \tag{B.36}$$

$p^2 < 0$:

$$\mathrm{Im}\left(iI_2(p_0,\vec{p})\right) = -\frac{T}{16\pi|\vec{p}|}\sigma_{p_0}\left[\log\left(\frac{1+e^{-\frac{1}{T}\left(\sqrt{\Delta}+\left|\frac{p_0}{2}\right|-\mu\right)}}{1+e^{-\frac{1}{T}\left(\sqrt{\Delta}-\left|\frac{p_0}{2}\right|-\mu\right)}}\right)+\log\left(\frac{1+e^{-\frac{1}{T}\left(\sqrt{\Delta}+\left|\frac{p_0}{2}\right|+\mu\right)}}{1+e^{-\frac{1}{T}\left(\sqrt{\Delta}-\left|\frac{p_0}{2}\right|+\mu\right)}}\right)\right]. \tag{B.37}$$

The vacuum part in Equation (B.36) still has to be regularized. This can be done by simply replacing the masses with the Pauli-Villars masses.

Armed with these expression we can calculate the real parts of the integral with the Kramers-Kronig relation, which leads to the results shown in Section 3.2.2.

C Details on Inhomogeneous Propagators and the Gap Equation

C.1 Mass Function from the Chiral Transformations

In Section 4.1 we started from the definition of the condensates

$$\langle\overline{\psi}\psi\rangle = -\frac{M}{2G_S}\cos(\vec{q}\vec{x}), \qquad \langle\overline{\psi}i\gamma^5\tau^3\psi\rangle = -\frac{M}{2G_S}\sin(\vec{q}\vec{x}) \tag{C.1}$$

and it remains to be shown, that the combination in Equation (3.53) equals

$$-2G_S\left[\langle\overline{\psi}\psi\rangle + i\gamma^5\tau^3\langle\overline{\psi}i\gamma^5\tau^3\psi\rangle\right] = M\exp(i\gamma^5\tau^3\vec{q}\vec{x}). \tag{C.2}$$

To do so we start from the slightly more general formulation of the exponential function in the mass function, with $\pm\alpha \in \mathbb{R}$ an additional multiplicative factor that will be convenient later

$$e^{\pm i\gamma^5\tau^3\alpha\vec{q}\vec{x}} = \sum_n \frac{1}{n!}\left(\pm i\gamma^5\tau^3\alpha\vec{q}\vec{x}\right)^n \tag{C.3}$$

$$= \sum_n \frac{1}{(2n)!}\left(\pm i\gamma^5\tau^3\alpha\vec{q}\vec{x}\right)^{2n} + \sum_n \frac{1}{(2n+1)!}\left(\pm i\gamma^5\tau^3\alpha\vec{q}\vec{x}\right)^{2n+1} \tag{C.4}$$

and with $(\gamma^5\tau^3)^2 = \mathbb{1}$, we can write

$$e^{\pm i\gamma^5\tau^3\alpha\vec{q}\vec{x}} = \mathbb{1}\sum_n \frac{(-1)^n}{(2n)!}(\alpha\vec{q}\vec{x})^{2n} \pm i\gamma^5\tau^3\sum_n \frac{(-1)^n}{(2n+1)!}(\vec{q}\vec{x})^{2n+1} \tag{C.5}$$

$$= \mathbb{1}\cos(\alpha\vec{q}\vec{x}) \pm i\gamma^5\tau^3\sin(\alpha\vec{q}\vec{x}), \tag{C.6}$$

with the series representation of sine and cosine. With $\alpha = 1$ and the positive sign we find that this fulfills (C.2), with the definitions (C.1).

Now we want to show how to perform a Fourier transformation on the mass function. With the additional $\pm\alpha$, this applies for the chiral transformation matrices $U(\vec{x})$ as well if we set $\alpha = 1/2$. With the definition of the Fourier transformation from Appendix A

$$\int d^4x \int d^4x' e^{ipx}\delta^{(4)}(x-x')e^{\pm i\gamma^5\tau^3\alpha\vec{q}\vec{x}}e^{-ip'x'} \tag{C.7}$$

$$= \int d^4x\, e^{i(p-p')x}\left[\mathbb{1}\cos(\alpha\vec{q}\vec{x}) \pm i\gamma^5\tau^3\sin(\alpha\vec{q}\vec{x})\right] \tag{C.8}$$

$$= \int d^4x\, e^{i(p-p')x}\left[\frac{1}{2}(\mathbb{1}\pm\gamma^5\tau^3)e^{i\alpha\vec{q}\vec{x}} + \frac{1}{2}(\mathbb{1}\mp\gamma^5\tau^3)e^{-i\alpha\vec{q}\vec{x}}\right] \tag{C.9}$$

$$= \frac{1}{2}\left[(\mathbb{1}\pm\gamma^5\tau^3)(2\pi)^4\delta^{(4)}\left(p-p'+\alpha\vec{q}\right) + (\mathbb{1}\mp\gamma^5\tau^3)(2\pi)^4\delta^{(4)}\left(p-p'-\alpha\vec{q}\right)\right]. \tag{C.10}$$

C.2 Inverting the Gap Equation

We start from Equation (4.26)

$$iS(p',p) = iS_0(p',p) + \int \frac{d^4p_1}{(2\pi)^4} \int \frac{d^4p_2}{(2\pi)^4} iS_0(p',p_2)(-i\Sigma(p_2,p_1))iS(p_1,p) \tag{C.11}$$

and multiply with the inverse bare propagator $S_0^{-1}(r',p')$ from the left, the full inverse propagator $S^{-1}(p,r)$ from the right and integrate over the momenta p and p'

$$\begin{aligned} & i \int \frac{d^4p'}{(2\pi)^4} S_0^{-1}(r',p') \int \frac{d^4p}{(2\pi)^4} S(p',p)S^{-1}(p,r) \qquad (C.12)\\ & = i \int \frac{d^4p'}{(2\pi)^4} \int \frac{d^4p}{(2\pi)^4} S_0^{-1}(r',p')S_0(p',p)S^{-1}(p,r) \\ & + i \int \frac{d^4p'}{(2\pi)^4} \int \frac{d^4p}{(2\pi)^4} \int \frac{d^4p_1}{(2\pi)^4} \int \frac{d^4p_2}{(2\pi)^4} S_0^{-1}(r',p')S_0(p',p_2)\Sigma(p_2,p_1)S(p_1,p)S^{-1}(p,r) \end{aligned}$$

and with the definitions of the inverse matrix in momentum space

$$\begin{aligned} & \int \frac{d^4p'}{(2\pi)^4} S_0^{-1}(r',p')(2\pi)^4\delta^{(4)}\left(p'-r\right) = \int \frac{d^4p}{(2\pi)^4} (2\pi)^4\delta^{(4)}\left(r'-p\right)S^{-1}(p,r) \qquad (C.13)\\ & \quad + \int \frac{d^4p_2}{(2\pi)^4} \int \frac{d^4p_1}{(2\pi)^4} (2\pi)^4\delta^{(4)}\left(r'-p_2\right)\Sigma(p_2,p_1)(2\pi)^4\delta^{(4)}(p_1-r) \\ \Rightarrow \quad & S_0^{-1}(r',r) = S^{-1}(r',r) + \Sigma(r',r) \qquad (C.14)\\ \Rightarrow \quad & S^{-1}(p',p) = S_0^{-1}(p',p) - \Sigma(p',p), \qquad (C.15) \end{aligned}$$

where in the last step we relabeled the momenta to read p and p' again.

C.3 Matsubara Formalism for the Gap Equation

In order to calculate the Matsubara sum we follow largely the same steps as for the homogeneous case (see Section B.1).

Here we start from the gap equation where we already took the trace over the propagator and made the replacements for the Matsubara formalism

$$M = -8G_S N_f N_c M T \sum_m \int \frac{d^3k}{(2\pi)^3} \frac{(i\omega_m+\mu)^2 - \left(E_+^2(\vec{k}) + E_-^2(\vec{k})\right)/2 + 2Q^2}{\left((i\omega_m+\mu)^2 - E_+^2(\vec{k})\right)\left((i\omega_m+\mu)^2 - E_-^2(\vec{k})\right)}. \tag{C.16}$$

We can interpret the sum as a sum over residues, following the residue theorem. We are searching for a function that has poles at all Matsubara frequencies. Here we take

$$n_F(z) = (1+\exp(z/T))^{-1}, \tag{C.17}$$

which has the residue $-T$ and an integration contour Γ of infinitesimal width in real direction around it. We can write

$$M = 8G_S N_f N_c M \frac{1}{2\pi i} \oint_\Gamma dz \int \frac{d^3k}{(2\pi)^3} n_F(z) \frac{(z+\mu)^2 - \left(E_+^2(\vec{k}) + E_-^2(\vec{k})\right)/2 + 2Q^2}{\left((z+\mu)^2 - E_+^2(\vec{k})\right)\left((z+\mu)^2 - E_-^2(\vec{k})\right)} \tag{C.18}$$

We can deform the path Γ to a path Γ' which includes the residues from the denominator $z_{1..4} = \pm E_\pm(\vec{k}) - \mu$. By doing so, we can utilize the residue theorem again

$$\begin{aligned} &\frac{1}{2\pi i} \oint_{\Gamma'} dz \int \frac{d^3k}{(2\pi)^3} n_F(z) \frac{(z+\mu)^2 - \left(E_+^2(\vec{k}) + E_-^2(\vec{k})\right)/2 + 2Q^2}{\left((z+\mu)^2 - E_+^2(\vec{k})\right)\left((z+\mu)^2 - E_-^2(\vec{k})\right)} \\ &= -\sum_{i=1}^{4} \int \frac{d^3k}{(2\pi)^3} \mathrm{Res}_{z=z_i} n_F(z) \frac{(z+\mu)^2 - \left(E_+^2(\vec{k}) + E_-^2(\vec{k})\right)/2 + 2Q^2}{\left((z+\mu)^2 - E_+^2(\vec{k})\right)\left((z+\mu)^2 - E_-^2(\vec{k})\right)}, \end{aligned} \tag{C.19}$$

where we picked up an additional -1 from the winding number of Γ'. Carrying out the sum over the residues we find

$$\begin{aligned} &-\int \frac{d^3k}{(2\pi)^3} \left[n_F(E_+(\vec{k}) - \mu) \frac{E_+^2(\vec{k}) - \left(E_+^2(\vec{k}) + E_-^2(\vec{k})\right)/2 + 2Q^2}{2E_+(\vec{k})\left(E_+(\vec{k}) - E_-(\vec{k})\right)\left(E_+(\vec{k}) + E_-(\vec{k})\right)} \right. \\ &\qquad - n_F(-E_+(\vec{k}) - \mu) \frac{E_+^2(\vec{k}) - \left(E_+^2(\vec{k}) + E_-^2(\vec{k})\right)/2 + 2Q^2}{2E_+(\vec{k})\left(-E_+(\vec{k}) - E_-(\vec{k})\right)\left(-E_+(\vec{k}) + E_-(\vec{k})\right)} \\ &\qquad + n_F(E_-(\vec{k}) - \mu) \frac{E_-^2(\vec{k}) - \left(E_+^2(\vec{k}) + E_-^2(\vec{k})\right)/2 + 2Q^2}{2E_-(\vec{k})\left(E_-(\vec{k}) - E_+(\vec{k})\right)\left(E_-(\vec{k}) + E_+(\vec{k})\right)} \\ &\qquad \left. - n_F(-E_-(\vec{k}) - \mu) \frac{E_-^2(\vec{k}) - \left(E_+^2(\vec{k}) + E_-^2(\vec{k})\right)/2 + 2Q^2}{2E_-(\vec{k})\left(-E_-(\vec{k}) - E_+(\vec{k})\right)\left(-E_-(\vec{k}) + E_+(\vec{k})\right)} \right] \\ &= \int \frac{d^3k}{(2\pi)^3} \left[\frac{E_+^2(\vec{k}) - E_-^2(\vec{k}) + 4Q^2}{4E_+(\vec{k})\left(E_+^2(\vec{k}) - E_-^2(\vec{k})\right)} \left(n_F(-E_+(\vec{k}) - \mu) - n_F(E_+(\vec{k}) - \mu)\right) \right. \\ &\qquad \left. + \frac{E_-^2(\vec{k}) - E_+^2(\vec{k}) + 4Q^2}{4E_-(\vec{k})\left(E_-^2(\vec{k}) - E_+^2(\vec{k})\right)} \left(n_F(-E_-(\vec{k}) - \mu) - n_F(E_-(\vec{k}) - \mu)\right) \right]. \end{aligned} \tag{C.20}$$

With $n_F(-z) = 1 - n_F(z)$ we find the gap-equation to be

$$M = 8G_S N_f N_c M \int \frac{d^3k}{(2\pi)^3} \left[\frac{E_+^2(\vec{k}) - E_-^2(\vec{k}) + 4Q^2}{4E_+(\vec{k})\left(E_+^2(\vec{k}) - E_-^2(\vec{k})\right)} \left(1 - n_F(E_+(\vec{k}) + \mu) - n_F(E_+(\vec{k}) - \mu)\right) \right. \tag{C.21}$$

$$\left. + \frac{E_-^2(\vec{k}) - E_+^2(\vec{k}) + 4Q^2}{4E_-(\vec{k})\left(E_-^2(\vec{k}) - E_+^2(\vec{k})\right)} \left(1 - n_F(E_-(\vec{k}) + \mu) - n_F(E_-(\vec{k}) - \mu)\right) \right]$$

$$= 8G_S N_f N_c M \int \frac{d^3k}{(2\pi)^3} \left[\frac{\sqrt{k_z^2 + M^2} + Q}{4E_+(\vec{k})\sqrt{k_z^2 + M^2}} \left(1 - n_F(E_+(\vec{k}) + \mu) - n_F(E_+(\vec{k}) - \mu)\right) \right. \tag{C.22}$$

$$\left. + \frac{\sqrt{k_z^2 + M^2} - Q}{4E_-(\vec{k})\sqrt{k_z^2 + M^2}} \left(1 - n_F(E_-(\vec{k}) + \mu) - n_F(E_-(\vec{k}) - \mu)\right) \right]$$

$$= 2G_S N_f N_c M \int \frac{d^3k}{(2\pi)^3} \frac{1}{\sqrt{k_z^2 + M^2}} \left[\frac{\sqrt{k_z^2 + M^2} + Q}{E_+(\vec{k})} \left(1 - n_F(E_+(\vec{k}) + \mu) - n_F(E_+(\vec{k}) - \mu)\right) \right. \tag{C.23}$$

$$\left. + \frac{\sqrt{k_z^2 + M^2} - Q}{E_-(\vec{k})} \left(1 - n_F(E_-(\vec{k}) + \mu) - n_F(E_-(\vec{k}) - \mu)\right) \right].$$

D Details on the Calculations in the Bethe-Salpeter Equation

D.1 Resummation of the Bethe-Salpeter Equation

In this section we want to show how to do the resummation of the BSE in the case of inhomogeneous propagators. We will do everything in collective indices, denoted by lower case Greek letters $\alpha, \beta, \cdots$, where summation over reoccurring indices is implied. These indices encapsulate Dirac , color and flavor structure, as well as momentum dependence.

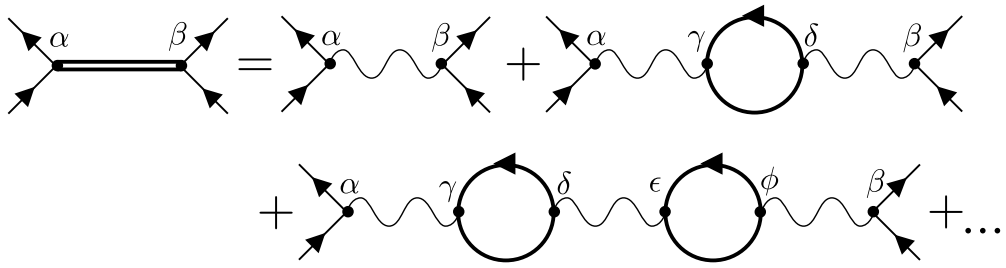

From the figure we get the equation

$$-\Gamma_\alpha D_{\alpha\beta}\bar{\Gamma}_\beta = \Gamma_\alpha K_{\alpha\beta}\bar{\Gamma}_\beta + \Gamma_\alpha K_{\alpha\gamma}\bar{\Gamma}_\gamma \hat{J}\Gamma_\delta K_{\delta\beta}\bar{\Gamma}_\delta + \Gamma_\alpha K_{\alpha\gamma}\bar{\Gamma}_\gamma \hat{J}\Gamma_\delta K_{\delta\epsilon}\bar{\Gamma}_\epsilon \hat{J}\Gamma_\phi K_{\phi\beta}\bar{\Gamma}_\beta + \cdots \tag{D.1}$$

We leave the first summand untouched and from the second summand onwards we take out the part $\Gamma_\alpha K_{\alpha\gamma}\bar{\Gamma}_\gamma \hat{J}$

$$-\Gamma_\alpha D_{\alpha\beta}\bar{\Gamma}_\beta = \Gamma_\alpha K_{\alpha\beta}\bar{\Gamma}_\beta + \Gamma_\alpha K_{\alpha\gamma}\bar{\Gamma}_\gamma \hat{J}\left(\Gamma_\delta K_{\delta\beta}\bar{\Gamma}_\beta + \Gamma_\delta K_{\delta\epsilon}\bar{\Gamma}_\epsilon \hat{J}\Gamma_\phi K_{\phi\beta}\bar{\Gamma}_\beta + \cdots\right) \tag{D.2}$$

and since this is an infinite sum, we can identify it with $-\Gamma_\delta D_{\delta\beta}\bar{\Gamma}_\beta$, which leads to the resummed equation

$$-\Gamma_\alpha D_{\alpha\beta}\bar{\Gamma}_\beta = \Gamma_\alpha K_{\alpha\beta}\bar{\Gamma}_\beta - \Gamma_\alpha K_{\alpha\gamma}\bar{\Gamma}_\gamma \hat{J}\Gamma_\delta D_{\delta\beta}\bar{\Gamma}_\delta, \tag{D.3}$$

which is exactly what we start our calculation off in Equation (6.4).

D.2 Transformation for the Meson Type

From the Lagrangian of the model, we get two types of vertices in Dirac and flavor space: $\mathbb{1}$ and $i\gamma_5\tau_3$. If we also take momentum space into account we find four distinct vertices we have to deal with

$$(\Gamma_\sigma(p))_{k',k} = \mathbb{1}(2\pi)^4\delta^{(4)}\left(k'-k-p\right), \qquad \left(\bar{\Gamma}_\sigma(p)\right)_{k',k} = \mathbb{1}(2\pi)^4\delta^{(4)}\left(k'-k+p\right), \tag{D.4}$$

$$(\Gamma_\pi(p))_{k',k} = i\gamma_5\tau_3(2\pi)^4\delta^{(4)}\left(k'-k-p\right), \quad \left(\bar{\Gamma}_\pi(p)\right)_{k',k} = i\gamma_5\tau_3(2\pi)^4\delta^{(4)}\left(k'-k+p\right), \tag{D.5}$$

which is diagrammatically

$(\Gamma_M(p))_{k',k} =$ 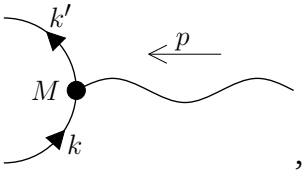

, $(\bar{\Gamma}_M(p))_{k',k} =$ 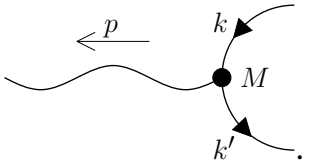

.

We already know which vertices we want in the end, namely those, where the transformations on the inner momenta from the propagators and the transformations of the outer momenta from the vertices cancel out. We can calculate the desired vertices from

$$\left(\Gamma'_M(p)\right)_{k',k} = \int \frac{d^4r'}{(2\pi)^4} \int \frac{d^4r}{(2\pi)^4} U^\dagger(k',r') \left(\Gamma_M(p)\right)_{r',r} U^\dagger(r,k), \tag{D.6}$$

$$\left(\bar{\Gamma}'_M(p)\right)_{k',k} = \int \frac{d^4r'}{(2\pi)^4} \int \frac{d^4r}{(2\pi)^4} U^\dagger(k',r') \left(\bar{\Gamma}_M(p)\right)_{r',r} U^\dagger(r,k), \tag{D.7}$$

which results in

$$\left(\Gamma'_\sigma(p)\right)_{k',k} = \frac{1}{2}\left[(\mathbb{1}+\gamma_5\tau_3)(2\pi)^4\delta^{(4)}\left(k'-k-p+q\right) + (\mathbb{1}-\gamma_5\tau_3)(2\pi)^4\delta^{(4)}\left(k'-k-p-q\right)\right], \tag{D.8}$$

$$\left(\bar{\Gamma}'_\sigma(p')\right)_{k',k} = \frac{1}{2}\left[(\mathbb{1}+\gamma_5\tau_3)(2\pi)^4\delta^{(4)}\left(k'-k+p'+q\right) + (\mathbb{1}-\gamma_5\tau_3)(2\pi)^4\delta^{(4)}\left(k'-k+p'-q\right)\right], \tag{D.9}$$

$$\left(\Gamma'_\pi(p)\right)_{k',k} = \frac{i}{2}\left[(\mathbb{1}+\gamma_5\tau_3)(2\pi)^4\delta^{(4)}\left(k'-k-p+q\right) + (-\mathbb{1}+\gamma_5\tau_3)(2\pi)^4\delta^{(4)}\left(k'-k-p-q\right)\right], \tag{D.10}$$

$$\left(\bar{\Gamma}'_\pi(p')\right)_{k',k} = \frac{i}{2}\left[(\mathbb{1}+\gamma_5\tau_3)(2\pi)^4\delta^{(4)}\left(k'-k+p'+q\right) + (-\mathbb{1}+\gamma_5\tau_3)(2\pi)^4\delta^{(4)}\left(k'-k+p'-q\right)\right]. \tag{D.11}$$

We can this express in terms of the untransformed vertices as

$$\Gamma'_\sigma(p) = \frac{1}{2}\left[\Gamma_\sigma(p-q) + \Gamma_\sigma(p+q) - i\Gamma_\pi(p-q) + i\Gamma_\pi(p+q)\right], \tag{D.12}$$

$$\bar{\Gamma}'_\sigma(p') = \frac{1}{2}\left[\bar{\Gamma}_\sigma(p'-q) + \bar{\Gamma}_\sigma(p'+q) + i\bar{\Gamma}_\pi(p'-q) - i\bar{\Gamma}_\pi(p'+q)\right], \tag{D.13}$$

$$\Gamma'_\pi(p) = \frac{1}{2}\left[i\Gamma_\sigma(p-q) - i\Gamma_\sigma(p+q) + \Gamma_\pi(p-q) + \Gamma_\pi(p+q)\right], \tag{D.14}$$

$$\bar{\Gamma}'_\pi(p') = \frac{1}{2}\left[-i\bar{\Gamma}_\sigma(p'-q) + i\bar{\Gamma}_\sigma(p'+q) + \bar{\Gamma}_\pi(p'-q) + \bar{\Gamma}_\pi(p'+q)\right]. \tag{D.15}$$

Now we want transformations on the external momenta p' and p which ensure

$$\bar{\Gamma}'_\alpha = W_{\alpha\beta}\bar{\Gamma}_\beta \qquad \text{and} \qquad \Gamma'_\alpha = \Gamma_\beta W^\dagger_{\beta\alpha} \tag{D.16}$$

and we find these to be

$$W_{\sigma\sigma}(p',k) = \frac{1}{2}\left[(2\pi)^4\delta^{(4)}\left(p'+q-k\right) + (2\pi)^4\delta^{(4)}\left(p'-q-k\right)\right], \tag{D.17}$$

$$W_{\sigma\pi}(p',k) = \frac{i}{2}\left[-(2\pi)^4\delta^{(4)}\left(p'+q-k\right) + (2\pi)^4\delta^{(4)}\left(p'-q-k\right)\right], \tag{D.18}$$

$$W_{\pi\sigma}(p',k) = \frac{i}{2}\left[(2\pi)^4\delta^{(4)}\left(p'+q-k\right) - (2\pi)^4\delta^{(4)}\left(p'-q-k\right)\right] = W^*_{\sigma\pi}(p',k), \tag{D.19}$$

$$W_{\pi\pi}(p',k) = \frac{1}{2}\left[(2\pi)^4\delta^{(4)}\left(p'+q-k\right) + (2\pi)^4\delta^{(4)}\left(p'-q-k\right)\right] = W_{\sigma\sigma}(p',k) \tag{D.20}$$

and

$$W^{\dagger}_{\sigma\sigma}(k,p) = \frac{1}{2}\left[(2\pi)^4\delta^{(4)}(p+q-k) + (2\pi)^4\delta^{(4)}(p-q-k)\right], \tag{D.21}$$

$$W^{\dagger}_{\sigma\pi}(k,p) = \frac{i}{2}\left[-(2\pi)^4\delta^{(4)}(p+q-k) + (2\pi)^4\delta^{(4)}(p-q-k)\right], \tag{D.22}$$

$$W^{\dagger}_{\pi\sigma}(k,p) = \frac{i}{2}\left[(2\pi)^4\delta^{(4)}(p+q-k) - (2\pi)^4\delta^{(4)}(p-q-k)\right] = \left(W^{\dagger}_{\sigma\pi}(k,p)\right)^*, \tag{D.23}$$

$$W^{\dagger}_{\pi\pi}(k,p) = \frac{1}{2}\left[(2\pi)^4\delta^{(4)}(p+q-k) + (2\pi)^4\delta^{(4)}(p-q-k)\right] = W^{\dagger}_{\sigma\sigma}(k,p). \tag{D.24}$$

These transformations are unitary, so that

$$WW^{\dagger} \equiv \int \frac{d^4k}{(2\pi)^4} \sum_N W_{M'N}(p',k) W^{\dagger}_{NM}(k,p) = \delta_{M'M}(2\pi)^4\delta^{(4)}\left(p'-p\right) \mathbb{1}_{D,f,c}. \tag{D.25}$$

Now we want to impose these transformations on the polarization loop, to see if they have the desired effects. From the polarization loop we get

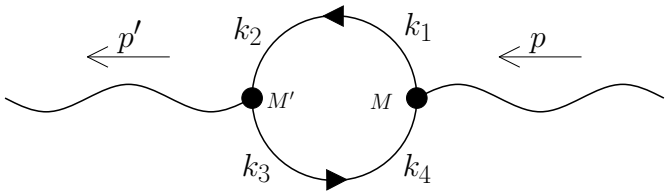

$$J_{M'M}(p'p) = i\left(\prod_{j=1}^{4}\int \frac{d^4k_j}{(2\pi)^4}\right) \mathrm{tr}\left[\left(\bar{\Gamma}_{M'}(p')\right)_{k_3,k_2} iS(k_2,k_1)\left(\Gamma_M(p)\right)_{k_1,k_4} iS(k_4,k_3)\right] \tag{D.26}$$

$$=: i\mathrm{Tr}\left[\bar{\Gamma}_{M'}(p')iS\Gamma_M(p)iS\right], \tag{D.27}$$

where in the second line the trace goes over momentum space, as well as the usual color-, flavor- and Dirac space and internal momenta need not be displayed. We get the transformed polarization loop by applying our transformations

$$J'_{M'M}(p',p) = i\int \frac{d^4k'}{(2\pi)^4} \int \frac{d^4k}{(2\pi)^4} \sum_{N',N} W_{M'N'}(p',k')\mathrm{Tr}\left[\bar{\Gamma}_{N'}(k')iS\Gamma_N(k)iS\right] W^{\dagger}_{NM}(k,p). \tag{D.28}$$

D.3 Traces in the Polarization Loop

Now we want to calculate the traces in the polarization loop

$$J'_{M'M}(p',p) = i\left(\prod_{j=1}^{4}\int \frac{d^4k_j}{(2\pi)^4}\right) \mathrm{tr}\left[\left(\bar{\Gamma}'_{M'}(p')\right)_{k_3,k_2} iS(k_2,k_1)\left(\Gamma'_M(p)\right)_{k_1,k_4} iS(k_4,k_3)\right]. \tag{D.29}$$

By replacing the propagator with the transformations from Chapter 4

$$S(k,k') = \int \frac{d^4r}{(2\pi)^4} \int \frac{d^4r'}{(2\pi)^4} U(k,r)S'(r)(2\pi)^4\delta^{(4)}\left(r-r'\right)U(r',k') \tag{D.30}$$

we find

$$J'_{M'M}(p',p) = i\left(\prod_{j=1}^{4}\int \frac{d^4k_j}{(2\pi)^4}\right)\left(\prod_{j=1}^{4}\int \frac{d^4r_j}{(2\pi)^4}\right)\times$$
$$\times \mathrm{tr}\Big[\left(\bar{\Gamma}'_{M'}(p')\right)_{k_3,k_2} U(k_2,r_2) iS(r_2)(2\pi)^4\delta^{(4)}(r_2-r_1)\,U(r_1,k_1) \tag{D.31}$$
$$\times \left(\Gamma'_M(p)\right)_{k_1,k_4} U(k_4,r_4) iS(r_4)(2\pi)^4\delta^{(4)}\left(r_4-r_3\right)U(r_3,k_3)\Big]$$
$$= i\left(\prod_{j=1}^{4}\int \frac{d^4k_j}{(2\pi)^4}\right)\int \frac{d^4r_1}{(2\pi)^4}\int \frac{d^4r_3}{(2\pi)^4}\times \tag{D.32}$$
$$\times \mathrm{tr}\Big[U(r_3,k_3)\left(\bar{\Gamma}'_{M'}(p')\right)_{k_3,k_2} U(k_2,r_1) iS(r_1) U(r_1,k_1)\left(\Gamma'_M(p)\right)_{k_1,k_4} U(k_4,r_3) iS(r_3)\Big].$$

Here we can define new vertices

$$\left(\bar{\Gamma}''_{M'}(p')\right)_{r_3,r_1} = \int \frac{d^4k_3}{(2\pi)^4}\int \frac{d^4k_2}{(2\pi)^4}\, U(r_3,k_3)\left(\bar{\Gamma}'_{M'}(p')\right)_{k_3,k_2} U(k_2,r_1), \tag{D.33}$$
$$\left(\Gamma''_M(p)\right)_{r_1,r_3} = \int \frac{d^4k_1}{(2\pi)^4}\int \frac{d^4k_4}{(2\pi)^4}\, U(r_1,k_1)\left(\Gamma'_M(p)\right)_{k_1,k_4} U(k_4,r_3) \tag{D.34}$$

and from the way we found the primed vertices in Equations (D.6) and (D.7) we immediately see, that the double primed vertices equal the untransformed vertices

$$\left(\bar{\Gamma}''_{M'}(p')\right)_{r_3,r_1} = \left(\bar{\Gamma}_{M'}(p')\right)_{r_3,r_1}, \qquad \left(\Gamma''_M(p)\right)_{r_1,r_3} = \left(\Gamma_M(p)\right)_{r_1,r_3}. \tag{D.35}$$

Therefore the transformed polarization loop can be written as

$$J'_{M'M}(p',p) = i\int \frac{d^4r_1}{(2\pi)^4}\int \frac{d^4r_3}{(2\pi)^4}\,\mathrm{tr}\Big[\left(\bar{\Gamma}_{M'}(p')\right)_{r_3,r_1} iS'(r_1)\left(\Gamma_M(p)\right)_{r_1,r_3} iS'(r_3)\Big] \tag{D.36}$$
$$= i\int \frac{d^4k'}{(2\pi)^4}\int \frac{d^4k}{(2\pi)^4}\,\mathrm{tr}\Big[\left(\bar{\Gamma}_{M'}(p')\right)_{k,k'} iS'(k')\left(\Gamma_M(p)\right)_{k',k} iS'(k)\Big], \tag{D.37}$$

where in the second step we just relabeled the internal momenta.

The four possible combinations of vertices are

$$J'_{\sigma\sigma}(p',p) = i\int\frac{d^4k'}{(2\pi)^4}\int\frac{d^4k}{(2\pi)^4}\,\mathrm{tr}\Big[\mathbb{1}(2\pi)^4\delta^{(4)}\big(k-k'+p'\big)iS'(k')\times \tag{D.38}$$
$$\times\,\mathbb{1}(2\pi)^4\delta^{(4)}\big(k'-k-p\big)iS'(k)\Big]$$
$$= i\int\frac{d^4k}{(2\pi)^4}\,\mathrm{tr}\big[iS'(k+p')iS'(k)\big](2\pi)^4\delta^{(4)}\big(p'-p\big), \tag{D.39}$$
$$J'_{\pi\pi}(p',p) = i\int\frac{d^4k'}{(2\pi)^4}\int\frac{d^4k}{(2\pi)^4}\,\mathrm{tr}\Big[i\gamma_5\tau_3(2\pi)^4\delta^{(4)}\big(k-k'+p'\big)iS'(k')\times \tag{D.40}$$
$$\times\,i\gamma_5\tau_3(2\pi)^4\delta^{(4)}\big(k'-k-p\big)iS'(k)\Big]$$
$$= i\int\frac{d^4k}{(2\pi)^4}\,\mathrm{tr}\big[i\gamma_5\tau_3iS'(k+p')i\gamma_5\tau_3iS'(k)\big](2\pi)^4\delta^{(4)}\big(p'-p\big), \tag{D.41}$$
$$J'_{\sigma\pi}(p',p) = i\int\frac{d^4k'}{(2\pi)^4}\int\frac{d^4k}{(2\pi)^4}\,\mathrm{tr}\Big[\mathbb{1}(2\pi)^4\delta^{(4)}\big(k-k'+p'\big)iS'(k')\times \tag{D.42}$$
$$\times\,i\gamma_5\tau_3(2\pi)^4\delta^{(4)}\big(k'-k-p\big)iS'(k)\Big]$$
$$= i\int\frac{d^4k}{(2\pi)^4}\,\mathrm{tr}\big[iS'(k+p')i\gamma_5\tau_3iS'(k)\big](2\pi)^4\delta^{(4)}\big(p'-p\big), \tag{D.43}$$
$$J'_{\pi\sigma}(p',p) = i\int\frac{d^4k'}{(2\pi)^4}\int\frac{d^4k}{(2\pi)^4}\,\mathrm{tr}\Big[i\gamma_5\tau_3(2\pi)^4\delta^{(4)}\big(k-k'+p'\big)iS'(k')\times \tag{D.44}$$
$$\times\,\mathbb{1}(2\pi)^4\delta^{(4)}\big(k'-k-p\big)iS'(k)\Big]$$
$$= i\int\frac{d^4k}{(2\pi)^4}\,\mathrm{tr}\big[i\gamma_5\tau_3iS'(k+p')iS'(k)\big](2\pi)^4\delta^{(4)}\big(p'-p\big). \tag{D.45}$$

Now we can actually calculate the traces with the propagators

$$S'(k) = \frac{1}{N(k)}\big[A(k)+\gamma_5\tau_3B(k)+\gamma_\mu C^\mu(k)+\gamma_5\tau_3\gamma_\mu D^\mu(k)+\gamma_5\tau_3\gamma_\mu\gamma_\nu E^{\mu\nu}(k)\big], \tag{D.46}$$
$$\gamma_5\tau_3S'(k) = \frac{1}{N(k)}\big[B(k)+\gamma_5\tau_3A(k)+\gamma_\mu D^\mu(k)+\gamma_5\tau_3\gamma_\mu C^\mu(k)+\gamma_\mu\gamma_\nu E^{\mu\nu}(k)\big]. \tag{D.47}$$

This yields

$$J'_{\sigma\sigma}(p',p) = i\int \frac{d^4k}{(2\pi)^4}\,\frac{-4(2\pi)^4\delta^{(4)}(p'-p)}{N(k+p')N(k)}\Big[A(k+p')A(k)+B(k+p')B(k) \tag{D.48}$$
$$+ g_{\mu\nu}\Big\{B(k+p')E^{\mu\nu}(k)+E^{\mu\nu}(k+p')B(k)$$
$$+ C^{\mu}(k+p')C^{\nu}(k)-D^{\mu}(k+p')D^{\nu}(k)\Big\}$$
$$+\left(g_{\mu\nu}g_{\rho\sigma}-g_{\mu\rho}g_{\nu\sigma}+g_{\mu\sigma}g_{\nu\rho}\right)E^{\mu\nu}(k+p')E^{\rho\sigma}(k)\Big],$$

$$J'_{\pi\pi}(p',p) = i\int \frac{d^4k}{(2\pi)^4}\,\frac{4(2\pi)^4\delta^{(4)}(p'-p)}{N(k+p')N(k)}\Big[A(k+p')A(k)+B(k+p')B(k) \tag{D.49}$$
$$+ g_{\mu\nu}\Big\{B(k+p')E^{\mu\nu}(k)+E^{\mu\nu}(k+p')B(k)$$
$$- C^{\mu}(k+p')C^{\nu}(k)+D^{\mu}(k+p')D^{\nu}(k)\Big\}$$
$$+\left(g_{\mu\nu}g_{\rho\sigma}-g_{\mu\rho}g_{\nu\sigma}+g_{\mu\sigma}g_{\nu\rho}\right)E^{\mu\nu}(k+p')E^{\rho\sigma}(k)\Big],$$

$$J'_{\sigma\pi}(p',p) = i\int \frac{d^4k}{(2\pi)^4}\,\frac{-4i(2\pi)^4\delta^{(4)}(p'-p)}{N(k+p')N(k)}\Big[B(k+p')A(k)+A(k+p')B(k) \tag{D.50}$$
$$- 4i\epsilon_{\mu\nu\rho\sigma}E^{\mu\nu}(k+p')E^{\rho\sigma}(k)$$
$$+ g_{\mu\nu}\Big\{A(k+p')E^{\mu\nu}(k)+E^{\mu\nu}(k+p')A(k)$$
$$+ C^{\mu}(k+p')D^{\nu}(k)-D^{\mu}(k+p')C^{\nu}(k)\Big\}\Big],$$

$$J'_{\pi\sigma}(p',p) = i\int \frac{d^4k}{(2\pi)^4}\,\frac{-4i(2\pi)^4\delta^{(4)}(p'-p)}{N(k+p')N(k)}\Big[B(k+p')A(k)+A(k+p')B(k) \tag{D.51}$$
$$- 4i\epsilon_{\mu\nu\rho\sigma}E^{\mu\nu}(k+p')E^{\rho\sigma}(k)$$
$$+ g_{\mu\nu}\Big\{A(k+p')E^{\mu\nu}(k)+E^{\mu\nu}(k+p')A(k)$$
$$- C^{\mu}(k+p')D^{\nu}(k)+D^{\mu}(k+p')C^{\nu}(k)\Big\}\Big].$$

This will simplify in some ways once we enter the functions A to E, i.e. the part with the Levi-Civita symbol will vanish, but of course the expressions will be much longer. To highlight the differences in the different vertex components one can write in shorthand

$$f_{ABE} = A(k+p')A(k)+B(k+p')B(k)+g_{\mu\nu}\left\{B(k+p')E^{\mu\nu}(k)+E^{\mu\nu}(k+p')B(k)\right\} \tag{D.52}$$
$$+\left(g_{\mu\nu}g_{\rho\sigma}-g_{\mu\rho}g_{\nu\sigma}+g_{\mu\sigma}g_{\nu\rho}\right)E^{\mu\nu}(k+p')E^{\rho\sigma}(k),$$
$$f_{CD} = g_{\mu\nu}\left\{C^{\mu}(k+p')C^{\nu}(k)-D^{\mu}(k+p')D^{\nu}(k)\right\}, \tag{D.53}$$
$$g_{ABE} = B(k+p')A(k)+A(k+p')B(k)-4i\epsilon_{\mu\nu\rho\sigma}E^{\mu\nu}(k+p')E^{\rho\sigma}(k) \tag{D.54}$$
$$+ g_{\mu\nu}\left\{A(k+p')E^{\mu\nu}(k)+E^{\mu\nu}(k+p')A(k)\right\},$$
$$g_{CD} = g_{\mu\nu}\left\{C^{\mu}(k+p')D^{\nu}(k)-D^{\mu}(k+p')C^{\nu}(k)\right\}. \tag{D.55}$$

This allows the polarization loop to be written in a shorter fashion

$$\underline{J}'(p',p) = i\int \frac{d^4k}{(2\pi)^4}\,\frac{4(2\pi)^4\delta^{(4)}(p'-p)}{N(k+p')N(k)}\begin{pmatrix} -(f_{ABE}+f_{CD}) & -i(g_{ABE}+g_{CD}) \\ -i(g_{ABE}-g_{CD}) & f_{ABE}-f_{CD}\end{pmatrix}, \tag{D.56}$$

where the matrix is meant as

$$\begin{pmatrix}\sigma\sigma & \sigma\pi \\ \pi\sigma & \pi\pi\end{pmatrix}.$$

After evaluating g_{ABE} we find it vanishes, so the matrix simplifies to

$$\underline{J}'(p',p) = i\int \frac{d^4k}{(2\pi)^4}\,\frac{4(2\pi)^4\delta^{(4)}(p'-p)}{N(k+p')N(k)}\begin{pmatrix} -(f_{ABE}+f_{CD}) & -ig_{CD} \\ ig_{CD} & f_{ABE}-f_{CD}\end{pmatrix}. \tag{D.57}$$

D.4 Abridged Functions in the Polarization Loop

Common Abbreviations

Since the expressions for the polarization loop are quite long, we introduced a lot of abbreviations inside the expressions. To help the reader not loose track of all these functions, we list the in this section

$$p_3^2 = p_0^2 - p_\perp^2, \tag{D.58}$$

$$E_{k,\pm} = \sqrt{k_z^2 + k_\perp^2 + M^2 + Q^2 \pm 2Q\sqrt{k_z^2+M^2}}, \tag{D.59}$$

$$E_{p,\pm} = \sqrt{(k_z+p_z)^2 + (k_\perp+p_\perp)^2 + M^2 + Q^2 \pm 2Q\sqrt{(k_z+p_z)^2+M^2}}, \tag{D.60}$$

$$d_k = E_{k,+}^2 - E_{k,-}^2 = 4Q\sqrt{k_z^2+M^2}, \tag{D.61}$$

$$d_p = E_{p,+}^2 - E_{p,-}^2 = 4Q\sqrt{(k_z+p_z)^2+M^2}, \tag{D.62}$$

$$d_{k,0} = 4\sqrt{k_z^2+M^2}, \tag{D.63}$$

$$d_{p,0} = 4\sqrt{(k_z+p_z)^2+M^2}, \tag{D.64}$$

$$\epsilon_{k,\pm} = E_{k,\pm}(k_\perp = 0) = \left|\sqrt{k_z^2+M^2} \pm Q\right|, \tag{D.65}$$

$$\epsilon_{p,\pm} = E_{p,\pm}(k_\perp = 0) = \left|\sqrt{(k_z+p_z)^2+M^2} \pm Q\right|, \tag{D.66}$$

$$\Delta\epsilon = \epsilon_{k,\pm}^2 - \epsilon_{p,\pm}^2, \tag{D.67}$$

$$\Sigma\epsilon = \epsilon_{k,\pm}^2 + \epsilon_{p,\pm}^2 + 2Q^2, \tag{D.68}$$

$$\alpha = \frac{p_0}{2p_3^2}\left(p_3^2 + \Delta\epsilon\right), \tag{D.69}$$

$$\beta = \sqrt{\frac{p_\perp^2}{4p_3^2}\left[\frac{(p_3^2+\Delta\epsilon)^2}{p_3^2} - 4\epsilon_{k,\pm}^2\right]}. \tag{D.70}$$

D.4.1 Integrand Functions j_i

The first function we introduced, is

$$\underline{j_1}(k,p) = \begin{pmatrix} -(f_{ABE}+f_{CD}) & -ig_{CD} \\ ig_{CD} & f_{ABE}-f_{CD} \end{pmatrix}. \tag{D.71}$$

The next one is

$$\begin{aligned} &\left(j_{2\pm\pm\pm}(\vec{k},\vec{p}\,')\right)_{\sigma\sigma} \\ &= \frac{\pm\pm N_f N_c k_\perp}{4 d_k d_p E_{k,\pm} E_{p,\pm}} \Big[-4Q^2 \Big(-4(k_z^2-M^2)^2 \pm d_p k_z p_z' - 8k_z^3 p_z' + 8k_z M^2 p_z' - 4k_z^2 p_z'^2 + 4M^2 p_z'^2 \\ &\quad \pm 4E_{k,\pm}E_{p,\pm}(-M^2 + k_z(k_z+p_z')) - 4k_\perp^2(-M^2+k_z(k_z+p_z')) + 4(-M^2+k_z(k_z+p_z'))Q^2 \Big) \\ &\quad \pm d_k \Big(4p_z'(k_z+p_z')Q^2 \pm d_p(\pm E_{k,\pm}E_{p,\pm} - k_\perp^2 + M^2 - k_z(k_z+p_z') + Q^2) \Big) \\ &\quad + k_\perp p_\perp' (16(-M^2+k_z(k_z+p_z'))Q^2 \mp \pm d_k d_p)\cos\theta \Big], \end{aligned} \tag{D.72}$$

$$\begin{aligned} &\left(j_{2\pm\pm\pm}(\vec{k},\vec{p}\,')\right)_{\pi\pi} \\ &= \frac{\pm\pm N_f N_c k_\perp}{4 d_k d_p E_{k,\pm} E_{p,\pm}} \Big[4Q^2 \Big(4(k_z^2-M^2)^2 \mp d_p(2M^2 + k_z p_z') + 8k_z^3 p_z' - 8k_z M^2 p_z' + 4k_z^2 p_z'^2 - 4M^2 p_z'^2 \\ &\quad \mp 4E_{k,\pm}E_{p,\pm}(M^2 + k_z(k_z+p_z')) + 4k_\perp^2(M^2+k_z(k_z+p_z')) - 4(M^2+k_z(k_z+p_z'))Q^2 \Big) \\ &\quad \pm d_k \Big(4(-2M^2 + p_z'(k_z+p_z'))Q^2 \pm d_p(\pm E_{k,\pm}E_{p,\pm} - k_\perp^2 - M^2 - k_z(k_z+p_z') + Q^2) \Big) \\ &\quad + k_\perp p_\perp' (16(M^2+k_z(k_z+p_z'))Q^2 \mp \pm d_k d_p)\cos\theta \Big], \end{aligned} \tag{D.73}$$

$$\begin{aligned} &\left(j_{2\pm\pm\pm}(\vec{k},\vec{p}\,')\right)_{\sigma\pi} = -\left(j_{2\pm\pm\pm}(\vec{k},\vec{p}\,')\right)_{\pi\sigma} \\ &= \frac{\pm\pm i N_f N_c k_\perp Q}{4 d_k d_p E_{k,\pm} E_{p,\pm}} \Big[16p_z'(M^2 + k_z(k_z+p_z'))Q^2 \pm 4d_p \Big(\pm E_{k,\pm}E_{p,\pm}k_z - k_\perp^2 k_z - (k_z^2-M^2)(k_z+p_z') + k_z Q^2 \Big) \\ &\quad \mp d_k \Big(\pm d_p p_z' \pm 4E_{k,\pm}E_{p,\pm}(k_z+p_z') - 4k_\perp^2(k_z+p_z') - 4k_z(k_z - M + p_z')(k_z+M+p_z') + 4(k_z+p_z')Q^2 \Big) \\ &\quad + 4k_\perp p_\perp' (\mp d_p k_z \pm d_k(k_z+p_z'))\cos\theta \Big]. \end{aligned} \tag{D.74}$$

For the next one we simply put in the Fermi distributions (and the 1 for the vacuum part) for readability reasons, so

$$\underline{j_3}_{\pm\pm\pm}(\vec{k},\vec{p}\,') = [1 - n_F(E_{k,\pm}+\mu) - n_F(E_{k,\pm}-\mu)]\, \underline{j_2}_{\pm\pm\pm}(\vec{k},\vec{p}\,') \tag{D.75}$$

The fourth function we abbreviated reads

$$\begin{aligned}
&\left(j_{4\pm\pm}(\vec{k},\vec{p}\,')\right)_{\sigma\sigma} \qquad (D.76)\\
&= \frac{N_f N_c}{32 d_{k,0} d_{p,0} \pi^2}\Big[-32k_z^4 - 32M^4 - 64k_z^3 p_z' \pm d_{k,0}(-8p_z'^2 Q \pm d_{p,0}(p_3^2 - \Sigma\epsilon))\\
&\quad + 2M^2(16p_z'^2 + 8p_3^2 \mp \pm d_{k,0}d_{p,0} - 8\Sigma\epsilon) + 2k_z^2(32M^2 - 16p_z'^2 - 8p_3^2 \pm \pm d_{k,0}d_{p,0} + 8\Sigma\epsilon)\\
&\quad + 2k_z p_z'(32M^2 - 8p_3^2 \pm 4d_{p,0}Q \pm \pm d_{k,0}d_{p,0} \mp 4d_{k,0}Q + 8\Sigma\epsilon)\Big],
\end{aligned}$$

$$\begin{aligned}
&\left(j_{4\pm\pm}(\vec{k},\vec{p}\,')\right)_{\pi\pi} \qquad (D.77)\\
&= \frac{N_f N_c}{32 d_{k,0} d_{p,0} \pi^2}\Big[-32k_z^4 - 32M^4 - 64k_z^3 p_z' \pm d_{k,0}(-8p_z'^2 Q \pm d_{p,0}(p_3^2 - \Sigma\epsilon))\\
&\quad + 2k_z^2(32M^2 - 16p_z'^2 - 8p_3^2 \pm \pm d_{k,0}d_{p,0} + 8\Sigma\epsilon)\\
&\quad + 2M^2(16p_z'^2 - 8p_3^2 \pm 8d_{p,0}Q \pm \pm d_{k,0}d_{p,0} \pm 8d_{k,0}Q + 8\Sigma\epsilon)\\
&\quad + 2k_z P_z'(32M^2 - 8p_3^2 \pm 4d_{p,0}Q \pm \pm d_{k,0}d_{p,0} \mp 4d_{k,0}Q + 8\Sigma\epsilon)\Big],
\end{aligned}$$

$$\begin{aligned}
&\left(j_{4\pm\pm}(\vec{k},\vec{p}\,')\right)_{\sigma\pi} = -\left(j_{4\pm\pm}(\vec{k},\vec{p}\,')\right)_{\pi\sigma} \qquad (D.78)\\
&= \frac{iN_f N_c}{16 d_{k,0} d_{p,0} \pi^2}\Big[-2\Big(\pm 2d_{k,0}k_z^3 + 4k_z^2 p_z'(2Q \pm d_{k,0}) + p_z'(8M^2 Q \pm d_{k,0}(p_3^2 - \Sigma\epsilon)) + k_z(2p_z'^2(4Q \pm d_{k,0})\\
&\quad \pm d_{k,0}(-2M^2 + p_3^2 - \Sigma\epsilon))\Big) \pm d_{p,0}(4k_z^3 + 4k_z^2 p_z' - 4M^2 p_z' \pm d_{k,0}p_z' Q - 2k_z(2M^2 - p_3^2 + \Sigma\epsilon))\Big].
\end{aligned}$$

D.5 Substitution in the Polarization Loop

Starting from the last expression before the substitution

$$\begin{aligned}
\mathrm{Im}\left(\underline{J}'(p')\right) = -2\pi \sum_{\pm\pm\pm\pm} \int_{-\infty}^{\infty} \frac{dk_z}{(2\pi)^3} \int_{-\infty}^{\infty} dk_\perp\, k_\perp \int_{-\infty}^{\infty} dc\, (\pm\pm \underline{j_3}_{\pm\pm\pm}(k_z, k_\perp, c, \vec{p}\,')g(c)) \qquad (D.79)\\
\times \delta\left(-E_{p,\pm} \pm (E_{k,\pm} \pm p_0')\right)\theta(E_{k,\pm})\theta(E_{p,\pm})\theta(c+1)\theta(1-c)\theta(k_\perp), \qquad (D.80)
\end{aligned}$$

and inserting the substitutions yields

$$\begin{aligned}\mathrm{Im}\left(\underline{J}'(p')\right) = -2\pi \sum_{\pm\pm\pm\pm} \int_{-\infty}^{\infty} \frac{dk_z}{(2\pi)^3} \int_{-\infty}^{\infty} dE_{k,\pm} \int_{-\infty}^{\infty} dE_{p,\pm} \frac{\pm\pm E_{k,\pm} E_{p,\pm}}{p'_\perp \sqrt{E_{k,\pm}^2 - \epsilon_{k,\pm}^2}} \\ \times \underline{j_3}_{\pm\pm\pm} \left(k_z, \sqrt{E_{k,\pm}^2 - \epsilon_{k,\pm}^2}, \frac{E_{p,\pm}^2 - E_{k,\pm}^2 - {p'_\perp}^2 + \Delta\epsilon}{2p'_\perp \sqrt{E_{k,\pm}^2 - \epsilon_{k,\pm}^2}}, \vec{p}' \right) \\ \times g\left(\frac{E_{p,\pm}^2 - E_{k,\pm}^2 - {p'_\perp}^2 + \Delta\epsilon}{2p'_\perp \sqrt{E_{k,\pm}^2 - \epsilon_{k,\pm}^2}} \right) \delta\left(-E_{p,\pm} \pm (E_{k,\pm} \pm p'_0)\right) \\ \times \theta(E_{k,\pm}) \theta(E_{p,\pm}) \theta(\sqrt{E_{k,\pm}^2 - \epsilon_{k,\pm}^2}) \\ \times \theta\left(\frac{E_{p,\pm}^2 - E_{k,\pm}^2 - {p'_\perp}^2 + \Delta\epsilon}{2p'_\perp \sqrt{E_{k,\pm}^2 - \epsilon_{k,\pm}^2}} + 1 \right) \theta\left(1 - \frac{E_{p,\pm}^2 - E_{k,\pm}^2 - {p'_\perp}^2 + \Delta\epsilon}{2p'_\perp \sqrt{E_{k,\pm}^2 - \epsilon_{k,\pm}^2}} \right).\end{aligned} \tag{D.81}$$

This equation allows to directly integrate over $E_{p,\pm}$ to get rid of the delta function, where the integral boundaries have already been taken care off by the theta functions we introduced

$$\begin{aligned}\mathrm{Im}\left(\underline{J}'(p')\right) = -2\pi \sum_{\pm\pm\pm\pm} \int_{-\infty}^{\infty} \frac{dk_z}{(2\pi)^3} \int_{-\infty}^{\infty} dE_{k,\pm} \frac{\pm E_{k,\pm}^2 + E_{k,\pm} p'_0}{p'_\perp \sqrt{E_{k,\pm}^2 - \epsilon_{k,\pm}^2}} \\ \times \underline{j_3}_{\pm\pm\pm} \left(k_z, \sqrt{E_{k,\pm}^2 - \epsilon_{k,\pm}^2}, \frac{p_3^2 \pm E_{k,\pm} p'_0 + \Delta\epsilon}{2p'_\perp \sqrt{E_{k,\pm}^2 - \epsilon_{k,\pm}^2}}, \vec{p}' \right) g\left(\frac{p_3^2 \pm E_{k,\pm} p'_0 + \Delta\epsilon}{2p'_\perp \sqrt{E_{k,\pm}^2 - \epsilon_{k,\pm}^2}} \right) \\ \times \theta(E_{k,\pm}) \theta(\pm(E_{k,\pm} \pm p'_0)) \theta(\sqrt{E_{k,\pm}^2 - \epsilon_{k,\pm}^2}) \\ \times \theta\left(\frac{p_3^2 \pm E_{k,\pm} p'_0 + \Delta\epsilon}{2p'_\perp \sqrt{E_{k,\pm}^2 - \epsilon_{k,\pm}^2}} + 1 \right) \theta\left(1 - \frac{p_3^2 \pm E_{k,\pm} p'_0 + \Delta\epsilon}{2p'_\perp \sqrt{E_{k,\pm}^2 - \epsilon_{k,\pm}^2}} \right).\end{aligned} \tag{D.82}$$

To proceed we take a closer look at the theta functions, which we split up in terms of the signs $\pm$ and $\pm$ in the following table

$\pm$	$\pm$	
-1	-1	$\theta(p_3^2)\theta(p_0)\theta(p_3^2 - \epsilon_{k,\pm}^2)\theta(p_3^2 - (\epsilon_{k,\pm} + \epsilon_{p,\pm})^2)\chi_{[\alpha-\beta,\alpha+\beta]}(E_{k,\pm})$
1	-1	$\theta(p_3^2)\theta(-p_0)\theta(p_3^2 - \epsilon_{k,\pm}^2)\theta(p_3^2 - (\epsilon_{k,\pm} + \epsilon_{p,\pm})^2)\chi_{[-\alpha-\beta,-\alpha+\beta]}(E_{k,\pm})$
-1	1	$\theta(p_3^2)[\theta(-p_0)\theta(\epsilon_{p,\pm} - \epsilon_{k,\pm} - \lvert p_3\rvert)$ $+\theta(p_0)\theta(\epsilon_{k,\pm} - \lvert p_3\rvert)\theta(\epsilon_{k,\pm} - \epsilon_{p,\pm} - \lvert p_3\rvert)]\chi_{[\alpha-\beta,\alpha+\beta]}(E_{k,\pm})$ $+\theta(-p_3^2)\chi_{[\alpha+\beta,\infty]}(E_{k,\pm})$
1	1	$\theta(p_3^2)[\theta(-p_0)\theta(\epsilon_{k,\pm} - \lvert p_3\rvert)\theta(\epsilon_{k,\pm} - \epsilon_{p,\pm} - \lvert p_3\rvert)$ $+\theta(p_0)\theta(\epsilon_{p,\pm} - \epsilon_{k,\pm} - \lvert p_3\rvert)]\chi_{[-\alpha-\beta,-\alpha+\beta]}(E_{k,\pm})$ $+\theta(-p_3^2)\chi_{[-\alpha+\beta,\infty]}(E_{k,\pm})$

and we can further simplify this by neglecting redundant theta functions

$$\begin{aligned}\Xi_{\pm\pm}(E_{k,\pm}) = \theta(\mp)\big[\theta(p_3^2)\theta(\mp p_0)\theta(p_3^2-(\epsilon_{k,\pm}+\epsilon_{p,\pm})^2)\chi_{[\mp\alpha-\beta,\mp\alpha+\beta]}(E_{k,\pm})\big] \\ +\theta(\pm)\Big[\theta(p_3^2)\Big(\theta(\pm p_0)\theta(\epsilon_{p,\pm}-\epsilon_{k,\pm}-|p_3|) \\ +\theta(\mp p_0)\theta(\epsilon_{k,\pm}-\epsilon_{p,\pm}-|p_3|)\Big)\chi_{[\mp\alpha-\beta,\mp\alpha+\beta]}(E_{k,\pm}) \\ +\theta(-p_3^2)\chi_{[\mp\alpha+\beta,\infty]}(E_{k,\pm})\Big].\end{aligned} \tag{D.83}$$

The functions $\chi_{[a,b]}$ are now the only ones depending on the energy $E_{k,\pm}$ and should be understood as defining the integral boundaries in the form

$$\int_{-\infty}^{\infty} dx\, f(x)\chi_{[a,b]}(x) = \int_a^b dx\, f(x). \tag{D.84}$$

From here we continue in the main part of this work with Equation (6.87).

D.6 Analytic Evaluation of the Energy Integrals

To evaluate the integrals, we basically need two integrals

$$\int dz \frac{1}{\sqrt{z^2-a^2}} = \log\left(z+\sqrt{z^2-a^2}\right), \tag{D.85}$$

$$\int dz \frac{1}{\sqrt{a^2-z^2}} = \arctan\left(\frac{z}{\sqrt{a^2-z^2}}\right). \tag{D.86}$$

We start from the vacuum integral for $p_3^2 > 0$

$$I^+_{vac} = \sum_{\pm\pm}\int_{\mp\alpha-\beta}^{\mp\alpha+\beta} dE_{k,\pm}\,(\pm\pm\pm\pm)\frac{1}{\sqrt{-4p_3^2\left((E_{k,\pm}\pm\alpha)^2-\beta^2\right)}}\Theta_{\pm\pm\pm\pm}, \tag{D.87}$$

where $\Theta_{\pm\pm\pm\pm}$ reminds us, that additional theta functions prohibit us from straightforward summing up of $\pm$ and $\pm$, but is of no further interest in this calculation. We can substitute $z = E_{k,\pm}\pm\alpha$ and after some reordering

$$I^+_{vac} = \sum_{\pm\pm}\frac{(\pm\pm\pm\pm)\Theta_{\pm\pm\pm\pm}}{2\sqrt{p_3^2}}\int_{-\beta}^{\beta} dz\,\frac{1}{\sqrt{\beta^2-z^2}}. \tag{D.88}$$

In this simple form the integral is immediately recognizable and has the value π, so

$$I^+_{vac} = \sum_{\pm\pm}(\pm\pm\pm\pm)\Theta_{\pm\pm\pm\pm}\frac{\pi}{2\sqrt{p_3^2}}. \tag{D.89}$$

In the case for $p_3^2 < 0$ we find

$$I^-_{vac} = \sum_{\pm\pm} \frac{(\pm\pm\pm\pm)\theta(\pm)}{2\sqrt{-p_3^2}} \int_\beta^\infty dz \, \frac{1}{\sqrt{z^2-\beta^2}} \tag{D.90}$$

$$= \sum_{\pm} \frac{(\pm\pm\pm)}{2\sqrt{-p_3^2}} \left[\log\left(z+\sqrt{z^2-\beta^2}\right)\right]_\beta^\infty \tag{D.91}$$

$$= 0, \tag{D.92}$$

where in the last step we evaluated the sum over $\pm$.

Now we turn to the medium part, as said before, we only consider the limit of vanishing temperatures. For $p_3^2 > 0$ we have

$$I^+_{med} = \sum_{\pm\pm} \frac{(\pm\pm\pm\pm)\Theta_{\pm\pm\pm\pm}}{2\sqrt{p_3^2}} \int_{\mp\alpha-\beta}^{\mp\alpha+\beta} dE_{k,\pm} \, \frac{\theta(\mu - E_{k,\pm})}{\sqrt{\left(\beta^2-(E_{k,\pm}\pm\alpha)^2\right)}} \tag{D.93}$$

and can integrate by parts

$$I^+_{med} = \sum_{\pm\pm} \frac{(\pm\pm\pm\pm)\Theta_{\pm\pm\pm\pm}}{2\sqrt{p_3^2}} \left\{ \left[\arctan\left(\frac{E_{k,\pm}\pm\alpha}{\sqrt{\beta^2-(E_{k,\pm}\pm\alpha)^2}} \right) \theta(\mu - E_{k,\pm}) \right]_{\mp\alpha-\beta}^{\mp\alpha+\beta} \right. \tag{D.94}$$

$$\left. + \int_{\mp\alpha-\beta}^{\mp\alpha+\beta} dE_{k,\pm} \, \delta(\mu - E_{k,\pm}) \arctan\left(\frac{E_{k,\pm}\pm\alpha}{\sqrt{\beta^2-(E_{k,\pm}\pm\alpha)^2}} \right) \right\}$$

$$= \sum_{\pm\pm} \frac{(\pm\pm\pm\pm)\Theta_{\pm\pm\pm\pm}}{2\sqrt{p_3^2}} \left\{ \frac{\pi}{2} \left[\theta(\mu\pm\alpha-\beta) + \theta(\mu\pm\alpha+\beta) \right] \right. \tag{D.95}$$

$$+ \int_{-\infty}^{\infty} dE_{k,\pm} \, \delta(\mu - E_{k,\pm}) \arctan\left(\frac{E_{k,\pm}\pm\alpha}{\sqrt{\beta^2-(E_{k,\pm}\pm\alpha)^2}} \right) \times$$

$$\left. \times \, \theta(\mp\alpha+\beta-E_{k,\pm}) \theta(E_{k,\pm} - (\mp\alpha-\beta)) \right\}$$

$$= \sum_{\pm\pm} \frac{(\pm\pm\pm\pm)\Theta_{\pm\pm\pm\pm}}{2\sqrt{p_3^2}} \left\{ \frac{\pi}{2} \left[\theta(\mu\pm\alpha-\beta) + \theta(\mu\pm\alpha+\beta) \right] \right. \tag{D.96}$$

$$\left. + \arctan\left(\frac{\mu\pm\alpha}{\sqrt{\beta^2-(\mu\pm\alpha)^2}} \right) \theta(\beta - (\mu\pm\alpha)) \theta(\beta + \mu\pm\alpha)) \right\}.$$

Now for $p_3^2 < 0$ we go a similar route, but we keep the upper limit finite L and send it to ∞ later

$$I_{med}^{-} = \sum_{\pm\pm} \frac{(\pm\pm\pm\pm)\theta(\pm)}{2\sqrt{-p_3^2}} \int_{\mp\alpha+\beta}^{\infty} dE_{k,\pm} \frac{\theta(\mu - E_{k,\pm})}{\sqrt{(E_{k,\pm}\pm\alpha)^2 - \beta^2}} \tag{D.97}$$

$$= \lim_{L\to\infty} \sum_{\pm} \frac{(\pm\pm\pm)}{2\sqrt{-p_3^2}} \left[\log\left(E_{k,\pm}\pm\alpha + \sqrt{(E_{k,\pm}\pm\alpha)^2 - \beta^2}\right)\theta(\mu - E_{k,\pm})\right]_{\mp\alpha+\beta}^{L} \tag{D.98}$$

$$+ \sum_{\pm} \frac{(\pm\pm\pm)}{2\sqrt{-p_3^2}} \int_{-\infty}^{\infty} dE_{k,\pm}\delta(\mu - E_{k,\pm}) \log\left(E_{k,\pm}\pm\alpha + \sqrt{(E_{k,\pm}\pm\alpha)^2 - \beta^2}\right)\theta(E_{k,\pm} - (\mp\alpha+\beta))$$

$$= \lim_{L\to\infty} \frac{(\pm\pm)}{2\sqrt{-p_3^2}} \Bigg\{ \left[\log\left(L + \alpha + \sqrt{(L+\alpha)^2 - \beta^2}\right)\theta(\mu - L) - \log(\beta)\,\theta(\mu - (-\alpha+\beta))\right] \tag{D.99}$$

$$- \left[\log\left(L - \alpha + \sqrt{(L-\alpha)^2 - \beta^2}\right)\theta(\mu - L) - \log(\beta)\,\theta(\mu - (\alpha+\beta))\right] \Bigg\}$$

$$+ \sum_{\pm} \frac{(\pm\pm\pm)}{2\sqrt{-p_3^2}} \log\left(\mu\pm\alpha + \sqrt{(\mu\pm\alpha)^2 - \beta^2}\right)\theta(\mu - (\mp\alpha+\beta)).$$

The two parts containing L in the last equality cancel each other in the limit for large L and we are left with

$$I_{med}^{-} = \sum_{\pm} \frac{(\pm\pm\pm)}{2\sqrt{-p_3^2}} \left[-\log\beta + \log\left(\mu\pm\alpha + \sqrt{(\mu\pm\alpha)^2 - \beta^2}\right)\right]\theta(\mu - (\mp\alpha+\beta)) \tag{D.100}$$

$$= \sum_{\pm} \frac{(\pm\pm\pm)}{2\sqrt{-p_3^2}} \log\left(\frac{\mu\pm\alpha + \sqrt{(\mu\pm\alpha)^2 - \beta^2}}{\beta}\right)\theta(\mu - (\mp\alpha+\beta)). \tag{D.101}$$

Bibliography

[1] H. Fritzsch, M. Gell-Mann, and H. Leutwyler, "Advantages of the color octet gluon picture," *Physics Letters B* **47** no. 4, (1973) 365–368. http://linkinghub.elsevier.com/retrieve/pii/0370269373906254.

[2] S. Weinberg, "Non-Abelian Gauge Theories of the Strong Interactions," *Physical Review Letters* **31** no. 7, (1973) 494–497. https://link.aps.org/doi/10.1103/PhysRevLett.31.494.

[3] P. W. Higgs, "Broken Symmetries and the Masses of Gauge Bosons," *Physical Review Letters* **13** no. 16, (1964) 508–509. http://link.aps.org/doi/10.1103/PhysRevLett.13.508.

[4] F. Englert and R. Brout, "Broken Symmetry and the Mass of Gauge Vector Mesons," *Physical Review Letters* **13** no. 9, (1964) 321–323. http://link.aps.org/doi/10.1103/PhysRevLett.13.321.

[5] S. Chatrchyan, V. Khachatryan, A. M. Sirunyan, *et al.*, "Observation of a new boson at a mass of 125 GeV with the CMS experiment at the LHC," *Physics Letters, Section B: Nuclear, Elementary Particle and High-Energy Physics* **716** no. 1, (2012) 30–61, arXiv:1207.7235.

[6] G. Aad, T. Abajyan, B. Abbott, *et al.*, "Observation of a new particle in the search for the Standard Model Higgs boson with the ATLAS detector at the LHC," *Physics Letters, Section B: Nuclear, Elementary Particle and High-Energy Physics* **716** no. 1, (2012) 1–29, arXiv:1207.7214 [hep-ex].

[7] D. J. Gross and F. Wilczek, "Ultraviolet Behavior of Non-Abelian Gauge Theories," *Physical Review Letters* **30** no. 26, (1973) 1343–1346. http://link.aps.org/doi/10.1103/PhysRevLett.30.1343.

[8] H. D. Politzer, "Reliable Perturbative Results for Strong Interactions?," *Physical Review Letters* **30** no. 26, (1973) 1346–1349. http://link.aps.org/doi/10.1103/PhysRevLett.30.1346.

[9] M. L. Perl, E. R. Lee, and D. Loomba, "Searches for Fractionally Charged Particles," *Annual Review of Nuclear and Particle Science* **59** no. 1, (2009) 47–65. http://www.annualreviews.org/doi/10.1146/annurev-nucl-121908-122035.

[10] R. J. Jaffe, "Multiquark hadrons. I. Phenomenology of Q 2 Q - 2 mesons," *Physical Review D* **15** no. 1, (1977) 267–280. https://link.aps.org/doi/10.1103/PhysRevD.15.267.

[11] R. L. Jaffe, "Multiquark hadrons. II. Methods," *Physical Review D* **15** no. 1, (1977) 281–289. https://link.aps.org/doi/10.1103/PhysRevD.15.281.

[12] R. Aaij, B. Adeva, M. Adinolfi, *et al.*, "Observation of J / ψ p Resonances Consistent with Pentaquark States in Λ b 0 -> J / ψ K - p Decays," *Physical Review Letters* **115** no. 7, (2015) 072001. http://link.aps.org/doi/10.1103/PhysRevLett.115.072001.

[13] H. Fritzsch and M. Gell-Mann, "Current algebra: Quarks and what else?," *eConf* **C720906V2** (1972) 135–165. https://inspirehep.net/record/76232?ln=de.

[14] H. Fritzsch and P. Minkowski, "Ψ-resonances, gluons and the Zweig rule," *Il Nuovo Cimento A* **30** no. 3, (1975) 393–429. http://link.springer.com/10.1007/BF02730295.

[15] J. Goldstone, "Field theories with Superconductor solutions," *Il Nuovo Cimento* **19** no. 1, (1961) 154–164. http://link.springer.com/10.1007/BF02812722.

[16] K. Olive, D. Weinberg, K. Munig, *et al.*, "Review of Particle Physics," *Chinese Physics C* **38** no. 9, (2014) 090001. http://stacks.iop.org/1674-1137/38/i=9/a=090001?key=crossref.47735154e79ac9c858085df9b5a1f93a.

[17] K. G. Wilson, "Confinement of quarks," *Physical Review D* **10** no. 8, (1974) 2445–2459. http://link.aps.org/doi/10.1103/PhysRevD.10.2445.

[18] Z. Fodor and C. Hoelbling, "Light hadron masses from lattice QCD," *Reviews of Modern Physics* **84** no. 2, (2012) 449–495. http://link.aps.org/doi/10.1103/RevModPhys.84.449.

[19] C. Gattringer and K. Langfeld, "Approaches to the sign problem in lattice field theory," *International Journal of Modern Physics A* **31** no. 22, (2016) 1643007. http://www.worldscientific.com/doi/abs/10.1142/S0217751X16430077.

[20] P. de Forcrand and O. Philipsen, "QCD phase diagram at small densities from simulations with imaginary mu," *Nucl. Phys. B. - Proc. Suppl.* **119** (2003) 535–537, arXiv:0301209 [hep-ph]. http://arxiv.org/abs/hep-ph/0301209.

[21] J. Günther, R. Bellwied, S. Borsanyi, *et al.*, "The QCD equation of state at finite density from analytical continuation," *EPJ Web of Conferences* **137** (2017) 07008. http://www.epj-conferences.org/10.1051/epjconf/201713707008.

[22] G. Endrődi, Z. Fodor, S. D. Katz, Szabó, and K. K., "The QCD phase diagram at nonzero quark density," *Journal of High Energy Physics* **2011** no. 4, (2011) 1. http://link.springer.com/10.1007/JHEP04(2011)001.

[23] O. Kaczmarek, F. Karsch, E. Laermann, *et al.*, "Phase boundary for the chiral transition in (2 + 1)-flavor QCD at small values of the chemical potential," *Physical Review D* **83** no. 1, (2011) 014504. http://link.aps.org/doi/10.1103/PhysRevD.83.014504.

[24] A. Bazavov, H.-T. Ding, P. Hegde, *et al.*, "QCD equation of state to O (μ B 6) from lattice QCD," *Physical Review D* **95** no. 5, (2017) 054504. https://link.aps.org/doi/10.1103/PhysRevD.95.054504.

[25] G. Aarts, I.-O. Stamatescu, Z. F. Katz, *et al.*, "Stochastic quantization at finite chemical potential," *Journal of High Energy Physics* **2008** no. 09, (2008) 018–018. http://stacks.iop.org/1126-6708/2008/i=09/a=018?key=crossref.cac062bdfd31e04de2c10d121cbb0656.

[26] D. Sexty, "Simulating full QCD at nonzero density using the complex Langevin equation," *Physics Letters B* **729** (2014) 108–111.

[27] P. Braun-Munzinger, J. Stachel, and C. Wetterich, "Chemical freeze-out and the QCD phase transition temperature," *Physics Letters B* **596** no. 1, (2004) 61–69. http://www.sciencedirect.com/science/article/pii/S0370269304008822.

[28] A. Andronic, P. Braun-Munzinger, and J. Stachel, "Hadron production in central nucleus-nucleus collisions at chemical freeze-out," *Nuclear Physics A* **772** no. 3-4, (2006) 167–199, arXiv:0511071 [nucl-th].

[29] F. J. Dyson, "The S matrix in quantum electrodynamics," *Physical Review* **75** no. 11, (1949) 1736–1755.

[30] J. Schwinger, "On the Green's functions of quantized fields. I," *Proceedings of the National Academy of Sciences* **37** no. 7, (1951) 452–455. http://www.pnas.org/cgi/content/short/37/7/452.

[31] J. Schwinger, "On the Green's functions of quantized fields. II," *Proceedings of the National Academy of Sciences* **37** no. 7, (1951) 455–459. http://www.pnas.org/cgi/content/short/37/7/455.

[32] C. Wetterich, "Exact evolution equation for the effective potential," *Physics Letters B* **301** no. 1, (1993) 90–94.

[33] M. Mitter, J. M. Pawlowski, and N. Strodthoff, "Chiral symmetry breaking in continuum QCD," *Physical Review D - Particles, Fields, Gravitation and Cosmology* **91** no. 5, (2015) 1–18, arXiv:1411.7978 [hep-ph].

[34] A. K. Cyrol, L. Fister, M. Mitter, J. M. Pawlowski, and N. Strodthoff, "Landau gauge Yang-Mills correlation functions," *Physical Review D - Particles, Fields, Gravitation and Cosmology* **94** no. 5, (2016) 1–20, arXiv:1605.01856.

[35] R. A. Tripolt, N. Strodthoff, L. Von Smekal, and J. Wambach, "Spectral functions for the quark-meson model phase diagram from the functional renormalization group," *Physical Review D - Particles, Fields, Gravitation and Cosmology* **89** no. 3, (2014) 156–167, arXiv:arXiv:1311.0630v1. http://dx.doi.org/10.1016/j.nuclphysa.2014.04.027.

[36] R. A. Tripolt, L. Von Smekal, and J. Wambach, "Flow equations for spectral functions at finite external momenta," *Physical Review D - Particles, Fields, Gravitation and Cosmology* **90** no. 7, (2014) 1–13, arXiv:arXiv:1408.3512v2.

[37] C. Jung, F. Rennecke, R.-A. Tripolt, L. von Smekal, and J. Wambach, "In-Medium Spectral Functions of Vector- and Axial-Vector Mesons from the Functional Renormalization Group," arXiv:1610.08754. http://arxiv.org/abs/1610.08754.

[38] GSI Helmholtzzentrum für Schwerionenforschung, "The phase diagram of strongly interacting matter,".

[39] Y. Nambu and G. Jona-Lasinio, "Dynamical model of elementary particles based on an analogy with superconductivity. i," *Physical Review* **122** no. 1, (1961) 345–358.

[40] Y. Nambu and G. Jona-Lasinio, "Dynamical Model of Elementary Particles Based on an Analogy with Superconductivity. ii," *Phys. Rev.* **124** (1961) 246–254.

[41] M. Buballa, "NJL-model analysis of dense quark matter," *Physics Reports* **407** no. 4-6, (2005) 205–376, arXiv:0402234 [hep-ph].

[42] S. Klevansky, "The Nambu-Jona-Lasinio model of quantum chromodynamics," *Reviews of Modern Physics* **64** no. 3, (1992) 649–708.

[43] D. Ebert and H. Reinhardt, "Effective chiral hadron lagrangian with anomalies and skyrme terms from quark flavour dynamics," *Nuclear Physics B* **271** no. 1, (1986) 188–226. http://linkinghub.elsevier.com/retrieve/pii/0550321386903597.

[44] Christov, K. Goeke, and M. Polyakov, "NJL model with vector couplings vs. phenomenology," arXiv:9501383v1 [arXiv:hep-ph].

[45] M. Alford, K. Rajagopal, and F. Wilczek, "QCD at finite baryon density: nucleon droplets and color superconductivity," *Physics Letters B* **422** no. 1-4, (1998) 247–256, arXiv:9711395 [hep-ph]. http://arxiv.org/abs/hep-ph/9711395.

[46] R. Rapp, T. Schäfer, E. Shuryak, and M. Velkovsky, "Diquark Bose Condensates in High Density Matter and Instantons," *Physical Review Letters* **81** no. 1, (1998) 53–56, arXiv:9711396 [hep-ph]. http://arxiv.org/abs/hep-ph/9711396.

[47] A. W. Overhauser, "Structure of Nuclear Matter," *Phys. Rev. Lett.* **4** no. 8, (1960) 415–418. http://link.aps.org/doi/10.1103/PhysRevLett.4.415.

[48] P. Fulde and R. A. Ferrell, "Superconductivity in a Strong Spin-Exchange Field," *Phys. Rev.* **135** no. 3A, (1964) A550—-A563. http://link.aps.org/doi/10.1103/PhysRev.135.A550.

[49] A. I. Larkin and Y. N. Ovchinnikov, "Nonuniform state of superconductors," *Zh.Eksp.Teor.Fiz.* **47** (1964) 1136–1146.

[50] D. J. Gross and A. Neveu, "Dynamical symmetry breaking in asymptotically free field theories," *Phys. Rev. D* **10** no. 10, (1974) 3235–3253. http://link.aps.org/doi/10.1103/PhysRevD.10.3235.

[51] O. Schnetz, M. Thies, and K. Urlichs, "Phase diagram of the Gross-Neveu model: Exact results and condensed matter precursors," *Annals Phys.* **314** (2004) 425–447, arXiv:hep-th/0402014 [hep-th].

[52] D. Nickel, "Inhomogeneous phases in the Nambu-Jona-Lasino and quark- meson model," *Phys. Rev.* **D80** (2009) 74025, arXiv:0906.5295 [hep-ph].

[53] M. Buballa and S. Carignano, "Inhomogeneous chiral condensates," *Progress in Particle and Nuclear Physics* **81** (2015) 39–96, arXiv:1406.1367.

[54] D. Nickel, "How Many Phases Meet at the Chiral Critical Point?," *Physical Review Letters* **103** no. 7, (2009) 072301. https://link.aps.org/doi/10.1103/PhysRevLett.103.072301.

[55] S. Carignano, D. Nickel, and M. Buballa, "Influence of vector interaction and Polyakov loop dynamics on inhomogeneous chiral symmetry breaking phases," *Physical Review D* **82** no. 5, (2010) 054009. https://link.aps.org/doi/10.1103/PhysRevD.82.054009.

[56] M. Schramm, *Inhomogeneous phases in the Vector Interaction Extended Nambu-Jona-Lasinio Model*. Master's Thesis, TU Darmstadt, 2013. http://theorie.ikp.physik.tu-darmstadt.de/nhq/downloads/thesis/master.schramm.pdf.

[57] D. Nowakowski, M. Buballa, S. Carignano, and J. Wambach, "Inhomogeneous chiral symmetry breaking phases in isospin-asymmetric matter," arXiv:1506.04260. http://arxiv.org/abs/1506.04260.

[58] S. Carignano, M. Buballa, and B.-J. Schaefer, "Inhomogeneous phases in the quark-meson model with vacuum fluctuations," *Physical Review D* **90** no. 1, (2014) 014033. https://link.aps.org/doi/10.1103/PhysRevD.90.014033.

[59] D. Müller, M. Buballa, and J. Wambach, "Dyson-Schwinger study of chiral density waves in QCD," *Physics Letters B* **727** no. 1-3, (2013) 240–243. http://linkinghub.elsevier.com/retrieve/pii/S0370269313008575.

[60] S. Carignano and M. Buballa, "Two-dimensional chiral crystals in the Nambu-Jona-Lasinio model," *Physical Review D* **86** no. 7, (2012) 074018. https://link.aps.org/doi/10.1103/PhysRevD.86.074018.

[61] L. D. Landau and E. M. Lifshitz, *Statistical physics*. Pergamon Press, Oxford, 1969. http://www.sciencedirect.com/science/book/9780080570464.

[62] T.-G. Lee, E. Nakano, Y. Tsue, T. Tatsumi, and B. Friman, "Landau-Peierls instability in a Fulde-Ferrell type inhomogeneous chiral condensed phase," *Physical Review D* **92** no. 3, (2015) 034024. https://link.aps.org/doi/10.1103/PhysRevD.92.034024.

[63] Y. Hidaka, K. Kamikado, T. Kanazawa, and T. Noumi, "Phonons, pions, and quasi-long-range order in spatially modulated chiral condensates," *Physical Review D* **92** no. 3, (2015) 034003. https://link.aps.org/doi/10.1103/PhysRevD.92.034003.

[64] Y. Nambu, "Quasi-Particles and Gauge Invariance in the Theory of Superconductivity," *Physical Review* **117** no. 3, (1960) 648–663. http://link.aps.org/doi/10.1103/PhysRev.117.648.

[65] M. Buballa and S. Carignano, "Inhomogeneous chiral condensates," *Progress in Particle and Nuclear Physics* **81** (2015) 39–96.

[66] J. Kapusta and C. Gale, *Finite Temperature Field Theory*. Cambridge University Press, 2005.

[67] T. D. Cohen, "Functional Integrals for QCD at Nonzero Chemical Potential and Zero Density," *Physical Review Letters* **91** no. 22, (2003) 222001. http://link.aps.org/doi/10.1103/PhysRevLett.91.222001.

[68] E. E. Salpeter and H. A. Bethe, "A Relativistic Equation for Bound-State Problems," *Physical Review* **84** no. 6, (1951) 1232–1242. http://link.aps.org/doi/10.1103/PhysRev.84.1232.

[69] J. Hubbard, "Calculation of Partition Functions," *Physical Review Letters* **3** no. 2, (1959) 77–78. http://link.aps.org/doi/10.1103/PhysRevLett.3.77.

[70] R. L. Stratonovich, "On a Method of Calculating Quantum Distribution Functions," *Soviet Physics Doklady, Vol. 2, p.416* **2** (1957) 416.

[71] E. Alert, *Gap equations at inhomogeneous phases in the Nambu-Jona-Lasinio Model*. Master's Thesis, TU Darmstadt, 2017. http://theorie.ikp.physik.tu-darmstadt.de/nhq/downloads/thesis/master.alert.pdf.

[72] F. Dautry and E. M. Nyman, "Pion condensation and the σ-model in liquid neutron matter," *Nuclear Physics A* **319** no. 3, (1979) 323–348. http://linkinghub.elsevier.com/retrieve/pii/0375947479905189.

[73] S. Carignano, *Inhomogeneous chiral symmetry breaking phases*. PhD thesis, Technische Universität, Darmstadt, November, 2012. http://tuprints.ulb.tu-darmstadt.de/3149/.

[74] O. Schnetz, M. Thies, and K. Urlichs, "Phase diagram of the Gross-Neveu model: exact results and condensed matter precursors," *Annals of Physics* **314** no. 2, (2004) 425–447. https://www.sciencedirect.com/science/article/pii/S0003491604001241.

[75] D. Nickel, "Inhomogeneous phases in the Nambu-Jona-Lasinio and quark-meson model," *Physical Review D* **80** no. 7, (2009) 074025. https://link.aps.org/doi/10.1103/PhysRevD.80.074025.

[76] W. Pauli and F. Villars, "On the Invariant Regularization in Relativistic Quantum Theory," *Reviews of Modern Physics* **21** no. 3, (1949) 434–444. http://link.aps.org/doi/10.1103/RevModPhys.21.434.

[77] J. Schwinger, "On Gauge Invariance and Vacuum Polarization," *Physical Review* **82** no. 5, (1951) 664–679. https://link.aps.org/doi/10.1103/PhysRev.82.664.

[78] J. Gasser and H. Leutwyler, "Low energy theorems as precision tests of {QCD}," *Physics Letters B* **125** no. 4, (1983) 325–329. http://www.sciencedirect.com/science/article/pii/0370269383912947.

[79] J. Goldstone, A. Salam, and S. Weinberg, "Broken Symmetries," *Physical Review* **127** no. 3, (1962) 965–970. https://link.aps.org/doi/10.1103/PhysRev.127.965.

[80] I. Low and A. V. Manohar, "Spontaneously Broken Spacetime Symmetries and Goldstone's Theorem," *Physical Review Letters* **88** no. 10, (2002) 101602. https://link.aps.org/doi/10.1103/PhysRevLett.88.101602.

[81] H. Watanabe and H. Murayama, "Redundancies in Nambu-Goldstone Bosons," *Physical Review Letters* **110** no. 18, (2013) 181601. https://link.aps.org/doi/10.1103/PhysRevLett.110.181601.

[82] T. Hayata and Y. Hidaka, "Broken spacetime symmetries and elastic variables," *Physics Letters B* **735** (2014) 195–199. https://www.sciencedirect.com/science/article/pii/S0370269314004444.

[83] H. Kramers, "La diffusion de la lumière par les atomes," *Atti del Congresso Internationale dei Fisici, Como* **2** (1927) 545–557.

[84] R. d. L. Kronig, "On the Theory of Dispersion of X-Rays," *Journal of the Optical Society of America* **12** no. 6, (1926) 547. https://www.osapublishing.org/abstract.cfm?URI=josa-12-6-547.

[85] Y. W. Sokhotskii, *On definite integrals and functions used in series expansions*. St. Petersburg, 1873.

[86] J. Plemelj, *Problems in the sense of Riemann and Klein*. Interscience Publishers, New York, 1964.

[87] C. Kittel, *Introduction to Solid State Physics*. John Wiley & Sons, Inc., New York, 8th ed., 2005.

[88] P. Bedaque and A. W. Steiner, "Sound velocity bound and neutron stars," *Phys. Rev. Lett.* **114** (2015) 031103. https://link.aps.org/doi/10.1103/PhysRevLett.114.031103.

[89] T. Schulz, *Expectation values in the Nambu–Jona-Lasinio model*. Master's Thesis, TU Darmstadt, 2017. http://theorie.ikp.physik.tu-darmstadt.de/nhq/downloads/thesis/master.schulz.pdf.

[90] D. Nowakowski, *Inhomogeneous chiral symmetry breaking in isospin-asymmetric strong-interaction matter*. PhD thesis, Technische Universität Darmstadt, Darmstadt, 2017. http://tuprints.ulb.tu-darmstadt.de/6157/.

Acknowledgements

First of all, I would like to thank Prof. Dr. Wambach for giving me the opportunity to do research and work in his group. His continued support, whether it being guidance on my topic or helping me navigate the the depths of bureaucracy, is very much appreciated.

I am especially thankful to Dr. Michael Buballa, who has helped me with advice and ideas since my Bachelor thesis. It was great to have a supervisor, who always had an open door and often took two hours out of his time to answer "just one quick question".

I should also thank Dr. Stefano Carignano, who was also always willing to help and whose strong opinions on German culture and food were always delightful.

Another big thank you goes to my colleagues and friends from the third floor. First off Dr. Daniel Müller, Dr. Pascal Büscher, Dr. Daniel Nowakowski, Dr. David Scheffler and Dr. Peter Piasecki, who welcomed my to the office and made for a great atmosphere and stimulating discussions about physics, life, the universe and everything, occasionally helped by an after-work beer. I would also like to thank the people from the "other" office, especially Dr. Arno Tripolt, for organizing many a board game evening and Dr. Philipp Scior, for sharing my interest in Whisky, the proper cooking of meat and Eintracht Frankfurt. The "Lungerbalken" crew should not go unmentioned, turning many a smoking break into a fun time. Thanks also goes to the "Rothis" who (almost) always joined for Pappapizza Tag. Thanks goes to my four to five Master students, who where great to work with and who taught me patience and resilience. There are many more people who made my time in the Theory center great and I want to thank you all.

For the financial support during my thesis I would like to thank HIC for Fair and HGS-HIRe, who made it possible for me to go to interesting conferences, where I learned a lot and met great people.

Last but not least, I want to thank my friends and family, who supported and motivated me throughout my studies and all my life.

Lebenslauf

Name	Marco Schramm
Geburtstag	12. Juli 1986
Geburtsort	Frankfurt am Main
Staatsangehörigkeit	deutsch
Familienstand	ledig

2013 - 2017	Promotionsstudium in Physik an der Technischen Universität Darmstadt
Mai 2013	Abschluss "M.Sc. in Physics" Thesis: "Inhomogenous Phases in the Vector Interaction Extended Nambu–Jona-Lasinio Model"
2011 - 2013	Masterstudium in Physik an der Technischen Universität Darmstadt
Februar 2011	Abschluss "B.Sc. in Physik" Thesis: "Study of Inhomogeneous Phases in the Walecka Model"
2007 - 2011	Bachelorstudium in Physik an der Technischen Universität Darmstadt
2006 - 2007	Zivildienst, Evangelisches Kinder- und Jugendheim "Haus Gottesgabe", Bad Homburg
Juni 2006	Abitur
1996 - 2006	Besuch des Gymnasiums, Christian Wirth Schule, Usingen

Erklärung zur Dissertation

Hiermit versichere ich, die vorliegende Dissertation ohne Hilfe Dritter nur mit den angegebenen Quellen und Hilfsmitteln angefertigt zu haben. Alle Stellen, die aus Quellen entnommen wurden, sind als solche kenntlich gemacht. Diese Arbeit hat in gleicher oder ähnlicher Form noch keiner Prüfungsbehörde vorgelegen. Es wurde zuvor noch keine Promotion angestrebt.

Darmstadt, den 29.06.2017

(Marco Schramm)